UNIVERSIDAD DE CÓRDOBA

Programa de doctorado: Química Fina

Título de la tesis:

Desarrollo de Nuevos Nano-Fotocatalizadores para su Aplicación en Procesos de Fotorreacción en Flujo Continuo

Design of Novel Nano-Photocatalytic Systems for Continuous Photoreaction Processes

Director: Rafael Luque Ávarez de Sotomayor

Autor de la tesis: Weiyi Ouyang

Fecha de depósito tesis en el Idep: 16 de Mayo, 2018

TITULO: *Design of Novel Nano-Photocatalytic Systems for Continuous Photoreaction Processes*

AUTOR: *Weiyi Ouyang*

Campus de Rabanales
Ctra. Nacional IV, Km. 396 A
14071 Córdoba

https://www.uco.es/ucopress/index.php/es/
ucopress@uco.es

Doctoral Thesis

Design of Novel Nanophotocatalytic Systems for Continuous Photoreaction Processes

Weiyi OUYANG

2018

DOCTORAL THESIS

DESIGN OF NOVEL NANO-PHOTOCATALYTIC SYSTEMS FOR CONTINUOUS PHOTOREACTION PROCESSES

WEIYI OUYANG

DEPARTAMENTO DE QUÍMICA ORGÁNICA

FACULTAD DE CIENCIAS

UNIVERSIDAD DE CÓRDOBA

2018

TÍTULO DE LA TESIS: DESIGN OF NOVEL NANO-PHOTOCATALYTIC SYSTEMS FOR CONTINUOUS PHOTOREACTION PROCESSES

DOCTORANDO/A: WEIYI OUYANG

INFORME RAZONADO DEL DIRECTOR DE LA TESIS

En esta Tesis Doctoral se han llevado a cabo investigaciones relacionadas con el desarrollo de nuevos nanomateriales y su estudio en procesos de transformación de biomasa y residuos en compuestos de alto valor añadido empleando sistemas de reacción en flujo continuo o bien mediante fotocatálisis.

En primer lugar, se funcionalizaron con diferentes metales como Cu, Pd, Pt y/o Fe_2O_3 silicatos y aluminosilicatos mesoporosos con estructura tipo SBA-15 empleando procedimientos como la mecnoquímica y la deposición en flujo. Los materiales sintetizados se estudiaron en la reacción de hidrogenación del furfural a alcohol furfurílico utilizando un reactor en flujo continuo. Los materiales sintetizados mostraron una elevada estabilidad en el tiempo, especialmente el material 5%Pd/MAGSNC, siendo su actividad catalítica similar a la del catalizador comercial 10%Pd/C, con un mayor contenido de Pd. Así, los resultados de actividad catalítica pusieron de manifiesto que los factores más influyentes en conversión de furfural y selectividad a los productos son: la naturaleza del catalizador, la temperatura a la cual se lleva la reacción y la velocidad espacial.

Seguidamente, se sintetizaron materiales catalíticos empleando como soporte salvado de trigo, un residuo agrícola muy abundante, e incorporándole mediante molienda diferentes contenidos de titanio. Los materiales sintetizados fueron evaluados en la fotooxidación del alcohol bencílico, mostrando estos una mayor selectividad hacia el benzaldehído que otros catalizadores comerciales, como el material P-25 Evonik. Los estudios de caracterización llevados a cabo empleando XPS, entre otras técnicas experimentales mostraron que dicho aumento de selectividad podría deberse a la incorporación de C en la red del TiO_2, que actuaría como fotosensibilizador, facilitando la transferencia de los electrones excitados a la banda de conducción del TiO_2.

Finalmente, se prepararon materiales de TiO_2 magnéticamente separables mediante un procedimiento mecanoquímico empleando SBA-15 como soporte. Estos materiales se estudiaron, al igual que los descritos anteriormente, en la oxidación fotocatalítica del alcohol bencílico para la cual mostró una elevada actividad catalítica. En este caso se observó una relación directa entre contenido en TiO_2, que son los centros activos, y conversión de alcohol bencílico.

Como fruto estas investigaciones, se han publicado tres artículos científicos en revistas incluidas en el “Journal Citation Reports”, que conforman esta Memoria de Tesis, en las cuales Weiyi Ouyang ha participado como primer autor:

1. **Título:** Towards industrial furfural conversion: Selectivity and stability of palladium and platinum catalysts under continuous flow regime.
   Autores: Weiyi Ouyang, Alfonso Yepez, Antonio A. Romero, Rafael Luque.
   Revista: Catalysis Today.
   Indicios de Calidad (2016):
   Categoría: Chemistry, Applied. Índice de impacto: 4,636.
   Posición dentro de la categoría: 6 de 72, primer cuartil (Q1).
   Volumen: 308; Páginas: 32-37; Año: 2018.

2. **Título:** Wheat bran valorisation: Towards photocatalytic nanomaterials for benzyl alcohol photo-oxidation.
   Autores: Weiyi Ouyang, Jose M. Reina, Ewelina Kuna, Alfonso Yepez, Alina M. Balu, Antonio A. Romero, Juan Carlos Colmenares, Rafael Luque.
   Revista: Journal of Environmental Management.
   Indicios de Calidad (2016):
   Categoría: Environmental Sciences. Índice de impacto: 4,010.
   Posición dentro de la categoría: 39 de 229, primer cuartil (Q1).
   Volumen: 203; Páginas: 768-773; Año: 2017.

3. **Título:** Mechanochemical synthesis of TiO_2 nanocomposites as photocatalysts for benzyl alcohol photo-oxidation.
   Autores: Weiyi Ouyang, Ewelina Kuna, Alfonso Yepez, Alina M. Balu, Antonio A. Romero, Juan Carlos Colmenares, Rafael Luque.
   Revista: Nanomaterials.
   Indicios de Calidad (2016):
   Categoría: Materials Science. Índice de impacto: 3,553.
   Posición dentro de la categoría: 59 de 275, primer cuartil (Q1).
   Volumen: 6; Página: 93; Año: 2016.

Por todo ello, se autoriza la presentación de la tesis doctoral.

Córdoba, 15 de Mayo de 2018

Firma del director

Fdo.: Rafael Luque Ávarez de Sotomayor

FQM-383 Group

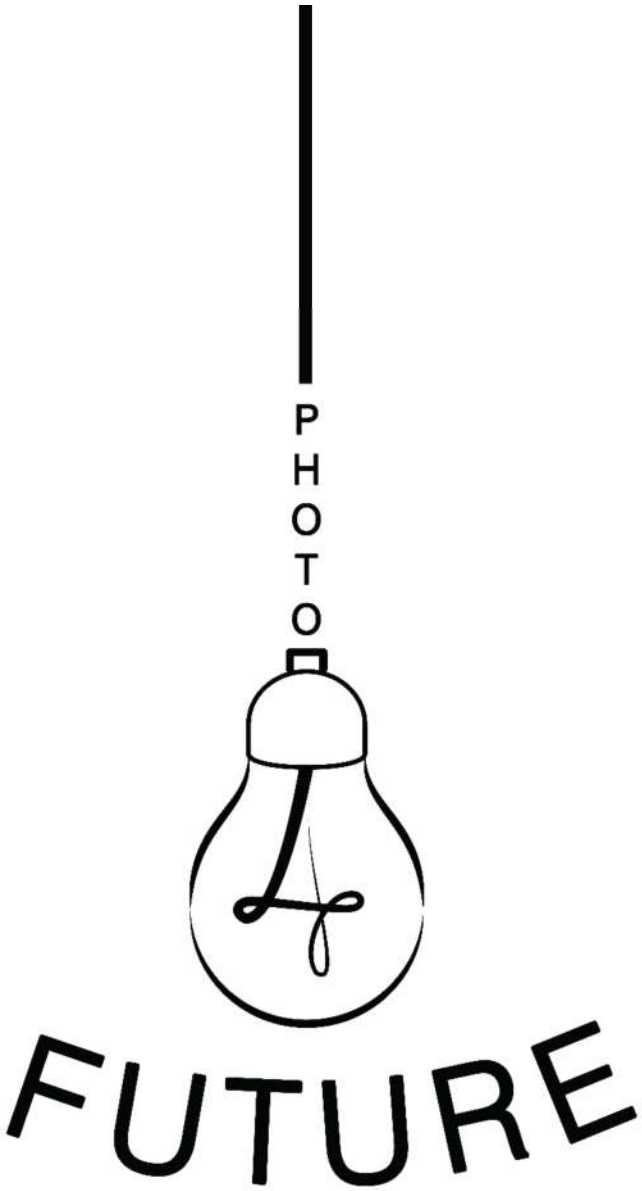

PHOTO4FUTURE

A Marie Skłodowska-Curie Innovative Training Network (ITN)

I would like to gratefully acknowledge funding from the European Union's Horizon 2020 research and innovation programme under the Marie Sklodowska-Curie grant agreement **No. 641861** for supporting all my PhD study, research and secondments.

Acknowledgements

The current research was carried out during 2015-2018 at Department of Organic Chemistry, University of Cordoba. Time flies that it is almost to the end of my PhD study. I am extraordinarily privileged to join as a Marie Sklodowska-Curie fellow in FQM-383 Group (NANOVAL), where I have conducted my PhD research for the past three years. Every single moment I experienced in NANOVAL counts and will become great treasure for my life. There were two remarkable fortunes for me in the past few years that I met two persons with significant importance to my life.

There is no doubt that the first one will be my most respected supervisor and life mentor, Prof. Rafael Luque Álvarez de Sotomayor. Knowing Prof. Luque in 2014, I was deeply inspired by his broad knowledge and innovative ideas, as well as his open-minded personality. I owe my deepest gratitude to Prof. Luque that I could not be a Marie Sklodowska-Curie fellow without his kind offer and hardly complete my research without his continuous and optimistic concern on this work, enthusiasm, encouragement and support. His inspiring ideas are also key stones securing the great success of the current research. As an ideal model, what I have learned from him will benefit me in both academic and life for my life time.

I am deeply grateful for the fortune that I met Li Hao, my wife, in 2015, who have been encouraging me with empathetic understanding since the very beginning and is very supportive for not only me but also the family. I am very appreciative that we went through the tough times hand in hand, and we will have an enjoyable life together in the near future.

I want to express my strong gratitude to Prof. Antonio Ángel Romero Reyes and Prof. Alina M. Balu for their great supports and kind help in the past three years. Besides, I would like to thank all the NANOVAL family members and alumni for supporting me in the research, sharing their knowledge and accompanying me through both the tough and happy moments, including Daily Rodriguez Padron, Antonio Pineda, Alfonso Yepez Gamboa, Ana Franco Losilla, Maria Dolores Marquez Medina, Layla Filiciotto, Alessio Zuliani & Camilla Maria Cova, Simona Polivia Consoletti, Pepijn Prinsen, Araceli Garcia Nunez, Maria Pinilla de Dios, Mario J. Munoz-Batista,

Soledad Cebrian Garcia, Esther Ricon Rubio, Kenneth Cerdán Gómez, Alain Puente Santiago, Sudipta De… as well as visitors from all over the world, including Yantao Wang, Deyang Zhao, Behgam Rahmani Vahid, Omar Perez Merino, Afsaneh Feiz, Sema Golonu, Virginia Aldabalde, Dovile Klupsaite, Tephilin Shilpa, Bingjie Wang, Gabriel Sathicq and so on… Special thanks to Antonio Pineda for his great assistance in the thesis, to Alfonso for his kind help in the lab instruments and to Daily & Andy for everything!

As a member of the outstanding Photo4Future team, I would like to thank all the principal investigators, including Prof. Timothy Noël, Prof. Rafael Luque, Prof. Samuel Marre, Prof. Simon Kuhn, Prof. Dorota Koziej, Prof. Kirsten Zeitler, Dr. Jesus Alcazar and Dr. Laszlo Kocsis, as well as Dr. Esther van Straten, for initiating such a fascinating project and building up this great team. I would like to thank Prof. Timothy Noël, Prof. Dorota Koziej and Prof. Samuel Marre for the inspiring encouragement. Besides, I would like to address my gratitude to all the other fellows within Photo4Future project, including Anca, Cecilia, Dario, Irini, Philipp, Prasaanth, Sztella and Xiao-Jing, for sharing the knowledge and brilliant ideas with me. I am very grateful that this project has offered me a lot of opportunities in learning, networking, etc, which is of great help for my career and my life.

My research could not have been completed without the excellent work from the outstanding collaborators and technicians. Therefore, I would like to acknowledge Prof. Juan Carlos Colmenares, Prof. Christophe Len and Prof. Marcos Fernandez-Garcia for their contributions in the collaboration. Many thanks to the technicians, including Pablo and Maria from the department, as well as Curro, Isabel, Juan Isidro, Macarena from SCAI for their support in material characterizations.

Thanks to ThalesNano Inc. and Institute of Catalysis and Petroleochemistry, CSIC for hosting me conduct my research during the secondments. Special appreciations for the people offering me kind helps during the secondments, including Olga, Ana, Mariela, Lucia, Tomas, Bernhard, Gabor, Dori, Miki, Peter.

Last but not least, I would like to my dear and lovely family: my parents, my parents-in-law, my wife, my brother and my uncles & aunts. Without their strong supports, I would not have been who I am today. Thank you very much! I love you all!

Contents

1. Introduction

Abstract

Energy and sustainability are two grand challenges for the 21st century. The society has been benefited from the manufacturing industry closely related to petroleum refining since the 20th century. However, great potential crisis lies in the supplements of chemicals, materials, polymers, energy and fuels due to the limited reserves of unrenewable crude oil. Meanwhile, the emerging trend of global warming and the raising public awareness on human and environmental safety are leading to more comprehensive legislations on environmental protection. These factors urge both scientific and industrial innovation in evolving substitutions for petrochemical industry from renewable resources to secure the sustainable development of society.

In this regard, environmental benign biorefineries can be a promising substitution to petroleum refineries. Tremendous amount of renewable lignocellulosic biomass, such as forestry waste and agricultural residues, can be used as sustainable carbon sources and prospective feedstocks for biorefineries. Unlike the open carbon cycle from the petroleum refinery, it is a close carbon cycle for biorefinery using biomass which is more eco-friendly and sustainable. Therefore, the shift from petroleum-based to renewable biomass-based refinery will be of great help for the development of sustainability and energy independence while reducing greenhouse gas emissions.[1,2]

Lignocellulosic biomass are complex materials comprising of three main fractions, namely cellulose, hemicellulose, and lignin, which can be deconstructed into platform molecules via thermal, biological or chemical conversion strategies. These platform molecules can be subsequently upgraded into various chemicals, materials and fuels, in which catalysis, especially heterogeneous catalysis, plays an essential role in the transformation.

Heterogeneous catalysts, most of which are solid state materials, function in different phase from reactants in the liquid or gaseous phasic reaction mixture. As compared to homogeneous catalysts, heterogeneous catalysts are advantageous in easier separation and reuse, higher high concentration

of active sites and stability under harsh conditions.[3] Apart from the intrinsic physical and chemical properties of the constitutive components, catalyst nanostructures, or the processing technology, has significant effect on the heterogeneous catalytic performance.[4] Nanocomposite catalysts synthesized by chemical processes can benefit from the possible synergetic catalytic effect that can greatly enhance the catalytic activity. Besides, the increase of catalyst surface area is also beneficial for the catalytic processes with enhancement in the contact between reactants and catalysts, as well as possible higher concentration of catalytic active sites. Therefore, there is great potential in the development of nanostructure composite materials for catalytic applications.

Flow chemistry and photochemistry are two appealing partners with green chemistry towards sustainability. In contrast to batch processes, flow ones are benefitted from the minimization of reaction time and waste generation, easy scale-up, energy and cost efficiency, together with improvement in safety.[5] Photocatalytic processes, utilizing photoenergy to drive many useful chemical reactions, have been considered as green technologies for both chemical and energy conversions since Fujishima and Honda first reported photocatalytic water splitting in 1972.[6]

In general, the current dissertation will be focused on the development of novel nanomaterials with the applications in valorizing biomass derived platform molecules using flow chemistry, photochemistry and, finally, photochemistry in flow.

1.1. Shift from petroleum refinery to biorefinery

1.1.1. Limits of petroleum refinery

The petroleum refinery industry has been developing dramatically over past centuries, providing both energy and materials as well as a wide range of useful chemical products. Though the fossil fuels will remain the role as major energy sources in the near future, it is coming to the crossroads for shifting to renewable and sustainable sources to secure the future energy and material supply, driven by number of factors.

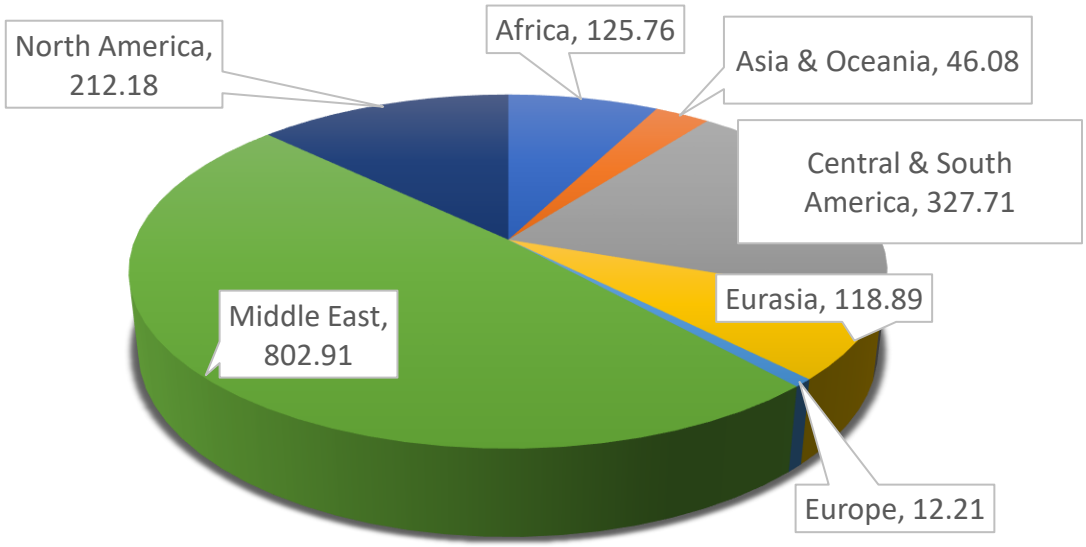

Figure 1. Global proven crude oil reserves of 2017. Unit: billion bbl. Data sources: U.S. Energy Information Administration, International Energy Statistics.[7]

Population growth is one of the critical factors (current population is about 7.6 billion, 2018) with numbers expanding to 9.2 billion in 2040. The demographic change together with improvement of living standards are raising the demand for energy and materials. The total primary energy demand at 2015 was 276.0 million barrels of oil equivalent per day (mboe/d), while it will increase by 35%, up to 372 mboe/d by 2040 according to the estimation from OPEC.[8] In particular, the long-term oil demand is anticipated to increase from 95.4 mb/d in 2016 to 111.1 mb/d in 2040. As known to all, fossil fuels are non-renewable resources and the current global proven crude oil

reserves are 1645.74 billion bbl (as shown in Figure 1). In other words, these might be exhausted in a foreseeable future (ca. 100-200 years).

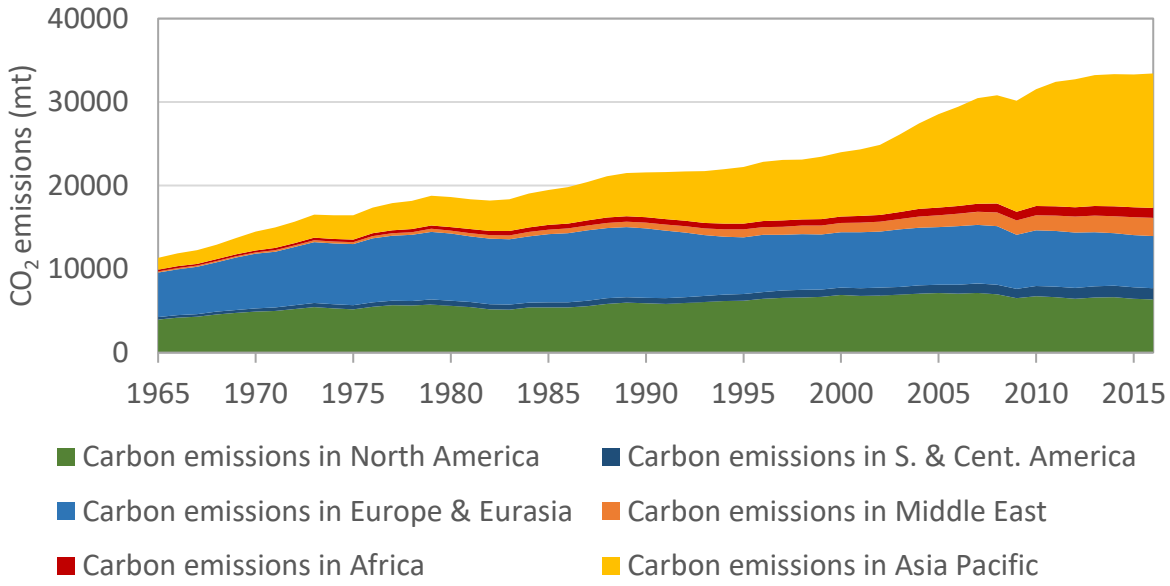

Figure 2. Regional CO_2 emissions from 1965 to 2016. Unit: million tonnes (mt). Data sources: BP Statistical Review of World Energy.[9]

Meanwhile, the massive use and burning of fossil fuels in the last century has contributed to enormous amount of CO_2 emissions into the atmosphere. The global CO_2 emissions are 33.4 billion tonnes (bt) in 2016, expected to increase to around 40.6 bt by 2040. As CO_2 is one of the main contributors to greenhouse gas (GHGs) emissions, the dramatic increase in CO_2 emissions is raising the potential of climate change, especially global warming. As shown in Figure 3, GHGs emissions of energy generated from fossil fuels are much higher than those from other sources. With the rising of public concern on global warming and environmental protection, various actions should be and are undertaking to control CO_2 emissions. In this regard, sustainable development goals (SDGs) were endorsed by the United Nations (UN in 2015, including affordable & clean energy (SDG 7) and climate action (SDG 13). Following the SDG 7 and SDG 13, the Paris Climate Agreement is targeting at dealing with greenhouse gas emissions mitigation, adaptation, and finance in respond to the trend of global warming. Though the announcement of US's withdrawal from the Paris Climate Agreement is bringing up uncertainty to the development of international environmental protection, the remaining countries and regions are still working closely to reduce

CO_2 emissions. For example, the EU's three-pronged energy policies (energy security, energy affordability, and sustainability) are targeting at reducing GHGs emissions by 20%, 40% and 80-95% of 1990 levels by 2020, 2030 and 2050 respectively, while increasing the share of renewables in its energy mix. According to the targets of China's Nationally Determined Contribution (NDC), a 64–70% reduction of GHGs emissions intensity below 2005 levels will be achieved by 2030 together with increasing share of non-fossil energy sources in the total primary energy supply to around 20%. Besides, India is also taking actions to fulfil such plan of reducing GHGs emissions intensity by 33-35% of 2005 levels by 2030. In general, these policies are aiming at reducing GHGs emissions by lowering share of fossil fuels while increasing those of renewables.

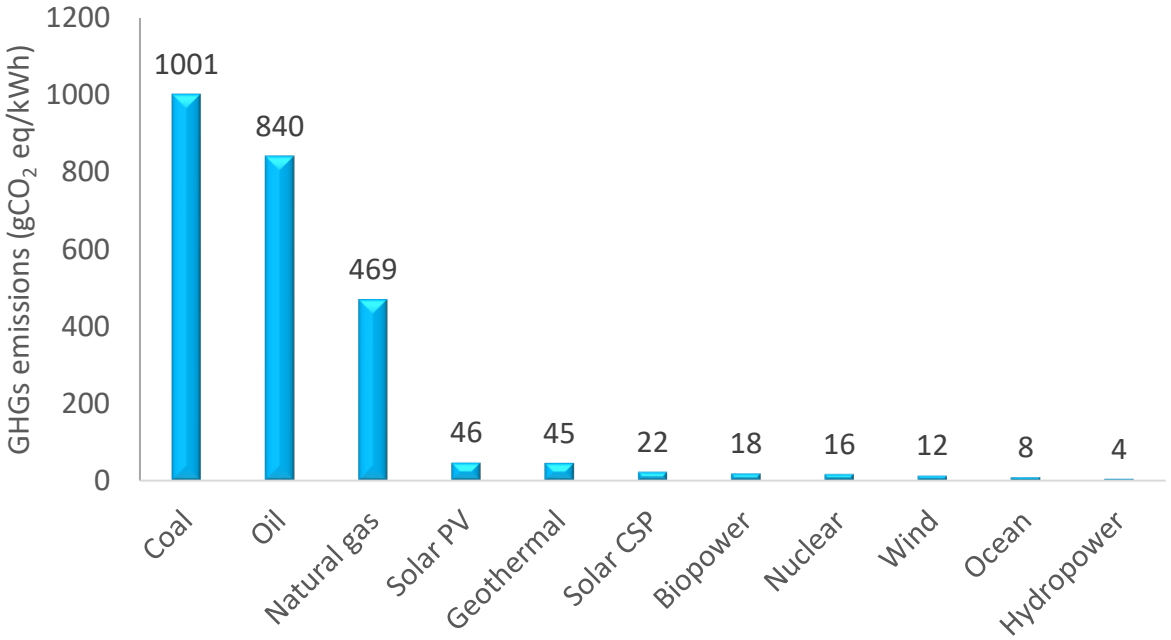

Figure 3. Lifecycle GHGs emissions from different electricity generation sources (within 50th percentile). Unit: $gCO_{2\ eq}$/kWh. [10]

The petroleum refinery based on limited reserves is encountering with the rising energy and material demand together with more strict legislations towards sustainable development. Therefore, there is strong necessity and urgency to develop sustainable alternatives to petroleum to secure energy and materials future supply. In this regard, biorefineries using renewable biomass resources can be considered as a perfect candidate that can provide biofuels for energy use, as well as various upstream materials for manufacturing industries.

1.1.2. The coming era of biorefinery

Biomass is inseparable to the human history so that human beings have been using biomass (such as woods, stalks, straws and animal manure) for energy purposes including cooking and heating. The traditional combustion of biomass is usually poorly efficient, while generating serious negative impacts on health and living conditions. Therefore, modern knowledge on chemistry and biology will benefit in more efficient and benign utilization of biomass, in the form of modern biorefinery.

Figure 4. Homo sapiens making fire by drilling wood.[11]

In the IEA Bioenergy Task 42, a thorough definition of biorefinery was introduced as "Biorefinery is the sustainable processing of biomass into a spectrum of marketable products (food, feed, materials, chemicals) and energy (fuels, power, heat)".[12] Unlike the broken cycle in petroleum refineries, biorefinery using biomass as carbon sources possesses an in principle closed carbon cycle (as shown in Figure 5). In detail, CO_2 generated from biorefinery using carbon-neutral biomass can gradually return to subsequent biomass regrowth under sunlight, while the CO_2 emitted from the petroleum refinery processes will mostly accumulate in the atmosphere, effectively off-setting the current carbon equilibrium because these carbon sources have been reserved for millions of years. Therefore, CO_2 emissions from fuels, chemicals and materials

produced with abundant and carbon-neutral renewable biomass can be in principle considered as reduced in comparison to CO_2 emissions from petroleum refineries.[13,14]

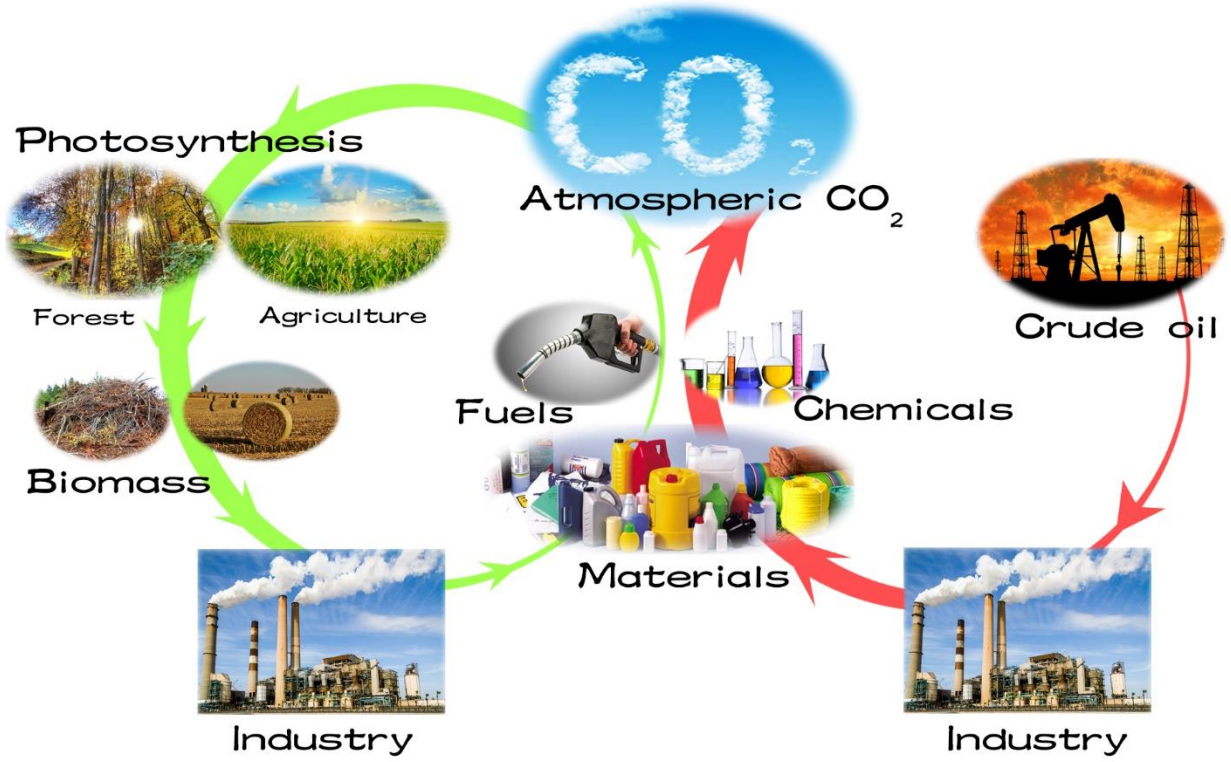

Figure 5. Comparison of carbon cycles between biorefinery and petroleum refinery

The biorefinery can be considered as an integrated unit with different technologies (i.e. extraction, biochemical, and thermochemical processes) that can transform biomass into useful value-added products such as fuels, chemicals and materials. An integrated, close-to-zero-waste biorefinery system was proposed, utilizing a sequential process of extractions and combination of biochemical and thermal processing steps together with internal recycle of energy and waste (Figure 6).[15]

As an analogue of petroleum refineries, integrated biorefineries utilizing renewable biomass as carbon sources can offer numerous alternatives in fuels, chemicals and materials to petroleum refineries, showing its great advantage in sustainability (in terms of feedstocks and low carbon emissions) and legislations. Therefore, the era of biorefinery is coming in a foreseeable future.

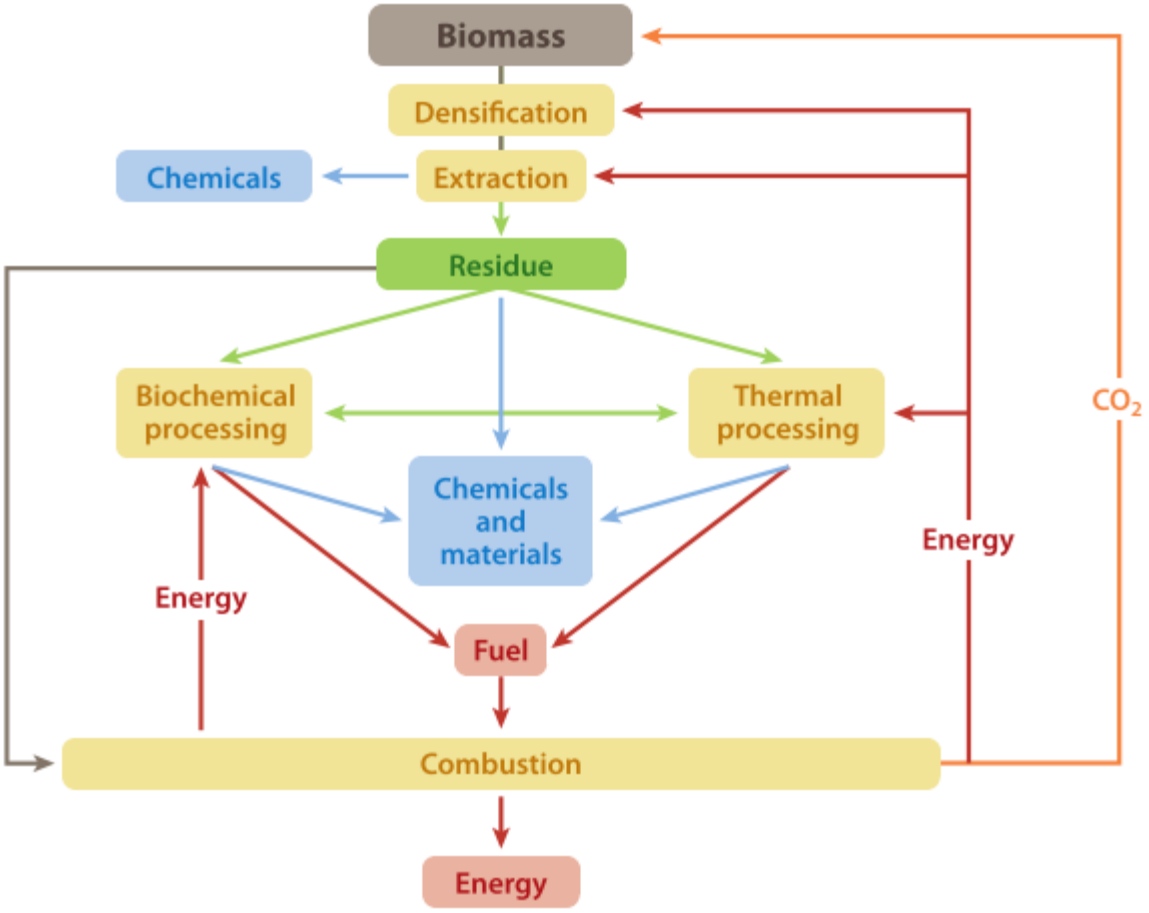

Figure 6. Integrated biorefinery system with internal energy and waste gases recycled[15]

1.1.3. Lignocellulosic biomass feedstocks for biorefineries

1.1.3.1. Opportunities for valorization of lignocellulosic biomass

There are mainly two sectors of feedstocks for biorefineries: dedicated feedstocks (dedicated crops, grasses, forestry, and aquaculture) and biomass (to be specific, biomass waste, including agricultural and agro-industrial waste, forestry residues, food waste and other organic residues).[16–40]

The current success of commercial biofuels is based on first-generation biofuel technologies: i) production of bioethanol via yeast fermentation of sugar and starch crops; ii) production of

biodiesel via chemical conversion of plant oils or animal fats.[15] Sugar crops (sugarcane and sugar beet) and starch crops (mainly corn and wheat) have been used as raw materials to produce bioethanol in quite large scale in European Union and countries such as USA and Brazil.[40–47] Besides, oil-based crops such as rapeseed and sunflower are also used to produce biodiesel in USA, Germany and other countries. [2,48,49,12] Indeed, first-generation biofuels can be alternatives to certain fuels from petroleum refining. However, these feedstocks compete with food/feed and demand huge amount of fertile land for growth that massive use of these feedstocks in biorefineries might result in an increase of feedstock prizes and food crisis. Therefore, first-generation of biofuels is limited by the unsustainable feedstock supply. Apart from crops, extensive use of grasses and forestry as raw materials may also destroy the ecology balance and damage the environment. Therefore, feedstocks from the first sectors can be used as raw materials in biorefineries, which might have passive effects to the human society or the environment.

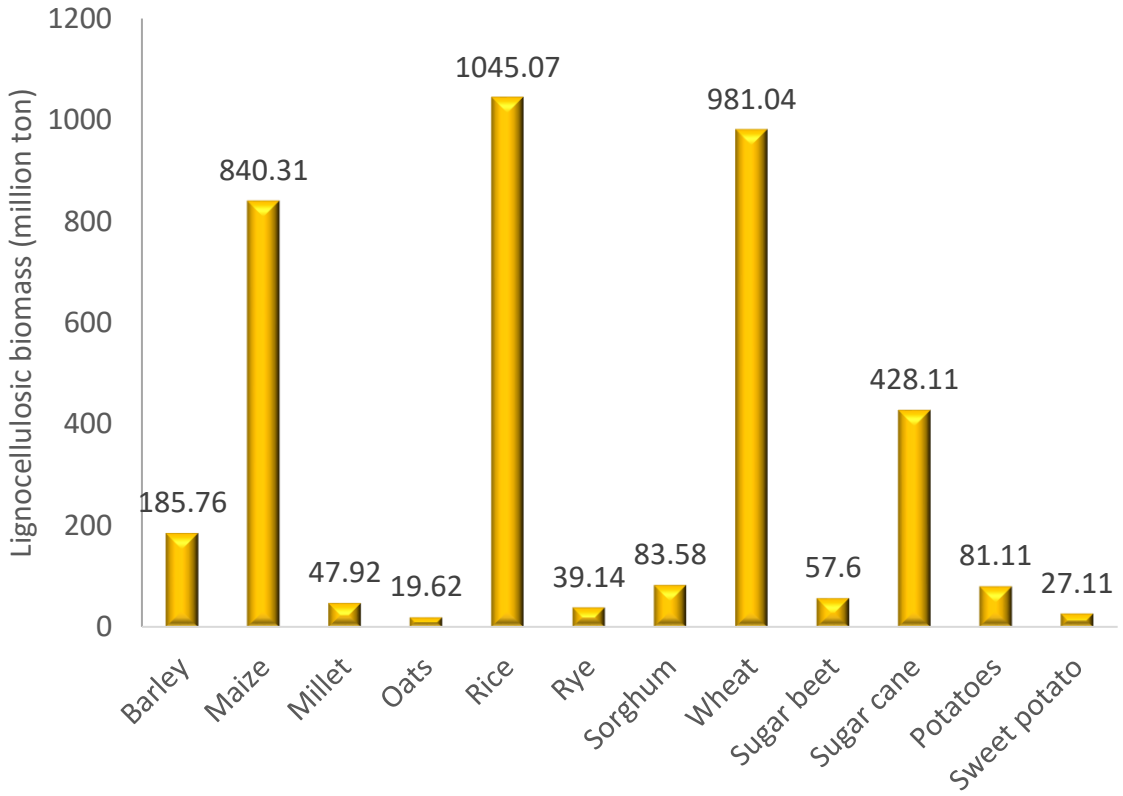

Figure 7. Annual estimate of world crop residue production in 2010[50]

In contrast, utilization of the largely available crop-derived and forest-derived lignocellulosic biomass can avoid the struggle of food versus fuel and partially meet demands for energy and materials.[22] As shown in Figure 7, the total annual world crop residues was estimated as 3836.37 million tons, mainly consisting of stalks and straws from maize, rice, wheat and sugarcane bagasse.[50] Moreover, the global quantity of economically and ecologically recoverable forest-derived biomass (logging residues, processing residues, and discarded wood-based products) is projected to be 1780 million dry metric tons by 2050.[51,52] Herein, great potential lies in the valorization of enormous amounts of lignocellulosic biomass for fuels and chemicals production.

1.1.3.2. Compositions of lignocellulosic biomass

Lignocellulosic biomass comprise of three main fractions, namely cellulose, hemicellulose and lignin (Figure 8), being a non-edible and renewable feedstock with significant potential for the sustainable production of valuable fuels and chemicals.[53,54]

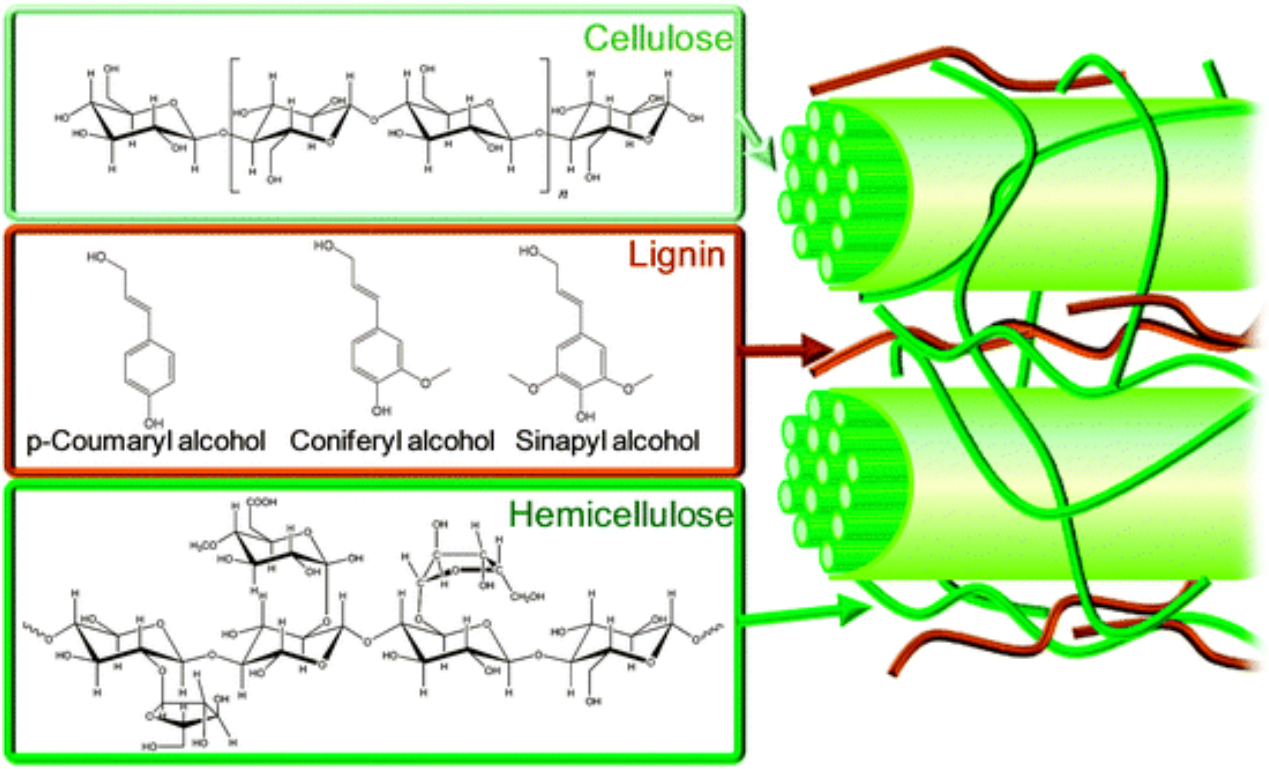

Figure 8. Cellulose, hemicellulose and lignin monomer species within the structure of lignocellulosic biomass.(adapted from[55])

Cellulose is a vital structural component of the primary cell wall of green plants and a crystalline homopolymer consisting of β (1 → 4) linked D-glucose units, which can be deconstructed into glucose monomers.[56] Unlike cellulose, hemicellulose comprises a mixture of C5 (mainly xylose) and C6 sugars, with a structure that varies in different lignocellulosic biomass.[57] Lignin is a complex cross-linked phenolic polymer composed of randomly branched phenylpropenoid building block units, with a different structure depending on the source.[58] The cellulose, hemicellulose and lignin compositions vary among different lignocellulosic biomass (Table 1).

Table 1. Compositions of different lignocellulosic biomass (adapted from[50])

Sources	Cellulose (%)	Hemicellulose (%)	Lignin (%)
Corn stover	31.0 (mf wt%)	43.0 (mf wt%)	13.0 (mf wt%)
Wheat straw	32.4 (mf wt%)	41.8 (mf wt%)	16.7 (mf wt%)
Cereal straws	35–40	26%	15-20
Poplar aspen	42.3 (mf wt%)	31.0 (mf wt%)	16.2 (mf wt%)
Rice straw	32.6	27.3	18.4
Baggase	65 (total carbohydrate)	-	18.4
Oil palm frond	49.8 (α)	83.5 (holocellulose)	20.5
Coconut	44.2 (α)	56.3 (holocellulose)	32.8
Pineapple leaf	73.4 (α)	80.5 (holocellulose)	10.5
Banana stem	63.9 (α)	65.2 (holocellulose)	18.6
Softwood	40–50	25–30	25-35
Hardwood	40–50	25–35	20-25
Big bluestem (whole plant)	29–37	21–25	17-24
Switchgrass (whole plant)	31–35	24–28	17-23
Jatropha waste	56.31	17.47	23.91

Considering the complex structures and various compositions of lignocellulosic sources, the development of integrated biorefinery processes is necessary for the effective transformation of lignocellulosic biomass to high value-added fuels, chemicals and materials. Integrated biorefinery

processes can be generally divided into two steps: i) decomposition of complicated lignocellulose structures into basic platform molecules; ii) sequential upgrading platform molecules to high value-added products (fuels, chemicals and materials).

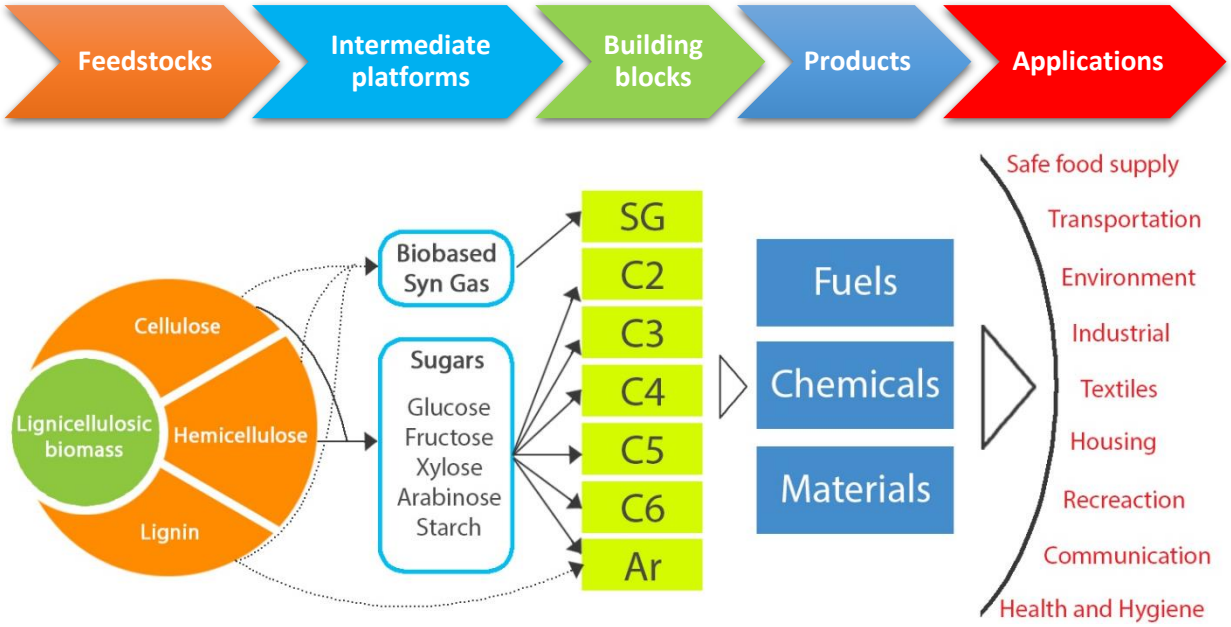

Figure 9. Flowchart of biobased products derived lignocellulosic biomass feedstocks. SG: syngas; Ar: aromatics

1.1.3.3. Promising platform molecules for upgrading

Extensive research efforts have been carried out aiming to deconstruct complex lignocellulosic feedstocks via biological, biochemical or thermochemical methods, obtaining prospective platform molecules (saccharides, polyols and alcohols, furans and acids).[59–67] For example, complete transformation of lignocellulosic biomass was achieved by utilizing integrated systems with catalyst recycling, obtaining aromatic monomers and aliphatic alcohols which can be further converted into valuable chemicals and fuels.[54]

Among various biomass derived platform molecules, furfural is a promising chemical for biofuels and chemicals production, which can be obtained from the hydrolysis and subsequent dehydration of hemicellulose-derived xylose. In the report from U.S. Department of Energy, furfural was selected as one of the top 30 biomass derived potential platform chemicals.[68]

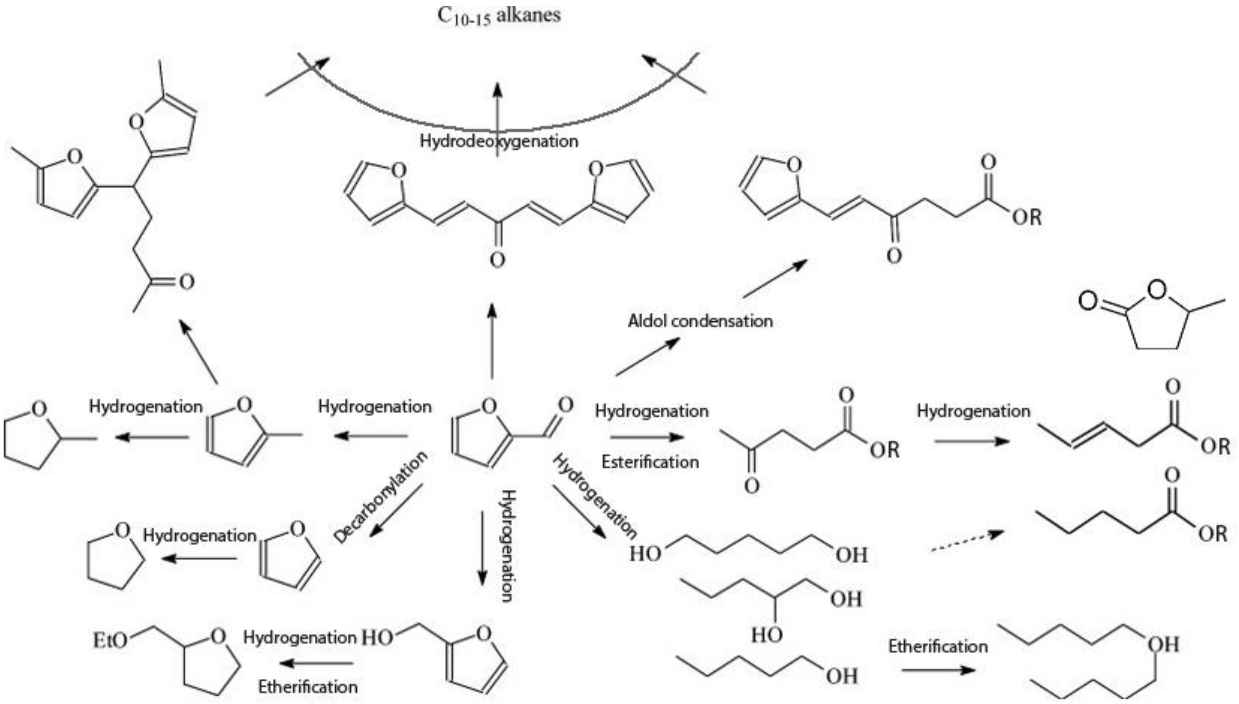

Figure 10. Furfural derived valuable chemicals and fuels (adapted from [69])

The most versatile pathway for upgrading furanic components is hydrogenation.[69] By controlling the degree of hydrogenation, various furfural derivatives can be obtained, such as furfuryl alcohol (FA), tetrahydrofurfuryl alcohol (THFA), 2-methyl furan (MF), 2-methyl tetrahydrofuran (MTHF) or further hydrogenation of the furan ring and its opening to alcohols, diols and, eventually, alkanes (Figure 11).[69–72] In this regard, around 60–70% of the global furfural production is transformed into FA, which can be further upgrade to alkyl levulinates via alcoholysis or direct hydrogenation of the furan ring to THFA. [73–81] Furthermore, alkyl levulinates can be subsequently converted to γ-valerolactone (GVL) by hydrogenation which has wide applications as solvent, fuel additive and liquid fuel, as well as precursor for valuable chemicals (e.g., olefins, polymers, 5-nanonone).[82–85] Though GVL can also be obtained by hydrogenation of levulinic acid, there are some limitations that should be taken into consideration for practical applications. Production of levulinic acid is usually conducted in acidic aqueous media in practical applications, which raises costs and difficulties for mineral acid recovery and separation of levulinic acid because of its high polarity and boiling point.[86–88] Therefore, the use of acid-free alkyl levulinates produced by alcoholysis of various carbohydrates for the production of GVL may be advantageous.

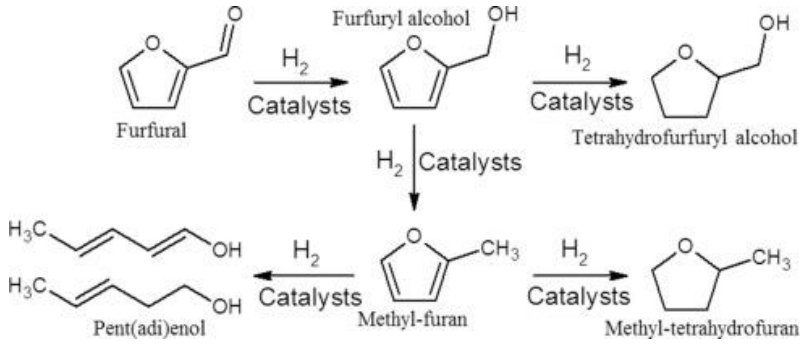

Figure 11. Reaction pathways in the catalytic hydrogenation of furfural[70]

As one of the main fractions of lignocellulosic biomass, lignin also provides great opportunities in valorization to useful products. Due to the complexity and great difference of lignin structures among various biomass sources, it is difficult to valorize lignin directly while depolymerization of lignin is necessary for downstream processes. The depolymerization of lignin targets low molecular weight mono- or oligomers, for which various methods (physical, chemical, and biological treatment) can be considered as pretreatment for breaking down the lignin structure.[89–95] The dominant chemical structures should be well identified after pretreatment to set up applicable industrial processes because the drastic change of lignin structure during the industrial extraction and isolation processes.[96] TiO_2 doped with rare earth or non-metallic elements (sulfur and boron) were found to be highly efficient in the degradation of lignin.[97,98] Photocatalytic depolymerization of lignin in rice husk was performed by Lu *et al.* using TiO_2 under UV irradiation, obtaining complex product mixtures including alkanes, alkenes, arenes, alkanols, alkenols, phenols, benzyl aldehyde, ketones, carbocyclic acids, alkanoates, phthalates, and nitrogen-, sulfur- and oxygen-containing organic compounds.[99] However, direct upgrading of lignin remains challenging because of the difficulty in the separation of the complex structure of lignin and extensive studies have been conducted on simpler model compounds that represent essential unit structures present in lignin.[100,101]

Among transformations of various lignin model molecules, the selective photocatalytic oxidation of benzyl alcohol to benzaldehyde is particularly attractive and has been intensively investigated.[102] Apart from providing potential reactivity and transformation strategies for the valorization of lignin compounds, the selective conversion of alcohols to the corresponding carbonyl compounds is of vital importance in organic chemistry. In addition, benzaldehyde is the

second most important aromatic molecule and has wide applications in various industrial sectors (cosmetic, food, pharmaceutical, and perfumery). Traditional routes for benzaldehyde production are either toluene chlorination or toluene oxidation, involving the use of toxic compounds (chromate, hypochlorite, peroxy acids, and other chemicals) while the photocatalytic selective oxidation of benzyl alcohol to generate benzaldehyde can provide a promising alternative protocol.[103] The mechanism for the photocatalytic oxidation of benzyl alcohol with TiO_2 was reported by Higashimoto et al. A strong interaction between the OH groups on the TiO_2 surface and benzyl alcohol (phenyl ring and alcohol group) forms a surface complex, enhancing the visible light absorption by ligand to metal charge transfer (Figure 12).[104]

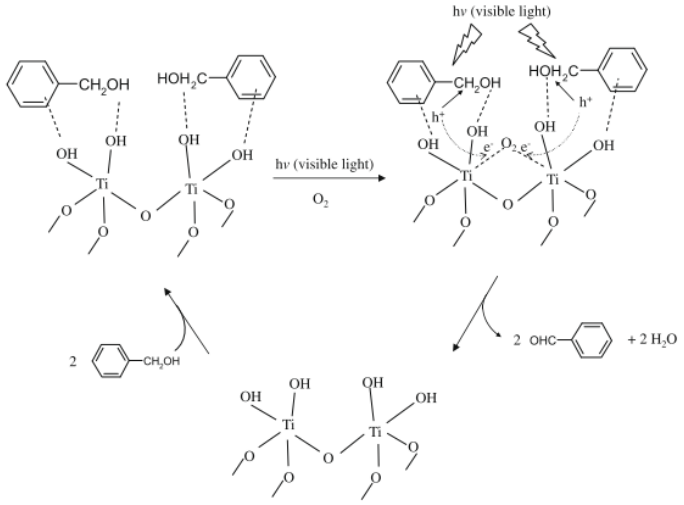

Figure 12. Proposed reaction mechanism for the selective photocatalytic oxidation of benzyl alcohol with molecule O_2 on TiO_2 surface under visible light irradiation (adapted from [104])

In general, a remarkable potential lies in valorization of platform molecules derived from abundant lignocellulosic biomass. It will be the next milestone in sustainability development if biomass valorization partners with modern technologies for the highly efficient production of fuels, chemicals and materials.

1.2. Modern technologies for biomass valorization

1.2.1. From batch to flow chemistry

Flow chemistry can partner ideally with green chemistry towards sustainability.[5] Continuous flow reactors have been applied in manufacture industries for over a century. With remarkable advances in microfabrication technology, flow chemistry and microreactors that involve chemical engineering, organic synthesis and green chemistry have received increasing attention as fascinating topics. Advances in flow chemistry led to significant improvement in safety, reduced energy consumption and expansion of reaction conditions.

In the flow process, reactants are introduced continuously into the reaction system where they react in contact with the catalytic active species with better defined temperature and flow fields, and subsequently leave the reaction space. The process variables (temperature, pressure, etc.) are better controlled in flow processes. Flow chemistry are significantly advantageous in different aspects listed below:[105,106]

1) Well-controlled mixing (micromixing) and extremely large surface-to-volume ratios
2) Well-controlled heat exchange and enhanced mass transfer
3) Increased multiphase interactions
4) Improved reaction selectivity and increased reproducibility
5) Multistep reaction sequences
6) Increased safety of operation
7) Possibility to use immobilized catalysts
8) Improved irradiation of the reaction mixture (photochemistry)
9) Increased electrode surface-to-reactor volume ratio (electrochemistry)
10) Increased capacity to run serial reactions.

The H-Cube is an emerging commercial continuous flow reactor from ThalesNano (Hungary) with real-time high-pressure hydrogenator based on water electrolysis, allowing the possibility to perform various hydrogenation reactions, including hydrogenation of various biomass derived platform molecules (levulinic acid, furfural, etc.).[106–111] Recently, Bottecchia et al. reported visible-light-induced photocatalytic aerobic oxidation of thiols to disulfides in a continuous-flow TiO_2 packed-bed reactor, achieving significant improvements in efficiency and yield of

disulfides.[112] g-C_3N_4 photocatalyzed radical cyclization in continuous flow using THF as electron and hydrogen donor was reported by Woźnica et al., which conversion >99% and selectivity >80% in most of the cases. The application of flow processes significantly improves the selectivity and drastically reduces reaction time.

There are also some challenges in use of flow reactors such as managing solids in flow, integration of reactor components (pumps, reactors, back- pressure regulators), and integration of new features (in-line monitoring and purification).[106] Regardless these limitations, flow chemistry is still a promising tool in green chemistry, that benefits in minimization of time and waste, optimization of time screening, high energy and cost efficiency, potential improvements in scale-up and improvement in safety.

1.2.2. Rising of TiO_2 based heterogeneous photocatalysis

According to the definition by IUPAC, photocatalysis is alteration of rate or initiation of a chemical reaction in presence of photocatalyst that absorbs ultraviolet, visible or infrared radiation and contributes to the chemical transformation of the reaction partners.[113] The idea of exploiting the solar energy is not novel concept as originally proposed by Ciamician in 1912.[114] However, it was not commonly used as a generally accepted term, photocatalysis, before the report by Fujishima and Honda in 1972 that utilized TiO_2 electrodes for water photolysis.[6]

Photocatalysis that can utilize abundant and inexpensive solar energy for chemical transformation is considered as one promising, sustainable, nonhazardous and economically feasible technology. Various heterogeneous photocatalysts have been extensively investigated, such as metal oxides nanoparticles, metal dichalcogenides, composite nanomaterials, metal organic frameworks, graphitic carbon nitride, etc.[115–127] Among these photocatalysts, TiO_2 materials have been intensively investigated and shown great potential as ideal and powerful photocatalysts for various chemical reactions due to their photocatalytic activity, high thermal and chemical stability, low cost, and non-toxicity.

TiO_2 is a type of semiconductor material with electrical conductivity between conductor and insulator. In semiconductor materials, the conduction band (CB) is formed by the interaction of the lowest unoccupied molecular orbital (LUMO), whereas the valence band (VB) of a

semiconductor is formed by the interaction of the highest occupied molecular orbital (HOMO), while the energy range between CB and VB is called forbidden bandgap (bandgap or energy gap), denoted as E_g. The light absorption property and redox capability of a semiconductor photocatalyst is determined by the band structure (bandgap and the locations of CB &VB).

A general photocatalytic process in a semiconductor material is illustrated in Figure 13, in which electrons are excited from VB to CB upon absorption of photons with energy no less than E_g, leaving the positive charge holes in VB. The electron excitation process of TiO_2 can be expressed as: $TiO_2 + h\nu \rightarrow e^-(TiO_2) + h^+(TiO_2)$. There are three possible pathways for photogenerated electron-hole pairs: (1) migration to the TiO_2 surface and subsequent participation in the photo-redox reaction; (2) trapping by the defective sites in the TiO_2 structure; (3) recombination and energy releasing in the form of either heat or photon. Only the first pathway is effectively contributing to the photocatalytic process, while the other two are generally considered as deactivation processes.

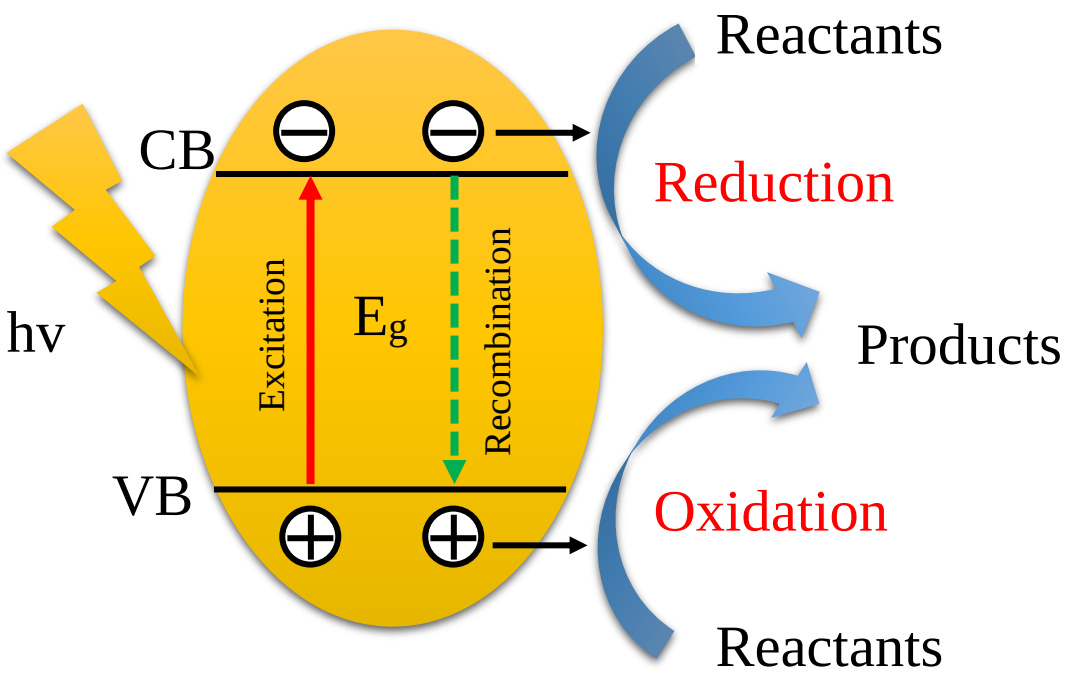

Figure 13. Schematic illustration of a typical photocatalytic process on semiconductor photocatalysts

The phase structure has significant impact of the physical/chemical properties of TiO_2 materials, especially on photocatalytic performance. There are main four polymorphs for TiO_2: anatase, brookite, rutile and TiO_2(B), comprising TiO_2 octahedra with different unit distortions and edge/corner sharing manners (Figure 14).[128] The difference in lattice structures cause the difference in density and electronic band structure that lead to different bandgaps. The bandgaps of bulk TiO_2 are 3.20, 2.96 and 3.02 eV for anatase, brookite, rutile phase respectively, which results in the different photocatalytic performances. Rutile is the most thermal stable phase, while the other three are metastable ones. Among the four polymorphs, anatase and rutile are the most frequently investigated photocatalysts.

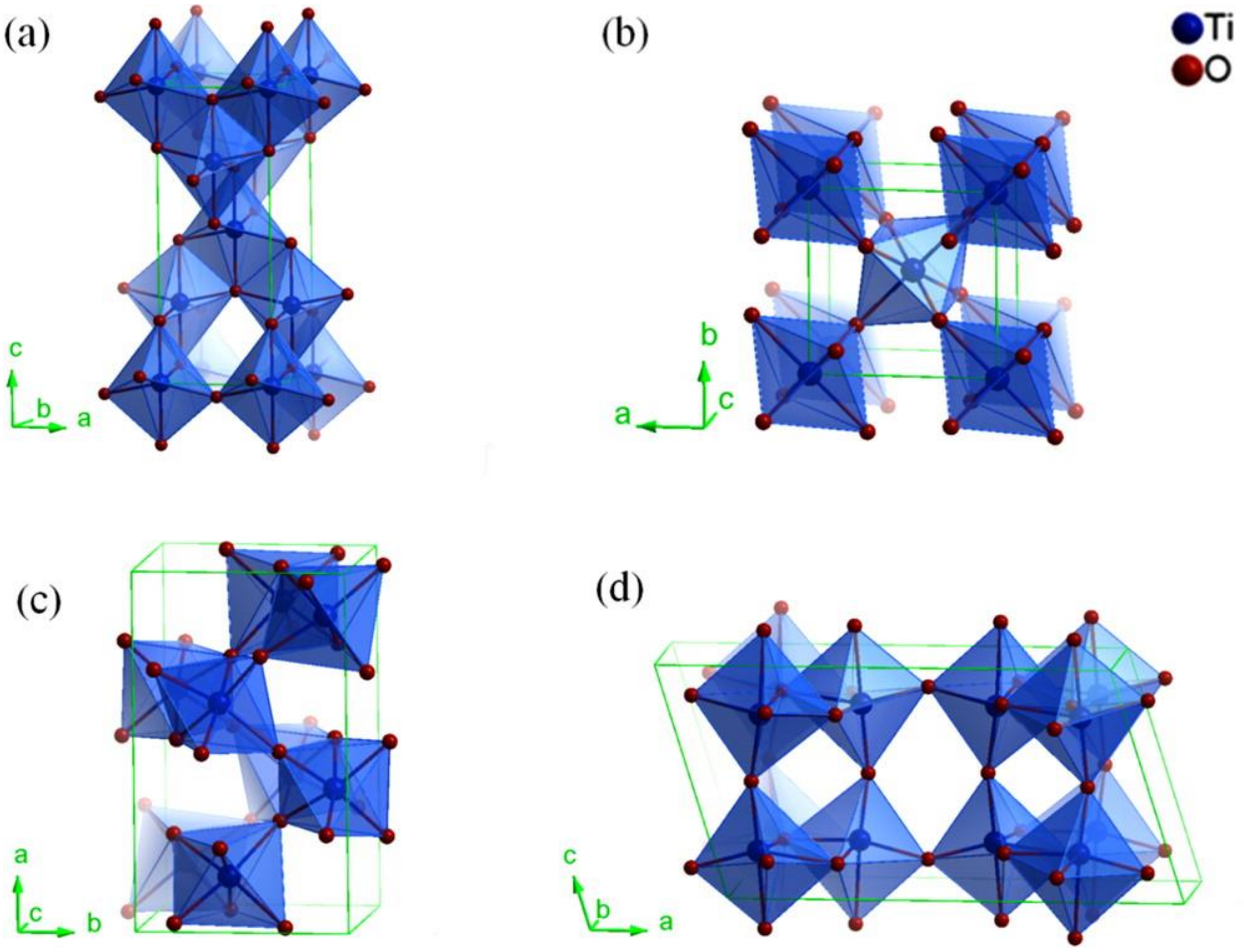

Figure 14. Crystalline structures of TiO_2 in different phases: (a) anatase, (b) rutile, (c) brookite, and (d) TiO_2(B). (Adapted from [128])

Though the range of light absorption of rutile are slightly more than that of anatase, anatase is still advantageous in several aspects that benefit for its photocatalytic performance: slightly higher redox driving force, higher surface area for enhancement in absorption capability and number of active sites, more efficient charge separation resulted from prolific oxygen vacancies. Therefore, anatase usually exhibits higher photocatalytic activity than rutile.

Since photocatalytic processes are initiated by light absorption and utilize the photogenerated electron-hole pairs for the redox reaction, the number and energy of photons absorbed by the photocatalyst have strong influence on the photocatalytic activity. The main drawback of anatase is the large bandgap, 3.2 eV, which means only UV light ($\lambda < 387$ nm) can be used for the electron excitation, limiting its utilization of the abundant solar light, especially visible light irradiation. Moreover, the photocatalytic activity of TiO_2 is also restricted by the fast recombination of photogenerated charge carriers. Therefore, it is necessary to expand the absorption capability of TiO_2 and delay the rate of recombination of electron-hole pairs to improve its photocatalytic activity from the fundamental point of view.

1.2.2.1. Visible Light-Responsive TiO_2

Enormous research efforts have been devoted to inducing visible light activity to TiO_2 that endow its activation for photocatalytic reaction by visible light, mainly by the following efficient strategies: (1) introduction of dopants into the TiO_2 matrix to narrow its bandgap; (2) surface sensitization with visible light materials as light harvesters.

Heteroatom doping. O 2p orbitals are dominant in VB of TiO_2, while Ti 3d, 4s, 4p orbitals contribute to the vacant CB of TiO_2 which lower position is decided by Ti 3d orbitals.[129,130] With the incorporation of cation dopants into the TiO_2 matrix, an impurity energy level could be introduced into the bandgap, which can act as either electron donor or acceptor, endowing visible light absorption capability to TiO_2.[131,132] TiO_2 doped with various cations (e.g. Cu^{2+}, Fe^{3+}, Nb^{5+}, Ni^{2+}, etc.) exhibited a significant enhancement in visible light absorption, responsible for the improvement in photocatalytic activity.[133–137] However, cation doping might cause structural instability, for which anion doping may be an alternatively interesting approach to enhanced the light absorption capability of TiO_2.[137] Rather than modifying the CB of TiO_2, narrowing the

bandgap of TiO_2 is achieved by reconstruction of the VB by shifting it upwards replacing O in TiO_2 crystals with various anions such as C, N, S, P, etc.[137–141] Likewise, the improvement in the light absorption of TiO_2 by anion doping also promotes the photocatalytic activity of TiO_2. Interestingly, Pal *et al.* reported decreasing photocatalytic activity in hydrogen production over TiO_2 doped with various anions in the following order: C-TiO_2 >S-TiO_2>N-TiO_2.[142]

Surface sensitization. Apart from introduction of dopants into the TiO_2 lattice, dye sensitization is another option for an extension of TiO_2 visible light absorption. The proposed mechanism for general photocatalytic process on dye-sensitized semiconductors is illustrated in Figure 15. In detail, the dye molecules are firstly absorbed onto the surface semiconductor as sensitizer. Upon visible light irradiation, the dye molecules are excited and generate electrons that are transferred to the CB of semiconductor. Reduction-half reaction and oxidation-half reaction occur separately in the dye-sensitized semiconductor system: reduction-half reaction takes place on the surface of semiconductor (reception of electrons in CB); while the sacrificial agent is oxidized during the regeneration of the excited dye molecules. Various dyes have been employed to sensitize TiO_2 such as Rhodamine B, Alizarin Red and Eosin Y and obtaining greatly improved photocatalytic activity, among which Eosin Y exhibits excellent light absorption ability and relatively high stability.[143–148]

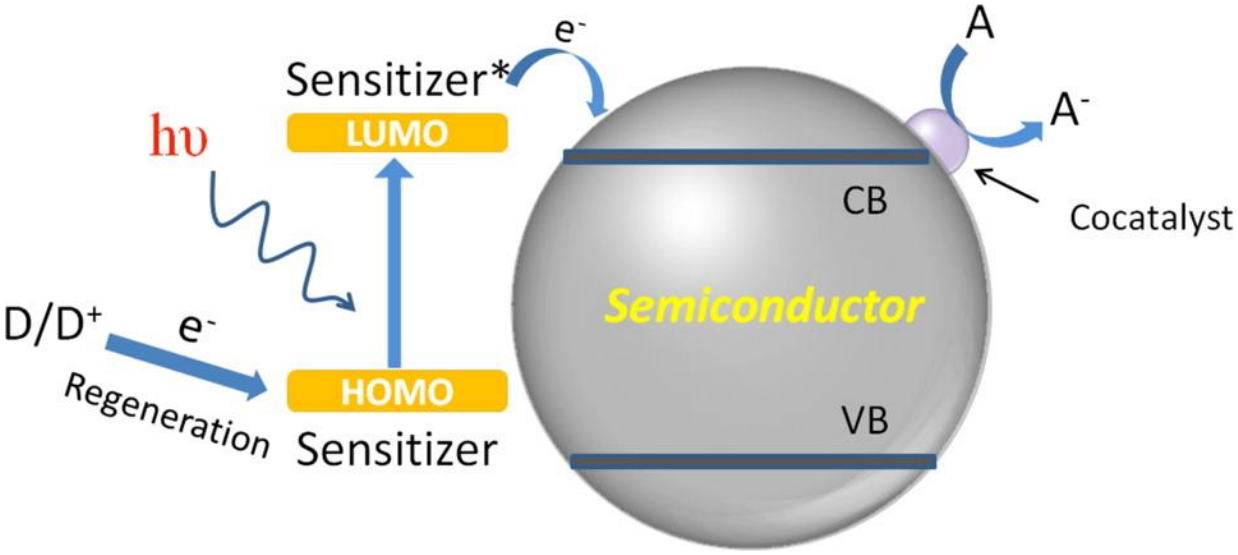

Figure 15. Schematic illustration of mechanism for general photocatalytic process on dye-sensitized semiconductor (adapted from [128])

1.2.2.2. Heterojunction TiO_2

The photogenerated charge carriers are either separated or recombined during transportation to the catalytic active sites on TiO_2 surface, while the effective charge separation is a crucial factor to secure the quantum efficiency. In this regard, creating heterojunctions between TiO_2 with other materials, mainly semiconductors, can promote the photocatalytic activity due to the extension of light absorption, increase of surface area and active site density and enhance spatial separation of the photogenerated charge carriers.

Heterojunction is defined as the interface between two different semiconductor materials with different band structure, causing energy band alignment, which can facilitate spatial separation of electron-hole pairs via migration of electron/hole between the semiconductors across the heterojunction.[149–151] Typically, there are three types of conventional heterojunctions photocatalysts (type I, II and III) which are illustrated in Figure 16.[152]

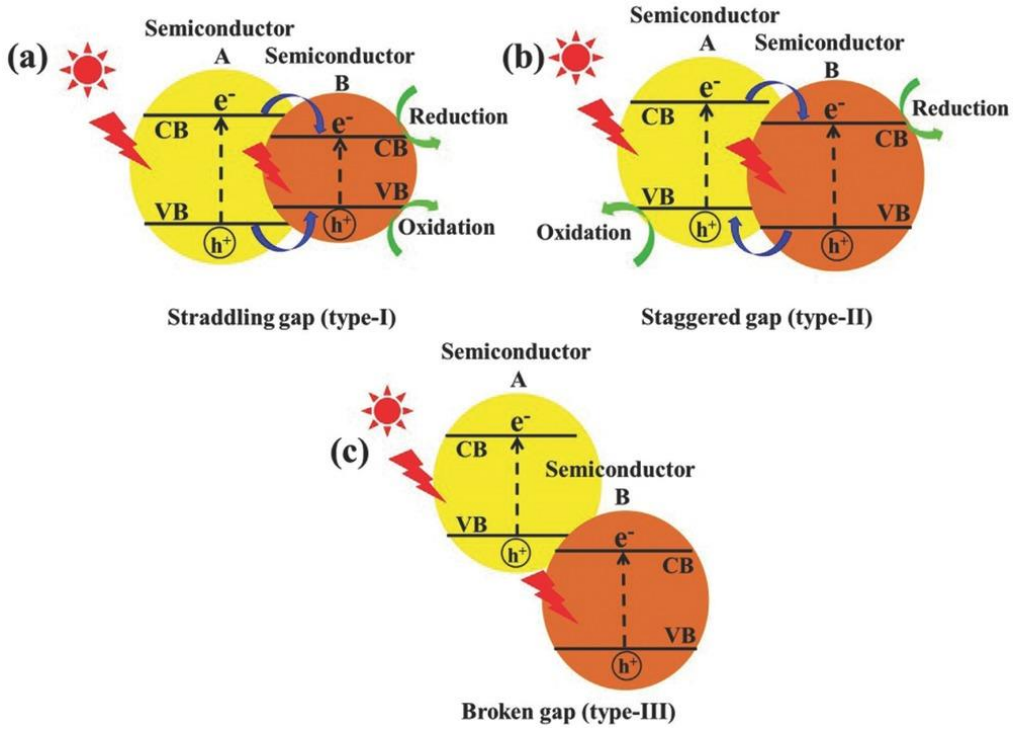

Figure 16. Schematic illustration of band structures and separation of charge carriers in three types of conventional heterojunction photocatalysts: a) type-I, b) type-II, and c) type-III heterojunctions (adapted from [152])

Type II heterojunction photocatalysts are the only one with effective spatial separation of charge carriers among conventional ones for which both electrons and holes accumulate on the same semiconductor (type I heterojunction photocatalysts), while electron-hole cannot migrate between the two semiconductors in type III heterojunction photocatalysts due to the staggered gap. For example, TiO_2/g-C_3N_4 is a typical type II heterojunction photocatalyst, which showed strong visible light absorption and great improvement in photocatalytic activity due to the presence of heterojunctions between TiO_2 and g-C_3N_4.[153–155] α-Fe_2O_3 is a visible light responsive *n*-type semiconductor, type II heterojunctions can be constructed in α-Fe_2O_3-TiO_2 heterostructured photocatalysts with strong visible light response and enhancement in photocatalytic performance, benefiting from the promoted light absorption and electron-hole pair separation.[156,157]

Due to the excellent electron conductivity of carbon materials, TiO_2/carbon material heterostructures have received increasing attention as photocatalysts. With the presence of sp^2-hybridized orbitals, carbon materials usually exhibit high electron conductivity, facilitating the charge transfer and inhibit the recombination of electron-hole pairs when coupled with TiO_2-based photocatalysts.[158–160]

1.2.2.3. TiO_2 based photocatalytic transformation of lignocellulose-based molecules

As discussed in previous sections, there is great potential in transforming lignocellulosic biomass derived molecules to valuable fuels, chemicals and materials. Due to the recent advances in photocatalysis, photocatalytic hydrogen production by reforming lignocellulosic biomass derived molecules and photocatalytic selective oxidation of platform molecules have attracted intensive attention and may be a promising alternative to conventional thermochemical biomass conversion processes. As compared to photocatalytic water-splitting, hydrogen production by photocatalytic reforming lignocellulosic biomass derived molecules maybe more viable and practical because it may be more efficient,[161] with these molecules potentially acting as sacrificial agents to delay the recombination rate of electron-hole pairs.[101] Meanwhile, photocatalysis also shows its advantages in transforming lignocellulosic biomass derived platform molecules such as alcohols, polyols and sugars, with high efficiency and selectivity.

Mesoporous carbon templated synthesized TiO_2 exhibited remarkable high photocatalytic generation rate in hydrogen production (188 μmol h^{-1}) under methanol reforming conditions, which can be attributed to the Ti^{3+} generated by hydrogen treatment.[162] Fontelles-Carceller *et al.* reported a highly efficient hydrogen production by photocatalytic reforming of the sacrificial agent, methanol, using Pt promoted TiO_2 photocatalysts.[163,164] Other biomass derived substrates can also be employed in hydrogen production via photoreforming such as alcohols (e.g. ethanol, glycol and polyols), aldehydes (e.g. formaldehyde, acetaldehyde), carboxylic acids (e.g. formic acid, acetic acid, lactic acid) and saccharides.[117] Sonication-assisted nanostructured synthesized TiO_2 was reported by Colmenares *et al.*, which showed higher selectivity towards glucaric acid, gluconic acid and arabitol in te selective photo-oxidation of glucose as compared to commercial TiO_2 P25.[165] Monolayer titanate nanosheets were reported to be active in selective oxidation of furfuryl alcohol to furfural under visible light irradiation with selectivity over 99%, in which the surface unsaturated Ti atoms can serve as Lewis acid sites that adsorb furfuryl alcohol forming surface coordination species.[166]

Due to the complex structure of lignocellulose, especially lignin, direct photocatalytic transformation of lignocellulosic feedstocks remains highly challenging, while aromatic alcohols have been used as model lignin compounds in relevant research. Among various alcohol oxidation processes, selective transformation of benzyl alcohol to benzaldehyde is particularly attractive because of the wide applications of the latter in cosmetics, flavor and perfumery industries. Anatase TiO_2 was employed in the systematic investigation of selective photo-oxidation of benzyl alcohol and derivatives to aldehydes under visible light irradiation.[104,167,168] The featured visible light induced photocatalytic activity could be ascribed to the formation of surface complex species by adsorption of aromatic alcohols which reacted with the OH group on the TiO_2 surface to form Ti–O–Ph species. In this regard, Kim *et al.* proposed a direct electron transfer from the surface complexes to CB of TiO_2 under visible light irradiation.[169] Fe^{3+}/TiO_2/zeolite Y composite photocatalyst prepared by sonophotodeposition exhibited outstanding performance in the oxidation of benzyl alcohol, in which the presence of a hematite phase promoted the photocatalytic efficiency.[170]

Photocatalytic selective transformation of lignocellulosic biomass to important chemicals and valuable products by utilizing the abundant solar light energy at room temperature and atmospheric

pressure is a highly innovative approach which can have several benefits from energy and environmental viewpoints. Several highly selective photocatalysts have been reported in related research. However, improving the conversion of substrates remains challenging and is of vital importance to boost up the process efficiency to make the photocatalytic valorization process more economically feasible. Therefore, the development of efficient photocatalysts together with system integration by coupling to scale-up facilities (e.g. solar plants) able to provide continuous flow equipment and large reactors is the main challenge to address in future years.

1.3. Nanocomposite materials as heterogeneous catalysts

Catalytic processes are of vital importance that account for >90% of the chemical manufacturing processes, where catalysts play essential roles in controlling reaction rates, conversion and product selectivity. Heterogeneous catalysis involves catalyst with phase differs from that of reactants, and heterogeneous catalysts are solids in most of the practical processes. As compared to homogeneous catalysis, the advantages of heterogeneous catalysis have been well-described in textbooks such as reusability, easy catalyst-reactant/product separation, low catalyst-originated product contamination, etc.

In typical heterogeneous catalytic reactions, reactants and products are transferred to and from the catalyst surface where the reaction takes place, which can be divided into the following elementary steps:[171]

1. Diffusion of reactants from the bulk fluid to the external catalyst surface
2. Intra-particle diffusion of reactants within the catalyst pores
3. Absorption of reactants onto the catalytic active sites
4. Reaction on the catalyst surface
5. Desorption of products from the catalyst surface
6. Intra-particle diffusion of products from the catalyst pores to external catalyst surface
7. Diffusion of products from the catalyst surface to bulk fluid

Apart from the intrinsic physical and chemical properties, the catalytic performance of heterogeneous catalysts is highly dependent on their structure. With the development of nanoscience or nanotechnology, nanoparticles are regarded as great progress to achieve miniaturization and nanoscaling effects and properties, which can potentially function as highly catalytic active sites for chemical processes. Improvement of the catalytic activity and selectivity of nanoparticles can be achieved by manipulating their size, shape and dispersity.[172] Single component heterogeneous catalysts have been reported to have good performance in chemical transformations including metals, metal oxides, zeolites and metal organic frameworks.[173–179]

Direct application of nanoparticles in catalysis may offer excellent performance, but there is difficulty in the recycle of the fine particles. Immobilization and stabilization nanoparticles on various materials/supports to create multicomponent composites is a promising alternative that can achieve better catalytic performance with enhanced activity and selectivity and reduced passive environmental side effects. The recent emerging metal organic frameworks are also promising as heterogeneous catalysts, featuring highly porous structures with massive nanochannels that can potentially provide more catalytic active sites and therefore facilitate the interaction between reactants and catalysts, improving the catalytic performance.

Heterogeneous bicomponent or multicomponent composite catalysts are generally composed of at least one catalytically active component and a functional support, having attracted intensive attention in recent years. Nanoparticles, particularly metal nanoparticles, are typical highly active centers for catalytic reactions but not thermodynamic stable due to their small sizes that haave associated large surface energy. Several methods have been carried out to stabilize the nanoparticles, for example, addition of organic ligands or inorganic capping agents.[172] Interestingly, the stabilization of nanoparticles on porous supports can effectively stabilize nanoparticles while maintaining their excellent catalytic performance, creating highly catalytic active nanocomposite materials. In addition, the interaction between the catalytic active species and the support materials can potentially reinforce the catalytic properties of the nanocomposite materials, such as remarkable improvements in activity, product selectivity and/or chemical stability. This interaction is denoted as synergetic catalytic effect, defined as a certain kind of cooperation between different components and/or active sites within one catalyst with consequence of significant or striking enhancement of catalytic performances superior to the arithmetic sum of those by the corresponding individual components. The synergetic catalytic effect makes catalysts supports highly relevant in heterogeneous composite catalysts, more than just simple carriers for catalytic active species. For example, titania nanoparticles can improve both the light absorption capability and charge separation by dispersion/deposition onto porous support materials such as carbons,[159,180–182] iron oxides,[157,183–185] g-C_3N_4,[152,154,155,186] CeO_2,[187] etc.

1.3.1 Carbon based nanocomposites

Carbon materials with various properties play an important role in heterogeneous catalysis as catalysts or catalyst supports. Applications of carbon materials as catalyst supports have been extensively investigated. Common used carbon materials are activated carbon,[188] carbon nanotubes (CNTs),[181,182] carbon fiber[160] and graphene,[189–191] which have been employed as supports for the synthesis of carbon-based titania composite materials to increase the photocatalytic efficiency.

Activated carbon is the most frequent used carbonaceous material in heterogeneous catalysis due to its excellent physical and chemical properties. The high surface area, highly porous structure and surface chemical properties are of vital importance for both the dispersion of the active phases and the absorption of organic compounds on its surface. In addition, surface functional groups with heteroatoms (O, N, H) can provide acid/basic sites and a hydrophilic character for the composite catalysts, favoring the chemisorption of the reactants, while they can also interact with the catalytically active components. Apart from activated carbon, graphene, a sp^2-hybridized 2D carbon nanosheet, featuring high surface area and excellent mechanical properties with high mobility of charge carriers has been a more recent alternative choice.[192,193] Due to its excellent properties, it is considered as a promising material and its composites with TiO_2 as photocatalysts have also recently received increasing attention.[158,194] Carbon Nanotubes (CNTs) can be viewed as graphene derived materials by rolling 2D graphene into 1D nanotubes, which retain several electronic properties and may also exhibit metallic conductivity, along with large electron storage capacity, implying the possibility in reception of photon-excited electrons from nanocomposites with TiO_2.[193,195]

Two mechanisms have been proposed to explain the improvement of photocatalytic properties of CNTs-TiO_2 composites.[196] Upon photo-excitation, an electron is excited from the VB to the CB of TiO_2 and subsequently transferred to CNTs, with the positive charge hole remaining on TiO_2 to take part in redox reactions (Figure 17 left). In contrast, CNTs act as sensitizers and transfer electrons to TiO_2 so that the photogenerated electron is injected from CNTs to the conduction band of TiO_2, while the positively charge CTNs remove one electron from the valence band of TiO_2, transferring a hole to TiO_2 for redox reactions (Figure 17 right).

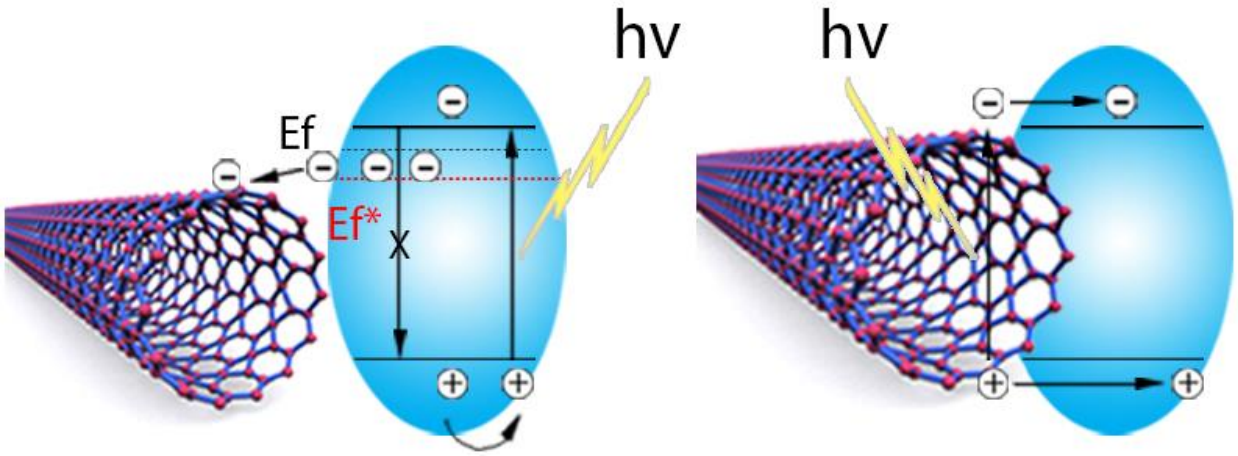

Figure 17. Proposed mechanisms for the enhancement of photocatalytic performance in. CNT-TiO_2 composites

In general, the improvement in photocatalytic activity of carbon-based TiO_2 composites can be attributed to the excellent electron conductivity of carbonaceous materials (e.g. graphene or CNTs) that facilitate the transfer of the photo-generated electron hole pair and inhibit their recombination, as well as the possible heterojunctions between TiO_2 and carbon materials.[159,195,197–199]

A biomass-based carbonaceous material, Starbon, was synthesized by Budarin *et al.* using starch as starting material.[200] Later, Colmenares *et al.* employed Starbons as support for the deposition of TiO_2 nanoparticles, obtaining TiO_2/Starbon composite photocatalysts which showed improved photocatalytic performance as compared to other carbon based supports.[201] Based on these recent results, there is great potential in the use biomass-derived carbonaceous materials (with rich oxygen and sp^2 hybridized electrons in the structures) as supports for photocatalysts.

1.3.2 Mesoporous metal oxide-based nanocomposites

With the advantages of high surface areas, well-ordered pore structures, finely tunable pore sizes and flexible wall-compositions, mesoporous metal oxide materials have been widely

investigated to explore their synthetic protocols and applications in absorption, catalysis, chemical sensing, etc.[202–207]

Mesoporous silicas are generally synthesized by soft-templating approaches by using conventional and market-available templates as the mesoporous porogens, such as TEA, F127, P123. Among various mesoporous silica materials, SBA-15 with 2D hexagonal structure with highly ordered mesoporous uniform channels (up to 500 Å) and walls (between 30 and 90 Å) are relatively more thermally and hydrothermally stable than other amorphous or mesostructured silica materials.[207] In a general protocol, SBA-15 type materials are synthesized in acidic medium (pH $\approx$1) using the triblock copolymer (P123) as structure directing agent, while the pore size and wall thickness can be varied during the synthetic protocol by controlling temperature and time.[208] Moreover, various metal cations can be introduced into the SBA-15 structure via *in-situ* incorporation by adding metal salts to the solutions, obtaining SBA-15 with various heteroatoms: Al-SBA-15, Fe-SBA-15, Ti-SBA-15 and Zr-SBA-15.[204,209–213] Soft templates can be removed by either solvent extraction or calcination.

Mesoporous silicas can be utilized as effective supports for guest catalytic species.[122,175,214–216] The interaction between the loaded/grafted catalytically active species and the *in-situ* present Si−OH groups or the two different kinds of introduced functional groups on the silica surface may result in catalytic synergetic effects.[4] As compared to commercial TiO_2 P25, improvements in catalytic performance could be obtained by using TiO_2-SBA-15 composite photocatalysts, profiting from the molecular sieve effect of SBA-15.[217–219] TiO_2-SBA-15 composites were found to be active in photocatalytic CO_2 reduction, and further increase of reduction rate could be achieved by decoration with Au nanoparticles.[220]

Coupling TiO_2 with other materials (metal, metal oxides, semiconductors, etc.) is one of the most common employed method to improve or delay charge separation and extend the light absorption capability of the composite materials, revealing a promising approach for developing highly efficient visible light activated photocatalysts.[221]

Magnetic iron oxide nanomaterials are of great interest as catalyst supports due to their response to an applied magnetic field.[222,223] Besides, the magnetic nanomaterials can play dual

role as both catalytic active species and magnetic carriers. The superparamagnetic property of magnetic nanomaterials facilitates the robust, highly efficient and rapid catalyst separation in the presence of magnetic field, superior to the conventional separation techniques such as liquid-liquid extraction, chromatography, filtration or centrifugation.

Various iron oxides (α-Fe_2O_3, γ-Fe_2O_3, Fe_3O_4) @ TiO_2 composites with core shell structure have been reported, exhibiting excellent photocatalytic performances that could be attributed to the fast charge transfer process, inhibited electron–hole recombination and wide spectral response.[157,184,185,224,225] The heterojunctions between iron oxides and TiO_2 can effectively extend the light absorption capability of the generated photocatalysts. The charge separation process under visible light irradiation within α-Fe_2O_3-TiO_2 composites is illustrated in Figure 18. Recently, magnetically separable nanocomposites (MAGSNCs) were reported by Ojeda *et al*. by introducing iron oxide nanoparticle onto mesoporous SBA-15 via mechanochemical methods.[226] MAGSNCs can be further functionalized by deposition of transition metal and metal oxide nanoparticles (e.g. Pd, Pt) for various catalytic applications.[227] The incorporation of TiO_2 on MAGSNCs can be consequently of interest for the design of advanced nanocomposite photocatalysts.

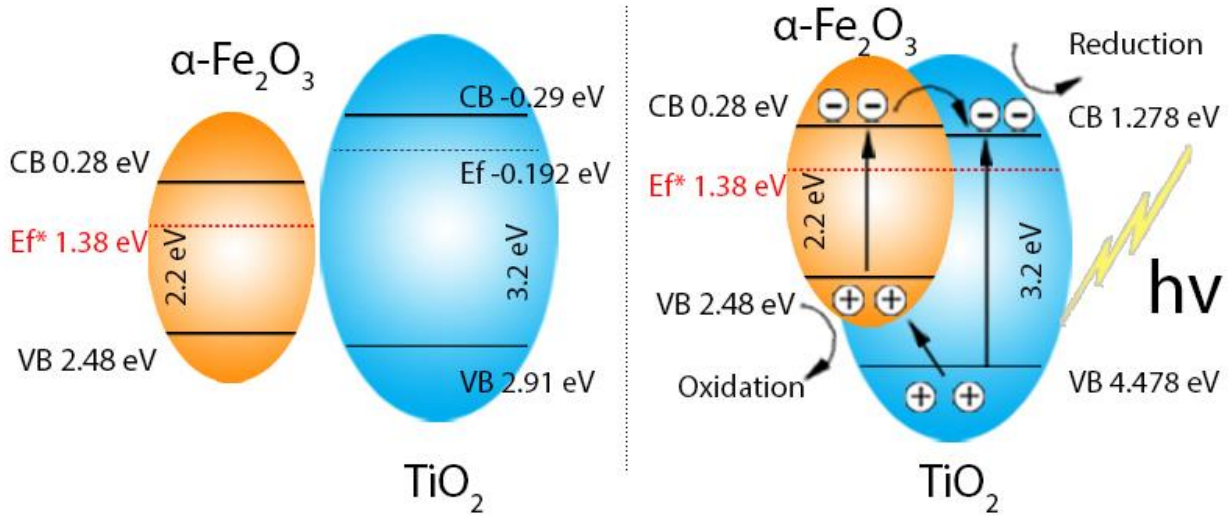

Figure 18. Schematic illustration of band gap location of on α-Fe_2O_3 and TiO_2 (left) and electron–hole separation on α-Fe_2O_3-TiO_2 under visible light irradiation (right)

1.3.3 Synthetic methods for (photo)catalyst preparation

Various chemical and physicochemical methods have been developed and employed in the synthesis of nanostructured materials including sol-gel, solvothermal, mechanochemical, sonochemical and electrochemical methods. In the synthesis of advanced functional materials with complicated structures, several methods are step-wise employed in synthetic processes.

1.3.3.1 Sol-gel methods

Sol-gel processes are common methods for the synthesis of porous metal oxides, ceramics and nanomaterials (e.g. TiO_2). TiO_2 materials have been extensively synthesized using sol-gel methods and subsequently explored in photocatalytic processes including water splitting, CO_2 reduction, decontamination of water, self-cleaning material and organic synthesis.[221,228–241]

In a typical sol-gel process, metal alkoxides, $M(OR)_x$, are commonly used precursors, which R represents alkyl group such as methyl, ethyl or propyl groups. Upon hydrolysis and condensation of the precursors, a diphasic gel-like system is gradually formed along with the formation of polymer oxide networks. In the synthesis of TiO_2, the theoretical hydrolysis process proceeds as shown in the below equations (1) & (2):

$$Ti(OR)_4 + 4H_2O \rightarrow Ti(OH)_4 + 4ROH \qquad (1)$$

$$Ti(OH)_4 \rightarrow TiO_2 + 2H_2O \qquad (2)$$

Nevertheless, the reactions does not proceed stoichiometrically, forming partially hydrolyzed compounds and further condensing into polymer networks, as shown in equation (3) & (4). [242]

$$Ti(OR)_4 + xH_2O \rightarrow Ti(OH)_x(OR)_{4-x} + xROH \qquad (4)$$

$$Ti(OH)_x(OR)_{4-x} + Ti(OR)_4 \rightarrow (OR)_{4-x}Ti\text{-}O_x\text{-}Ti(OR)_{4-x} + xROH \qquad (5)$$

The hydrolysis ratio r, H_2O/Ti ratio, plays an essential role in the synthesis of TiO_2, controlling the size, morphology, and crystallinity of the generated precipitates.[242] Partial hydrolysis usually

occurs with low hydrolysis ratios, while high ratios tend to result in nearly complete or fully complete hydrolysis.[243]

1.3.3.2 Solvothermal methods

Solvothermal methods have been widely employed in the synthesis of various well-defined nanostructure materials with excellent manipulation of morphology. Solvothermal synthesis is usually conducted in closed containers, allowing the temperature to exceed the boiling point of solvents. Higher solubility and reactivity of reagents can be achieved in solvothermal processes due to the increase of temperature and pressure that might facilitate unanticipated reactions.[244] Manipulation of experimental factors such as temperature, solvent and addition of facet-specific capping agent, can control the nuclei formation and growth that have vital impact of the crystal properties.

It is well-known that properties (viscosity, dielectric constant) of solvents can be greatly different under various temperatures, while the activity and stability of reagents can be very different at higher temperatures. Besides, solvent properties such as polarity, viscosity and dielectric constant, can significantly affect solvothermal processes and interactions between solvents and reactants/intermediates/products can have a remarkable impact on the reaction equilibriums, kinetics and the generated products. [245] Among various solvents, water, dimethylformamide (DMF), polyols, oleylamine and their mixtures are commonly employed in solvothermal syntheses due to their excellent compatibility with many reactants. In the synthesis of nanoparticles with specific facet explosion, facet-specific capping agents (acids, solvents, surfactants, polymers, etc.) are usually employed to promote the formation of the desired facet that can improve certain properties of the generated products. [246–248] For example, oleic acid and HF were employed in the synthesis of anatase phase TiO_2 featuring {100} and {001} facets which are more active than {101} in photocatalysis owing to the superior surface atomic structure and electronic structure.[249,250]

1.3.3.3 Mechanochemical methods

Mechanochemistry is not a novel method for material synthesis. Instead, it has long history, but it was mostly evolved in the recent decades with its application in synthetic organic chemistry, currently developing as the next platform for the design and synthesis of advanced materials.[251–253] According to the definition by IUPAC, mechanochemistry was defined as "a chemical reaction/synthesis that is induced by the direct absorption of mechanical energy".[254]

Conventional synthetic procedures such as sol-gel and solvothermal methods, employ large amount of solvents which have essential effects in energy dispersion, dissolution/solvation and transportation of chemicals.[255] In contrast, mechanochemical processes can quantitatively and quickly facilitate solid-phase reactions (dry milling) and/or reactions with the addition of small amounts of solvents (wet milling or liquid-assisted grinding). As a simple and promising approach, mechanochemistry is advantageous in the preparation of catalysts/nanomaterials in comparison to traditional protocols that involves multiple steps, heating and potential addition of expensive and hazardous reagents. These inherent disadvantages can be overcome by the accumulation of excess of potential energy along with strong shear and friction forces on the materials during grinding under ball milling conditions.[256] Therefore, mechanochemical protocols may offer advantages such as cost, efficiency, sustainability, reproducibility, suitability in large-scale production etc. Many (liquid-assisted) solid state reactions or syntheses can be completed in such high energy input system which can greatly change the materials or create defects on the surface of the final materials, drastically modifying their properties and reactivities. Especially, mechanochemical reactions can be accelerated by liquid-assisted grinding, which could be attributed to the enhancement of reactants' mobility on molecule level.[257] Meanwhile, the employed liquids can improve the co-crystallization processes and exert structure-directing properties.[253]

The energy employed in the grinding system is closely related to the grinding speed and time. There is no doubt that more energy intensive syntheses relate to higher speed milling and therefore will raise the system temperature. It will be favorable for diffusion of species and homogenization of material, but it may cause damage to temperature sensitive compounds or phases. Grinding time is another key parameter for the mechanochemical processes which should be selected appropriately to achieve the steady state of the solid particles between fracture and fusion. In this

regard, type of milling system, temperature, size of balls and the materials should be taken into consideration in mechanochemical syntheses.

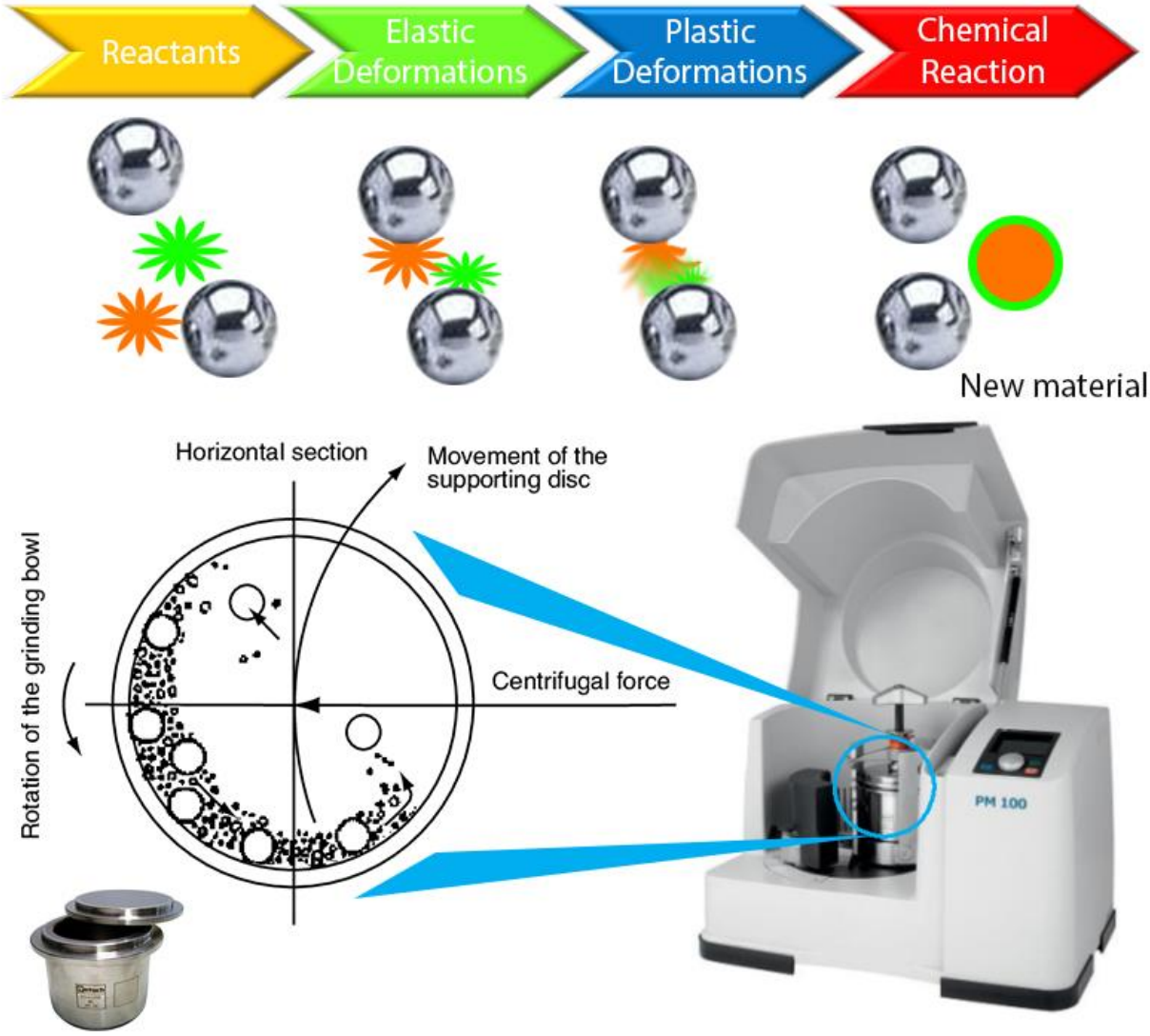

Figure 19. Procedures of material synthesis in mechanochemical process

A comprehensive schematic of the mechanochemical process is illustrated in Figure 19. Mechanochemical methods have been exploited in the synthesis of various materials, including supported metal nanoparticles, metal oxide nanoparticles, composite nanomaterials, metal organic frameworks and perovskite materials, among others.[226,227,258–263] Benefitting from the strong shear forces in the system, mechanical ball milling is an efficient tool for the exfoliation of bulk materials into 2D nanosheets nanosheets (e.g. g-C_3N_4, graphene, WSe_2, TaS_2, etc.).[264–266]

1.3.3.4 Sonochemical methods

Sonochemical syntheses are induced by energy generated by ultrasonic irradiation in liquids with exceptional reaction conditions that can hardly be achieved by other methods (Figure 20). Acoustic cavitation is generated by highly intensive ultrasonic irradiation over a wide range of frequencies, from 20 kHz to 15 MHz, which are much larger than the molecular size scale.[268] Upon sonication, bubbles are generated and oscillated by the acoustic waves in the liquids, which can grow to a certain size along with the accumulation of ultrasonic energy. The accumulated energy will be released within a very short time by the collapse of the overgrew bubbles, generating extremely high localized temperatures and pressures (temperature around 5000 K and pressure around 1000 bar).[269,270] Acoustic cavitation (bubble formation, growth and implosive collapse) accounts for the physical and chemical effects of ultrasound, not the direct interaction between the reagents and sound waves.[268]

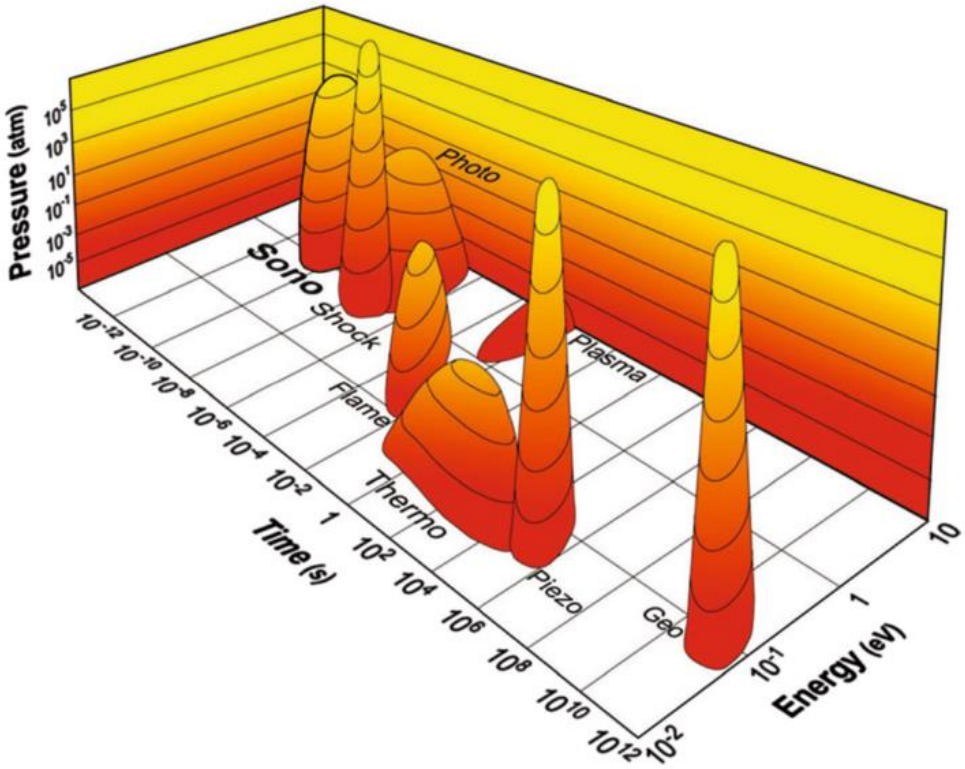

Figure 20. Comparison of time, energy and pressure scales among various chemical processes. (adapted from [267])

Due to the unique environment, ultrasounds have been widely employed in various areas such as pharmaceutical, food industries, material syntheses, waste water treatment, chemical transformations, etc.[269] In terms of material syntheses under ultrasonication, the formation and growth of nanomaterials will be favored in the following stages:

1. Formation of extra nuclei centers on the cavitation bubbles or nebulization microdroplets
2. Faster particle growth rate benefited from the enhanced mass transfer phenomena and the continuous regeneration of surface growing particles
3. Breakdown of particle aggregates in the presence of waves and microjets of molecules

The high temperature at the interface between the cavitation bubble and the bulk solution can accelerate the hydrolysis and condensation process, and therefore shorten the synthesis time, while obtaining particles with uniform size distribution, higher surface area, better thermal stability.[271] Hence, ultrasound has wide applications in synthesis of various nanostructured materials such as metals, metal oxides, metal carbides/nitrides/sulfides, zeolites, and nanocomposites.[272]

References

[1] M. FitzPatrick, P. Champagne, M. F. Cunningham, R. A. Whitney, *Bioresour. Technol.* **2010**, *101*, 8915–8922.

[2] R. Luque, L. Herrero-Davila, J. M. Campelo, J. H. Clark, J. M. Hidalgo, D. Luna, J. M. Marinas, A. A. Romero, *Energy Environ. Sci.* **2008**, *1*, 542–564.

[3] C. Chatterjee, F. Pong, A. Sen, *Green Chem.* **2015**, *17*, 40–71.

[4] J. Shi, *Chem. Rev.* **2013**, *113*, 2139–2181.

[5] L. Vaccaro, D. Lanari, A. Marrocchi, G. Strappaveccia, *Green Chem.* **2014**, *16*, 3680–3704.

[6] A. Fujishima, K. Honda, *Nature* **1972**, *213*, 8656.

[7] "U.S. Energy Information Administration, International Energy Statistics," can be found under https://www.eia.gov/beta/international/data/browser/#/?pa=0000000000000000000008&c=410000000200006000000000000g0002&tl_id=5-A&vs=INTL.57-6-AFRC-BB.A&cy=2014&vo=0&v=H

[8] Organization of the Petroleum Exporting Countries, *2017 World Oil Outlook*, **2017**.

[9] "Statistical Review of World Energy | Energy economics | BP," can be found under https://www.bp.com/en/global/corporate/energy-economics/statistical-review-of-world-energy.html

[10] O. Edenhofer, R. Pichs-Madruga, Y. Sokona, K. Seyboth, P. Matschoss, S. Kadner, T. Zwickel, P. Eickemeier, G. Hansen, S. Schlömer, *IPCC Special Report on Renewable Energy Sources and Climate Change Mitigation*, **2011**.

[11] "Homo sapiens is making fire by drilling wood," can be found under http://www.5011.net/lishi/58652.html

[12] F. A. O. GBEP, *A Review of the Current State of Bioenergy Development in G8 +5 Countries*, **2007**.

[13] M. Stöcker, *Angew. Chem. Int. Ed.* **2008**, *47*, 9200–9211.

[14] J. N. Chheda, G. W. Huber, J. A. Dumesic, *Angew. Chem. Int. Ed.* **2007**, *46*, 7164–7183.

[15] J. H. Clark, R. Luque, A. S. Matharu, *Annu. Rev. Chem. Biomol. Eng.* **2012**, *3*, 183–207.

[16] N. Puy, R. Murillo, M. V. Navarro, J. M. López, J. Rieradevall, G. Fowler, I. Aranguren, T. García, J. Bartrolí, A. M. Mastral, *Waste Manag.* **2011**, *31*, 1339–1349.

[17] Y. Yang, A. Gilbert, C. Xu, *AIChE J.* **2009**, *55*, 807–819.

[18] R. Datar, J. Huang, P. C. Maness, A. Mohagheghi, S. Czernik, E. Chornet, *Int. J. Hydrogen Energy* **2007**, *32*, 932–939.

[19] C. Huang, M. H. Zong, H. Wu, Q. P. Liu, *Bioresour. Technol.* **2009**, *100*, 4535–4538.

[20] J. K. Ko, J. S. Bak, M. W. Jung, H. J. Lee, I. G. Choi, T. H. Kim, K. H. Kim, *Bioresour. Technol.* **2009**, *100*, 4374–4380.

[21] P. Binod, R. Sindhu, R. R. Singhania, S. Vikram, L. Devi, S. Nagalakshmi, N. Kurien, R. K. Sukumaran, A. Pandey, *Bioresour. Technol.* **2010**, *101*, 4767–4774.

[22] S. Kim, B. E. Dale, *Biomass Bioenergy* **2004**, *26*, 361–375.

[23] N. Q. Diep, K. Sakanishi, N. Nakagoshi, S. Fujimoto, T. Minowa, *Renew. Energy* **2015**, *74*, 456–463.

[24] K. Karimi, G. Emtiazi, M. J. Taherzadeh, *Process Biochem.* **2006**, *41*, 653–658.

[25] N. Sarkar, S. K. Ghosh, S. Bannerjee, K. Aikat, *Renew. Energy* **2012**, *37*, 19–27.

[26] T. M. Mata, A. A. Martins, N. S. Caetano, *Renew. Sust. Energy Rev.* **2010**, *14*, 217–232.

[27] X. Miao, Q. Wu, *Bioresour. Technol.* **2006**, *97*, 841–846.

[28] Y. Chisti, *Trends Biotechnol.* **2008**, *26*, 126–131.

[29] H. Fukuda, A. Kondo, H. Noda, *J. Biosci. Bioeng.* **2001**, *92*, 405–416.

[30] B. Fu, L. Gao, L. Niu, R. Wei, G. Xiao, *Energy & Fuels* **2009**, *23*, 569–572.

[31] S. Saka, D. Kusdiana, *Fuel* **2001**, *80*, 225–231.

[32] D. Pleissner, T. H. Kwan, C. S. K. Lin, *Bioresour. Technol.* **2014**, *158*, 48–54.

[33] C. S. K. Lin, A. A. Koutinas, K. Stamatelatou, E. B. Mubofu, A. S. Matharu, N. Kopsahelis, L. A. Pfaltzgraff, J. H. Clark, S. Papanikolaou, T. H. Kwan, R. Luque., *Biofuels Bioprod. Bioref.* **2014**, *6*, 246–256.

[34] T. Silva-Fernandes, L. C. Duarte, F. Carvalheiro, S. Marques, M. C. Loureiro-Dias, C. Fonseca, F. Gírio, *Bioresour. Technol.* **2015**, *183*, 203–212.

[35] X. Yang, S. J. Lee, H. Y. Yoo, H. S. Choi, C. Park, S. W. Kim, *Bioresour. Technol.* **2014**, *159*, 17–23.

[36] R. C. Rivas-Cantu, K. D. Jones, P. L. Mills, *Waste Manag. Res.* **2013**, *31*, 413–20.

[37] A. Y. Zhang, Z. Sun, C. C. J. Leung, W. Han, K. Y. Lau, M. Li, C. S. K. Lin, *Green Chem.* **2013**, *15*, 690–695.

[38] A. Elmekawy, L. Diels, H. De Wever, D. Pant, *Environ. Sci. Technol.* **2013**, *47*, 9014-9027.

[39] D. Pleissner, C. S. K. Lin, *Sustain. Chem. Process.* **2013**, *1*, 21.

[40] A. P. de Souza, A. Grandis, D. C. C. Leite, M. S. Buckeridge, *Bioenergy Res.* **2014**, *7*, 24-35.

[41] D. Talukdar, D. K. Verma, K. Malik, B. Mohapatra, R. Yulianto, in *Sugarcane Biotechnol. Challenges Prospect.* (Ed.: C. Mohan), Springer International Publishing, Cham, **2017**, pp. 123–137.

[42] M. Gumienna, A. Szwengiel, A. Szczepańska-Alvarez, K. Szambelan, M. Lasik-Kurdyś, Z. Czarnecki, A. Sitarski, *Biomass Bioenergy* **2016**, *85*, 228–234.

[43] A. Alexiades, A. Kendall, K. S. Winans, S. R. Kaffka, *J. Clean. Prod.* **2018**, *172*, 3907-3917.

[44] E. Marris, *Nature* **2006**, *444*, 670–672.

[45] L. A. Martinelli, S. Filoso, *Ecol. Appl.* **2008**, *18*, 885–898.

[46] D. Pimentel, T. W. Patzek, *Nat. Resour. Res.* **2005**, *14*, 65–76.

[47] J. A. Quintero, M. I. Montoya, O. J. Sánchez, O. H. Giraldo, C. A. Cardona, *Energy* **2008**, *33*, 385–399.

[48] G. Taylor, *Energy Policy* **2008**, *36*, 4406–4409.

[49] H. Ohara, *Appl. Microbiol. Biotechnol.* **2003**, *62*, 474–477.

[50] A. Gupta, J. P. Verma, *Renew. Sust. Energy Rev.* **2015**, *41*, 550–567.

[51] C. M. Drapcho, N. P. Nhuan, T. H. Walker, *Biofuels Eng. Process Technol.* McGraw-Hill New York:, **2008**.

[52] E. M. W. Smeets, A. P. C. Faaij, *Clim. Change* **2007**, *81*, 353–390.

[53] L. Christopher, *Integrated Forest Biorefineries: Challenges and Opportunities*, Royal Society Of Chemistry, **2012**.

[54] Z. Sun, G. Bottari, A. Afanasenko, M. C. A. Stuart, P. J. Deuss, B. Fridrich, K. Barta, *Nat. Catal.* **2018**, *1*, 82–92.

[55] D. M. Alonso, S. G. Wettstein, J. A. Dumesic, *Chem. Soc. Rev.* **2012**, *41*, 8075–8098.

[56] C. O. Tuck, E. Perez, I. T. Horvath, R. A. Sheldon, M. Poliakoff, *Science* **2012**, *337*, 695-699.

[57] H. V. Scheller, P. Ulvskov, *Annu. Rev. Plant Biol.* **2010**, *61*, 263–289.

[58] S. E. Lebo, J. D. Gargulak, T. J. McNally, in *Kirk-Othmer Encycl. Chem. Technol.*, John Wiley & Sons, Inc., Hoboken, NJ, USA, **2001**, pp. 1–32.

[59] R. Luque, *Pure Appl. Chem.* **2014**, *86*, 843–857.

[60] R. O. M. A. de Souza, L. S. M. Miranda, R. Luque, *Green Chem.* **2014**, *16*, 2386–2405.

[61] H. A. Ruiz, R. M. Rodríguez-Jasso, B. D. Fernandes, A. A. Vicente, J. A. Teixeira, *Renew. Sust. Energy Rev.* **2013**, *21*, 35–51.

[62] R. Liguori, A. Amore, V. Faraco, *Appl. Microbiol. Biotechnol.* **2013**, *97*, 6129–6147.

[63] N. Johar, I. Ahmad, A. Dufresne, *Ind. Crops Prod.* **2012**, *37*, 93–99.

[64] R. A. Arancon, H. R. Barros Jr, A. M. Balu, C. Vargas, R. Luque, *Green Chem.* **2011**, *13*,

3162–3167.

[65] K. Niu, P. Chen, X. Zhang, W. S. Tan, *J. Chem. Technol. Biotechnol.* **2009**, *84*, 1240-1245.

[66] C. Liu, H. Wang, A. M. Karim, J. Sun, Y. Wang, *Chem. Soc. Rev.* **2014**, *43*, 7594–7623.

[67] H. Ma, W. W. Liu, X. Chen, Y. J. Wu, Z. L. Yu, *Bioresour. Technol.* **2009**, *100*, 1279–1284.

[68] T. Werpy, G. Petersen, *Top Value Added Chemicals from Biomass: Volume I -- Results of Screening for Potential Candidates from Sugars and Synthesis Gas*, Golden, CO, **2004**.

[69] J. P. Lange, E. Van Der Heide, J. Van Buijtenen, R. Price, *ChemSusChem* **2012**, *5*, 150-166.

[70] W. Ouyang, A. Yepez, A. A. Romero, R. Luque, *Catal. Today* **2018**, *308*, 32–37.

[71] P. Panagiotopoulou, N. Martin, D. G. Vlachos, *J. Mol. Catal. A Chem.* **2014**, *392*, 223–228.

[72] Y. Nakagawa, K. Tomishige, *Catal. Today* **2012**, *195*, 136–143.

[73] B. Chen, F. Li, Z. Huang, T. Lu, Y. Yuan, G. Yuan, *ChemSusChem* **2014**, *7*, 202–209.

[74] A. M. Hengne, S. B. Kamble, C. V. Rode, *Green Chem.* **2013**, *15*, 2540–2547.

[75] K. Yan, G. Wu, T. Lafleur, C. Jarvis, *Renew. Sust. Energy Rev.* **2014**, *38*, 663–676.

[76] N. Merat, C. Godawa, A. Gaset, *J. Chem. Technol. Biotechnol.* **2007**, *48*, 145–159.

[77] H. E. Hoydonckx, W. M. Van Rhijn, W. Van Rhijn, D. E. De Vos, P. A. Jacobs, in *Ullmann's Encycl. Ind. Chem.*, Wiley-VCH Verlag GmbH & Co. KGaA, Weinheim, Germany, **2007**.

[78] E. Ahmad, M. I. Alam, K. K. Pant, M. A. Haider, *Green Chem.* **2016**, *18*, 4804–4823.

[79] P. Neves, M. M. Antunes, P. A. Russo, J. P. Abrantes, S. Lima, A. Fernandes, M. Pillinger, S. M. Rocha, M. F. Ribeiro, A. A. Valente, *Green Chem.* **2013**, *15*, 3367–3376.

[80] H. Li, Z. Fang, J. Luo, S. Yang, *Appl. Catal. B Environ.* **2017**, *200*, 182–191.

[81] X. Hu, Y. Song, L. Wu, M. Gholizadeh, C.-Z. Li, *ACS Sustain. Chem. Eng.* **2013**, *1*, 1593–1599.

[82] D. M. Alonso, S. G. Wettstein, J. A. Dumesic, *Green Chem.* **2013**, *15*, 584–595.

[83] J. C. Serrano-Ruiz, D. Wang, J. A. Dumesic, *Green Chem.* **2010**, *12*, 574–577.

[84] Y. Kuwahara, W. Kaburagi, Y. Osada, T. Fujitani, H. Yamashita, *Catal. Today* **2017**, *281*, 418–428.

[85] D. Wang, S. H. Hakim, D. Martin Alonso, J. A. Dumesic, *Chem. Commun.* **2013**, *49*, 7040--7042.

[86] D. Zhao, P. Prinsen, Y. Wang, W. Ouyang, F. Delbecq, C. Len, R. Luque, *ACS Sustain. Chem. Eng.* **2018**, *6*, 6901–6909.

[87] X. Tang, L. Hu, Y. Sun, G. Zhao, W. Hao, L. Lin, *RSC Adv.* **2013**, *3*, 10277–10284.

[88] F. Yu, R. Zhong, H. Chong, M. Smet, W. Dehaen, B. F. Sels, *Green Chem.* **2017**, *19*, 153–163.

[89] O. Y. Abdelaziz, D. P. Brink, J. Prothmann, K. Ravi, M. Sun, J. García-Hidalgo, M. Sandahl, C. P. Hulteberg, C. Turner, G. Lidén, M.F. Gorwa-Grauslund, *Biotechnol. Adv.* **2016**, *34*, 1318–1346.

[90] R. Sun, J. Tomkinson, *Ultrason. Sonochem.* **2002**, *9*, 85–93.

[91] M.-F. Li, S.-N. Sun, F. Xu, R.-C. Sun, *Ultrason. Sonochem.* **2012**, *19*, 243–249.

[92] J. Zakzeski, A. L. Jongerius, P. C. A. Bruijnincx, B. M. Weckhuysen, *ChemSusChem* **2012**, *5*, 1602–1609.

[93] S. Dutta, K. C.-W. Wu, B. Saha, *Catal. Sci. Technol.* **2014**, *4*, 3785–3799.

[94] M. Zaheer, R. Kempe, *ACS Catal.* **2015**, *5*, 1675–1684.

[95] Q. Song, F. Wang, J. Cai, Y. Wang, J. Zhang, W. Yu, J. Xu, *Energy Environ. Sci.* **2013**, *6*, 994–1007.

[96] L. I. Granone, F. Sieland, N. Zheng, R. Dillert, D. W. Bahnemann, *Green Chem.* **2018**, *20*,

1169–1192.

[97] L. Song, X. Zhao, L. Cao, J.-W. Moon, B. Gu, W. Wang, *Nanoscale* **2015**, *7*, 16695–16703.

[98] E. Portjanskaja, K. Stepanova, D. Klauson, S. Preis, *Catal. Today* **2009**, *144*, 26–30.

[99] Y. Lu, X.-Y. Wei, Z. Wen, H.-B. Chen, Y.-C. Lu, Z.-M. Zong, J.-P. Cao, S.-C. Qi, S.-Z. Wang, L.-C. Yu, W. Zha, X. Fan, Y-P. Zhao, *Fuel Process. Technol.* **2014**, *117*, 8–16.

[100] V. Augugliaro, G. Camera-Roda, V. Loddo, G. Palmisano, L. Palmisano, J. Soria, S. Yurdakal, *J. Phys. Chem. Lett.* **2015**, *6*, 1968–1981.

[101] J. C. Colmenares, R. Luque, *Chem. Soc. Rev.* **2014**, *43*, 765–778.

[102] S.-H. Li, S. Liu, J. C. Colmenares, Y.-J. Xu, *Green Chem.* **2016**, *18*, 594–607.

[103] C. Zheng, G. He, X. Xiao, M. Lu, H. Zhong, X. Zuo, J. Nan, *Appl. Catal. B Environ.* **2017**, *205*, 201–210.

[104] S. Higashimoto, N. Kitao, N. Yoshida, T. Sakura, M. Azuma, H. Ohue, Y. Sakata, *J. Catal.* **2009**, *266*, 279–285.

[105] D. Cambié, C. Bottecchia, N. J. W. Straathof, V. Hessel, T. Noël, *Chem. Rev.* **2016**, *116*, 10276–10341.

[106] D. T. McQuade, P. H. Seeberger, *J. Org. Chem.* **2013**, *78*, 6384–6389.

[107] H. P. L. Gemoets, Y. Su, M. Shang, V. Hessel, R. Luque, T. Noël, *Chem. Soc. Rev.* **2016**, *45*, 83–117.

[108] T. Noël, S. L. Buchwald, *Chem. Soc. Rev.* **2011**, *40*, 5010–5029.

[109] R. Örkényi, J. Éles, F. Faigl, P. Vincze, A. Prechl, Z. Szakács, J. Kóti, I. Greiner, *Angew. Chem. Int. Ed.* **2017**, *56*, 8742–8745.

[110] M. Brzozowski, M. O'Brien, S. V. Ley, A. Polyzos, *Acc. Chem. Res.* **2015**, *48*, 349–362.

[111] M. Irfan, T. N. Glasnov, C. O. Kappe, *ChemSusChem* **2011**, *4*, 300–316.

[112] C. Bottecchia, N. Erdmann, P. M. A. Tijssen, L. G. Milroy, L. Brunsveld, V. Hessel, T.

Noël, *ChemSusChem* **2016**, *9*, 1781–1785.

[113] A. D. McNaught, A. W. Blackwel, *IUPAC Compendium of Chemical Terminology*, IUPAC, Research Triagle Park, NC, **2009**.

[114] G. Ciamician, *Science* **1912**, *36*, 385–394.

[115] S. Manzeli, D. Ovchinnikov, D. Pasquier, O. V. Yazyev, A. Kis, *Nat. Rev. Mater.* **2017**, *2*, 17033.

[116] M.-H. Pham, C.-T. Dinh, G.-T. Vuong, N.-D. Ta, T.-O. Do, *Phys. Chem. Chem. Phys.* **2014**, *16*, 5937–41.

[117] A. V. Puga, *Coord. Chem. Rev.* **2016**, *315*, 1–66.

[118] X. Zhang, X. Xie, H. Wang, J. Zhang, B. Pan, Y. Xie, *J. Am. Chem. Soc.* **2013**, *135*, 18–21.

[119] Y. H. Ng, A. Iwase, A. Kudo, R. Amal, *J. Phys. Chem. Lett.* **2010**, *1*, 2607–2612.

[120] H. Li, Y. Sun, Z.-Y. Yuan, Y.-P. Zhu, T. Ma, *Angew. Chem. Int. Ed.* **2018**, *57*, 3222–3227.

[121] J. Long, S. Wang, Z. Ding, S. Wang, Y. Zhou, L. Huang, X. Wang, *Chem. Commun.* **2012**, *48*, 11656–11658.

[122] S. Abedi, A. Morsali, *ACS Catal.* **2014**, *4*, 1398–1403.

[123] Y. Fu, D. Sun, Y. Chen, R. Huang, Z. Ding, X. Fu, Z. Li, *Angew. Chem. Int. Ed.* **2012**, *51*, 3364–3367.

[124] L. W. Zhang T., *Chem Soc Rev* **2014**, 43, 5982–5993.

[125] A. Mills, S. Le Hunte, *J. Photochem. Photobiol. A Chem.* **1997**, *108*, 1–35.

[126] W. He, H. Jia, J. Cai, X. Han, Z. Zheng, W. G. Wamer, J. J. Yin, *J. Phys. Chem. C* **2016**, *120*, 3187–3195.

[127] L.-Y. Yang, S.-Y. Dong, J.-H. Sun, J.-L. Feng, Q.-H. Wu, S.-P. Sun, *J. Hazard. Mater.* **2010**, *179*, 438–443.

[128] Y. Ma, X. Wang, Y. Jia, X. Chen, H. Han, C. Li, *Chem. Rev.* **2014**, *114*, 9987–10043.

[129] A. G. Thomas, W. R. Flavell, A. K. Mallick, A. R. Kumarasinghe, D. Tsoutsou, N. Khan, C. Chatwin, S. Rayner, G. C. Smith, R. L. Stockbauer, S. Warren, T. K. Johal, S. Patel, D. Holland, A. Taleb, F. Wiame, *Phys. Rev. B* **2007**, *75*, 35105.

[130] G. N. Raikar, P. J. Hardman, C. A. Muryn, G. van der Laan, P. L. Wincott, G. Thornton, D. W. Bullett, *Solid State Commun.* **1991**, *80*, 423–426.

[131] K. E. Karakitsou, X. E. Verykios, *J. Phys. Chem.* **1993**, *97*, 1184–1189.

[132] N. Serpone, *J. Phys. Chem. B* **2006**, *110*, 24287–24293.

[133] M. Khan, S. Woo, O. Yang, *Int. J. Hydrogen Energy* **2008**, *33*, 5345–5351.

[134] R. Dholam, N. Patel, M. Adami, A. Miotello, *Int. J. Hydrogen Energy* **2009**, *34*, 5337–5346.

[135] M. I. Litter, J. A. Navío, *J. Photochem. Photobiol. A Chem.* **1996**, *98*, 171–181.

[136] R. Dholam, N. Patel, A. Santini, A. Miotello, *Int. J. Hydrogen Energy* **2010**, *35*, 9581–9590.

[137] R. Niishiro, H. Kato, A. Kudo, *Phys. Chem. Chem. Phys.* **2005**, *7*, 2241–2245.

[138] E. M. Neville, M. J. Mattle, D. Loughrey, B. Rajesh, M. Rahman, J. M. D. MacElroy, J. A. Sullivan, K. R. Thampi, *J. Phys. Chem. C* **2012**, *116*, 16511–16521.

[139] X. Yang, C. Cao, L. Erickson, K. Hohn, R. Maghirang, K. Klabunde, *J. Catal.* **2008**, *260*, 128–133.

[140] T. Ohno, M. Akiyoshi, T. Umebayashi, K. Asai, T. Mitsui, M. Matsumura, *Appl. Catal. A Gen.* **2004**, *265*, 115–121.

[141] K. Yang, Y. Dai, B. Huang, *J. Phys. Chem. C* **2007**, *111*, 18985–18994.

[142] U. Pal, S. Ghosh, D. Chatterjee, *Transit. Met. Chem.* **2012**, *37*, 93–96.

[143] M. Zhang, C. Chen, W. Ma, J. Zhao, *Angew. Chem. Int. Ed.* **2008**, *120*, 9876–9879.

[144] H. Wang, Y. Liu, M. Li, H. Huang, H. M. Xu, R. J. Hong, H. Shen, *Optoelectron. Adv.*

Mater. Rapid Commun. **2010**, *4*, 1166–1169.

[145] K. Gurunathan, *J. Mol. Catal. A Chem.* **2000**, *156*, 59–67.

[146] S. S. Mali, C. A. Betty, P. N. Bhosale, P. S. Patil, *Electrochim. Acta* **2012**, *59*, 113–120.

[147] S. Min, G. Lu, *Int. J. Hydrogen Energy* **2012**, *37*, 10564–10574.

[148] N. Rungjaroentawon, S. Onsuratoom, S. Chavadej, *Int. J. Hydrogen Energy* **2012**, *37*, 11061–11071.

[149] K. T. Ranjit, B. Viswanathan, *J. Photochem. Photobiol. A Chem.* **1997**, *108*, 79–84.

[150] K. Vinodgopal, P. V. Kamat, *Environ. Sci. Technol.* **1995**, *29*, 841–845.

[151] S. J. A. Moniz, S. A. Shevlin, X. An, Z.-X. Guo, J. Tang, *Chem. Eur. J.* **2014**, *20*, 15571–15579.

[152] J. Fu, J. Yu, C. Jiang, B. Cheng, *Adv. Energy Mater.* **2018**, *8*, 1701503.

[153] X. Chen, J. Wei, R. Hou, Y. Liang, Z. Xie, Y. Zhu, X. Zhang, H. Wang, *Appl. Catal. B Environ.* **2016**, *188*, 342–350.

[154] R. Hao, G. Wang, H. Tang, L. Sun, C. Xu, D. Han, *Appl. Catal. B Environ.* **2016**, *187*, 47–58.

[155] K. Li, S. Gao, Q. Wang, H. Xu, Z. Wang, B. Huang, Y. Dai, J. Lu, *ACS Appl. Mater. Interfaces* **2015**, *7*, 9023–9030.

[156] D. Barreca, G. Carraro, A. Gasparotto, C. Maccato, M. E. A. Warwick, K. Kaunisto, C. Sada, S. Turner, Y. Gönüllü, T.-P. Ruoko, L. Borgese , E. Bontempi , G. Van Tendeloo , H. Lemmetyinen, S. Mathur, *Adv. Mater. Interfaces* **2015**, *2*, 1500313.

[157] J. Liu, S. Yang, W. Wu, Q. Tian, S. Cui, Z. Dai, F. Ren, X. Xiao, C. Jiang, *ACS Sust. Chem. Eng.* **2015**, *3*, 2975–2984.

[158] C. H. Kim, B.-H. Kim, K. S. Yang, *Carbon* **2012**, *50*, 2472–2481.

[159] X.-H. Xia, Z.-J. Jia, Y. Yu, Y. Liang, Z. Wang, L.-L. Ma, *Carbon* **2007**, *45*, 717–721.

[160] H. Meng, W. Hou, X. Xu, J. Xu, X. Zhang, *Particuology* **2014**, *14*, 38–43.

[161] J. R. Bolton, S. J. Strickler, J. S. Connolly, *Nature* **1985**, *316*, 495–500.

[162] Y. Xiong, D. Gu, X. Deng, H. Tüysüz, M. van Gastel, F. Schüth, F. Marlow, *Micropor. Mesopor. Mater.* **2018**, *268*, 162–169.

[163] O. Fontelles-Carceller, M. J. Muñoz-Batista, E. Rodríguez-Castellón, J. C. Conesa, M. Fernández-García, A. Kubacka, *J. Catal.* **2017**, *347*, 157–169.

[164] O. Fontelles-Carceller, M. J. Muñoz-Batista, J. C. Conesa, M. Fernández-García, A. Kubacka, *Appl. Catal. B Environ.* **2017**, *216*, 133–145.

[165] J. C. Colmenares, A. Magdziarz, A. Bielejewska, *Bioresour. Technol.* **2011**, *102*, 11254–11257.

[166] H. Wang, Y. Song, J. Xiong, J. Bi, L. Li, Y. Yu, S. Liang, L. Wu, *Appl. Catal. B Environ.* **2018**, *224*, 394–403.

[167] S. Higashimoto, N. Suetsugu, M. Azuma, H. Ohue, Y. Sakata, *J. Catal.* **2010**, *274*, 76–83.

[168] S. Higashimoto, K. Okada, T. Morisugi, M. Azuma, H. Ohue, T.-H. Kim, M. Matsuoka, M. Anpo, *Top. Catal.* **2010**, *53*, 578–583.

[169] S. Kim, S.-J. Hwang, W. Choi, *J. Phys. Chem. B* **2005**, *109*, 24260–24267.

[170] A. Magdziarz, J. C. Colmenares, O. Chernyayeva, D. Lisovytskiy, J. Grzonka, K. Kurzydłowski, K. Freindl, J. Korecki, *Ultrason. Sonochem.* **2017**, *38*, 187–196.

[171] J. J. Bravo-Suárez, R. V. Chaudhari, B. Subramaniam, in *Nov. Mater. Catal. Fuels Process.*, **2013**, pp. 3–68.

[172] R. J. White, R. Luque, V. L. Budarin, J. H. Clark, D. J. Macquarrie, *Chem. Soc. Rev.* **2009**, *38*, 481–494.

[173] J. M. Hernández Enríquez, L. A. Cortez Lajas, R. García Alamilla, A. Castillo Mares, G. Sandoval Robles, L. A. García Serrano, *J. Alloys Comp.* **2009**, *483*, 425–428.

[174] H. Zhou, J. Song, H. Fan, B. Zhang, Y. Yang, J. Hu, Q. Zhu, B. Han, *Green Chem.* **2014**, *16*, 3870–3875.

[175] A. H. Valekar, K.-H. Cho, S. K. Chitale, D.-Y. Hong, G.-Y. Cha, U.-H. Lee, D. W.

Hwang, C. Serre, J.-S. Chang, Y. K. Hwang, *Green Chem.* **2016**, *18*, 4542–4552.

[176] L. Shen, S. Liang, W. Wu, R. Liang, L. Wu, *Dalt. Trans.* **2013**, *42*, 13649–13657.

[177] F. G. Cirujano, A. Corma, F. X. Llabrés I Xamena, *Catal. Today* **2015**, *257*, 213–220.

[178] C.-H. Kuo, A. S. Poyraz, L. Jin, Y. Meng, L. Pahalagedara, S.-Y. Chen, D. A. Kriz, C. Guild, A. Gudz, S. L. Suib, *Green Chem.* **2014**, *16*, 785–791.

[179] J. Wang, S. Jaenicke, G.-K. Chuah, *RSC Adv.* **2014**, *4*, 13481–13489.

[180] P. Fu, Y. Luan, X. Dai, *J. Mol. Catal. A Chem.* **2004**, *221*, 81–88.

[181] A. Moya, A. Cherevan, S. Marchesan, P. Gebhardt, M. Prato, D. Eder, J. J. Vilatela, *Appl. Catal. B Environ.* **2015**, *179*, 574–582.

[182] J. Di, S. Li, Z. Zhao, Y. Huang, Y. A. Jia, H. Zheng, *Chem. Eng. J.* **2015**, *281*, 60–68.

[183] M. Wang, M. Pyeon, Y. Gönüllü, A. Kaouk, S. Shen, L. Guo, S. Mathur, *Nanoscale* **2015**, *7*, 10094–10100.

[184] Y. Xia, L. Yin, *Phys. Chem. Chem. Phys.* **2013**, *15*, 18627–18634.

[185] X. Zhang, Y. Xie, H. Chen, J. Guo, A. Meng, C. Li, *Appl. Surf. Sci.* **2014**, *317*, 43–48.

[186] H. Yan, H. Yang, *J. Alloys Compd.* **2011**, *509*, L26–L29.

[187] M. J. Muñoz-Batista, A. Kubacka, M. Fernández-García, *ACS Catal.* **2014**, *4*, 4277–4288.

[188] A. C. Martins, A. L. Cazetta, O. Pezoti, J. R. B. Souza, T. Zhang, E. J. Pilau, T. Asefa, V. C. Almeida, *Ceram. Int.* **2017**, *43*, 4411–4418.

[189] A. Trapalis, N. Todorova, T. Giannakopoulou, N. Boukos, T. Speliotis, D. Dimotikali, J. Yu, *Appl. Catal. B Environ.* **2016**, *180*, 637–647.

[190] P. Calza, C. Hadjicostas, V. A. Sakkas, M. Sarro, C. Minero, C. Medana, T. A. Albanis, *Appl. Catal. B Environ.* **2016**, *183*, 96–106.

[191] M. Minella, F. Sordello, C. Minero, *Catal. Today* **2017**, *281*, 29–37.

[192] A. K. Geim, *Science* **2009**, *324*, 1530–1534.

[193] A. K. Geim, K. S. Novoselov, *Nat. Mater.* **2007**, *6*, 183–191.

[194] G. Williams, B. Seger, P. V Kamat, *ACS Nano* **2008**, *2*, 1487–1491.

[195] A. Kongkanand, P. V. Kamat, *ACS Nano* **2007**, *1*, 13–21.

[196] K. Woan, G. Pyrgiotakis, W. Sigmund, *Adv. Mater.* **2009**, *21*, 2233–2239.

[197] W. Fan, Q. Lai, Q. Zhang, Y. Wang, *J. Phys. Chem. C* **2011**, *115*, 10694–10701.

[198] H. Li, X. Zhang, X. Cui, Y. Lin, *J. Nanosci. Nanotechnol.* **2012**, *12*, 1806–1811.

[199] P. Zeng, Q. Zhang, X. Zhang, T. Peng, *J. Alloys Comp.* **2012**, *516*, 85–90.

[200] V. Budarin, J. H. Clark, J. J. E. Hardy, R. Luque, K. Milkowski, S. J. Tavener, A. J. Wilson, *Angew. Chem. Int. Ed.* **2006**, *45*, 3782–3786.

[201] J. C. Colmenares, P. Lisowski, D. Łomot, *RSC Adv.* **2013**, *3*, 20186.

[202] M. J. Gracia, E. Losada, R. Luque, J. M. Campelo, D. Luna, J. M. Marinas, A. A. Romero, *Appl. Catal. A Gen.* **2008**, *349*, 148–155.

[203] A. Yepez, J. M. Hidalgo, A. Pineda, R. Černý, P. Jíša, A. Garcia, A. A. Romero, R. Luque, *Green Chem.* **2015**, *17*, 565–572.

[204] R. Huirache-Acuña, R. Nava, C. Peza-Ledesma, J. Lara-Romero, G. Alonso-Núñez, B. Pawelec, E. Rivera-Muñoz, *Materials* **2013**, *6*, 4139–4167.

[205] D. Zhao, J. Sun, Q. Li, G. D. Stucky, *Chem. Mater.* **2000**, *12*, 275–279.

[206] F. Kleitz, in *Handbook of Heterogeneous Catalysis*, Wiley-VCH Verlag GmbH & Co. KGaA, Weinheim, Germany, **2008**, pp. 131–149.

[207] M. Kruk, M. Jaroniec, C. H. Ko, R. Ryoo, *Chem. Mater.* **2000**, *12*, 1961–1968.

[208] D. Zhao, J. Feng, Q. Huo, N. Melosh, G. H. Fredrickson, B. F. Chmelka, G. D. Stucky, *Science* **1998**, *279*, 548–552.

[209] Y. Li, Z. Feng, Y. Lian, K. Sun, L. Zhang, G. Jia, Q. Yang, C. Li, *Micropor. Mesopor. Mater.* **2005**, *84*, 41–49.

[210] E. Sacaliuc, A. Beale, B. Weckhuysen, T. Nijhuis, *J. Catal.* **2007**, *248*, 235–248.

[211] Y. Li, W. Zhang, L. Zhang, Q. Yang, Z. Wei, Z. Feng, C. Li, *J. Phys. Chem. B* **2004**, *108*, 9739–9744.

[212] L. Fuxiang, Y. Feng, L. Yongli, L. Ruifeng, X. Kechang, *Micropor. Mesopor. Mater.* **2007**, *101*, 250–255.

[213] S.-Y. Chen, L.-Y. Jang, S. Cheng, *Chem. Mater.* **2004**, *16*, 4174–4180.

[214] D. Chen, X. Zhang, A. F. Lee, *J. Mater. Chem. A* **2015**, *3*, 14487–14516.

[215] R. Munirathinam, J. Huskens, W. Verboom, *Adv. Synth. Catal.* **2015**, *357*, 1093–1123.

[216] C. Chatterjee, F. Pong, A. Sen, *Green Chem.* **2015**, *17*, 40–71.

[217] M.-J. López-Muñoz, R. Van Grieken, J. Aguado, J. Marugan, *Catal. Today* **2005**, *101*, 307–314.

[218] H. Lachheb, O. Ahmed, A. Houas, J. P. Nogier, *J. Photochem. Photobiol. A Chem.* **2011**, *226*, 1–8.

[219] W.-T. Qiao, G.-W. Zhou, X.-T. Zhang, T.-D. Li, *Mater. Sci. Eng. C* **2009**, *29*, 1498–1502.

[220] B. Mei, A. Pougin, J. Strunk, *J. Catal.* **2013**, *306*, 184–189.

[221] M. Pelaez, N. T. Nolan, S. C. Pillai, M. K. Seery, P. Falaras, A. G. Kontos, P. S. M. Dunlop, J. W. J. Hamilton, J. A. Byrne, K. O'Shea, M.H. Entezari, D.D. Dionysiou, *Appl. Catal. B Environ.* **2012**, *125*, 331–349.

[222] K. Zhu, Y. Ju, J. Xu, Z. Yang, S. Gao, Y. Hou, *Acc. Chem. Res.* **2018**, *51*, 404–413.

[223] L. M. Rossi, N. J. S. Costa, F. P. Silva, R. Wojcieszak, *Green Chem.* **2014**, *16*, 2906–2933.

[224] I. Jang, K.-E. You, Y. C. Kim, S.-G. Oh, *Appl. Surf. Sci.* **2014**, *316*, 187–193.

[225] W. Li, J. Yang, Z. Wu, J. Wang, B. Li, S. Feng, Y. Deng, F. Zhang, D. Zhao, *J. Am. Chem. Soc.* **2012**, *134*, 11864–11867.

[226] M. Ojeda, A. M. Balu, V. Barron, A. Pineda, A. G. Coleto, A. A. Romero, R. Luque, *J. Mater. Chem. A* **2014**, *2*, 387–393.

[227] M. Ojeda, A. Pineda, A. A. Romero, V. Barron, R. Luque, *ChemSusChem* **2014**, *7*, 1876–1880.

[228] M. Baghbanzadeh, T. N. Glasnov, C. O. Kappe, *J. Flow Chem.* **2013**, *3*, 109–113.

[229] K. Qi, B. Fei, J. H. Xin, *Thin Solid Films* **2011**, *519*, 2438–2444.

[230] J.-M. Herrmann, H. Tahiri, C. Guillard, P. Pichat, *Catal. Today* **1999**, *54*, 131–141.

[231] C. Lettmann, K. Hildenbrand, H. Kisch, W. Macyk, W. F. Maier, *Appl. Catal. B Environ.* **2001**, *32*, 215–227.

[232] A. Fujishima, T. N. Rao, D. A. Tryk, *J. Photochem. Photobiol. C Photochem. Rev.* **2000**, *1*, 1–21.

[233] A. J. Cowan, J. Tang, W. Leng, J. R. Durrant, D. R. Klug, *J. Phys. Chem. C* **2010**, *114*, 4208–4214.

[234] J. Zoller, D. C. Fabry, M. Rueping, *ACS Catal.* **2015**, *5*, 3900–3904.

[235] M. Wang, J. Han, H. Xiong, R. Guo, *Langmuir* **2015**, *31*, 6220–6228.

[236] T. A. Kandiel, L. Robben, A. Alkaim, D. Bahnemann, *Photochem. Photobiol. Sci.* **2013**, *12*, 602–609.

[237] M. Sathish, B. Viswanathan, R. P. Viswanath, C. S. Gopinath, *Chem. Mater.* **2005**, *17*, 6349–6353.

[238] J. Liu, Q. Zhang, J. Yang, H. Ma, M. O. Tade, S. Wang, J. Liu, *Chem. Commun.* **2014**, *50*, 13971–13974.

[239] S. Yurdakal, G. Palmisano, V. Loddo, V. Augugliaro, L. Palmisano, *J. Am. Chem. Soc.* **2008**, *130*, 1568–1569.

[240] C. Aprile, A. Corma, H. Garcia, *Phys. Chem. Chem. Phys.* **2008**, *10*, 769–783.

[241] X. Lang, X. Chen, J. Zhao, *Chem. Soc. Rev.* **2014**, *43*, 473–486.

[242] D. A. H. Hanaor, I. Chironi, I. Karatchevtseva, G. Triani, C. C. Sorrell, *Adv. Appl. Ceram.* **2012**, *111*, 149–158.

[243] B. E. Yoldas, *J. Mater. Sci.* **1986**, *21*, 1087–1092.

[244] D. R. Modeshia, R. I. Walton, *Chem. Soc. Rev.* **2010**, *39*, 4303–4325.

[245] R. E. Morris, L. Brammer, *Chem. Soc. Rev.* **2017**, *46*, 5444–5462.

[246] Y. Cao, Q. Li, C. Li, J. Li, J. Yang, *Appl. Catal. B Environ.* **2016**, *198*, 378–388.

[247] H. G. Yang, G. Liu, S. Z. Qiao, C. H. Sun, Y. G. Jin, S. C. Smith, J. Zou, H. M. Cheng, G. Q. Lu, *J. Am. Chem. Soc.* **2009**, *131*, 4078–4083.

[248] J. Yu, J. Low, W. Xiao, P. Zhou, M. Jaroniec, *J. Am. Chem. Soc.* **2014**, *136*, 8839–8842.

[249] H. Xu, S. Ouyang, P. Li, T. Kako, J. Ye, *ACS Appl. Mater. Interfaces* **2013**, *5*, 1348–1354.

[250] J. Pan, G. Liu, G. Q. M. Lu, H.-M. Cheng, *Angew. Chem. Int. Ed.* **2011**, *50*, 2133–2137.

[251] V. Šepelák, A. Düvel, M. Wilkening, K.-D. Becker, P. Heitjans, *Chem. Soc. Rev.* **2013**, *42*, 7507–7520.

[252] A. L. Garay, A. Pichon, S. L. James, *Chem. Soc. Rev.* **2007**, *36*, 846–855.

[253] S. L. James, C. J. Adams, C. Bolm, D. Braga, P. Collier, T. Friščić, F. Grepioni, K. D. M. Harris, G. Hyett, W. Jones, A. Krebs, J. Mack, L. Maini, A. G. Orpen, I. P. Parkin, W. C. Shearouse, J. W. Steed, D. C. Waddell, *Chem. Soc. Rev.* **2012**, *41*, 413–447.

[254] K. Horie, M. Barón, R. B. Fox, J. He, M. Hess, J. Kahovec, T. Kitayama, P. Kubisa, E. Maréchal, W. Mormann, R. F. T. Stepto, Tabak, J. Vohlídal, E. S. Wilks, W. J. Work, *Pure Appl. Chem.* **2004**, *76*, 889–906.

[255] C. Xu, S. De, A. M. Balu, M. Ojeda, R. Luque, *Chem. Commun.* **2015**, *51*, 6698–6713.

[256] B. Kubias, M. J. G. Fait, R. Schlogl, in *Handbook of Heterogeneous Catalysis*, Wiley-VCH Verlag GmbH & Co. KGaA, Weinheim, Germany, **2008**, pp. 571–583.

[257] N. Stock, S. Biswas, *Chem. Rev.* **2012**, *112*, 933–969.

[258] A. Pineda, A. M. Balu, J. M. Campelo, A. A. Romero, D. Carmona, F. Balas, J. Santamaria, R. Luque, *ChemSusChem* **2011**, *4*, 1561–1565.

[259] M. Francavilla, A. Pineda, A. A. Romero, J. C. Colmenares, C. Vargas, M. Monteleone,

R. Luque, *Green Chem.* **2014**, *16*, 2876–2885.

[260] F. Schröder, M. Ojeda, N. Erdmann, J. Jacobs, R. Luque, T. Noël, L. Van Meervelt, J. Van der Eycken, E. V. Van der Eycken, *Green Chem.* **2015**, *17*, 3314–3318.

[261] W. Yuan, T. Friščič, D. Apperley, S. L. James, *Angew. Chem. Int. Ed.* **2010**, *49*, 3916–3919.

[262] J. Zhou, M. Zhang, Y. Zhu, *Phys. Chem. Chem. Phys.* **2014**, *16*, 17627–17633.

[263] W. Yuan, J. O'Connor, S. L. James, *CrystEngComm* **2010**, *12*, 3515–3517.

[264] H. Li, G. Lu, Y. Wang, Z. Yin, C. Cong, Q. He, L. Wang, F. Ding, T. Yu, H. Zhang, *Small* **2013**, *9*, 1974–1981.

[265] M. Yi, Z. Shen, *J. Mater. Chem. A* **2015**, *3*, 11700–11715.

[266] K. Zhu, W. Wang, A. Meng, M. Zhao, J. Wang, M. Zhao, D. Zhang, Y. Jia, C. Xu, Z. Li, *RSC Adv.* **2015**, *5*, 56239–56243.

[267] K. S. Suslick, D. J. Flannigan, *Annu. Rev. Phys. Chem.* **2008**, *59*, 659–683.

[268] H. Xu, B. W. Zeiger, K. S. Suslick, *Chem. Soc. Rev.* **2013**, *42*, 2555–2567.

[269] D. Chen, S. K. Sharma, A. Mudhoo, *Handbook on Applications of Ultrasound: Sonochemistry for Sustainability*, **2011**.

[270] K. S. Suslick, *Sci. Am.* **1989**, *260*, 80–86.

[271] J. H. Bang, K. S. Suslick, *Adv. Mater.* **2010**, *22*, 1039–1059.

[272] J. J. Hinman, K. S. Suslick, *Top. Curr. Chem.* **2017**, *375*, 1–36.

2. Hypothesis and Objectives

The hypotheses and objectives of the current doctoral thesis are summarized as below:

Hypothesis 1

With the depletion of the fossil fuels and the increasing concern of environmental protection, there is strong urgency in developing sustainable alternative fuels, chemicals and materials as substitutions for those derived from petroleum industry. In this regard, abundant lignocellulosic biomass can be utilized as renewable carbon sources to produce valuable fuels, chemicals and materials in the biorefinery process. Due to the structure complexity and difference of lignocellulosic biomass, it is difficult to achieve direct transformation, while it would be easier to convert biomass to platform molecules and subsequently upgrade the molecules to valuable products.

Furfural is a platform molecule derived from a key fraction of lignocellulosic biomass feedstocks (hemicelluloses). Hydrogenation of furfural has received intensive attention and promising results have been reported in batch condition. In contrast to batch process, flow processes will be more favorable because of the inherent advantages of flow chemistry including minimization of time and waste, optimization of time screening, efficient mixing and high surface-to-volume ratios, easy scale-up and improvement in safety. Therefore, performing hydrogenations of furfural in flow conditions is an attractive topic and can potentially offer a possibility for the valorization of biomass derived platform molecules under continuous flow.

Objective 1

Mesoporous silica supports (SBA-15, Al-SBA-15) will be firstly synthesized, followed by deposition of transition/noble metals or metal oxides as catalytic active species using various methods (flow deposition and mechanochemical deposition). Subsequently, as-synthesized catalysts will be employed in the hydrogenation of furfural in continuous flow reactors. Various reaction parameters will be optimized such as temperature and flow rate. The catalytic

performance of as-synthesized catalysts will be compared to commercial catalysts in terms of product yield and stability. To understand the deactivation process, analytical techniques such as ICP-MS, TEM and XPS, will be employed to analyze the catalysts and samples. This objective will be addressed in the work "***Towards industrial furfural conversion: Selectivity and stability of palladium and platinum catalysts under continuous flow regime***".

Hypothesis 2

TiO_2 photocatalysts have been reported in different applications in the last decades, including chemicals and fuels production from CO_2 reduction, water decontamination, organic synthesis and water splitting, etc. However, the application of TiO_2 (bulk anatase: 3.2 eV) is limited by its wide bandgap that means only UV light can the utilized for the electron excitation in the photocatalytic process. Meanwhile, the fast recombination of the photogenerated electron-hole pairs will inhibit the quantum efficiency. Therefore, it is necessary modify TiO_2 to improve its photocatalytic activity. In this regard, deposition of TiO_2 on carbon materials can well address these limitations due to the excellent electron conductivity of carbon materials that can promote the charge separation process. The abundant agro-industrial residue, wheat bran, can be potentially used as support for synthesis of TiO_2/carbon-based nanocomposite.

Benzyl alcohol is a model molecule of the lignin structure, which can be oxidized into benzaldehyde, an attractive chemical with wide applications in food, perfumery and pharmaceutical industries, as well as its use as precursor in various chemical industries. Photocatalytic conversion of benzyl alcohol to benzaldehyde is very attractive, which can potentially offer an alternative to the traditional synthetic routes - either by benzyl chloride hydrolysis or through oxidation of toluene, as well as provide the reactivity and transformation strategies for the valorization of lignocellulose-based biomass.

Objective 2

Different amounts of titanium precursor will be introduced onto the wheat bran support via mechanochemical methods, following by calcination. As-synthesized samples will be fully characterized by different techniques, including N_2 physisorption, TEM, XRD, XPS, UV-Vis and ICP-MS. The photocatalytic activity of as-synthesized materials will be investigated in the selective oxidation of benzyl alcohol. The proposed research will be addressed in the work "***Wheat bran valorization: Towards photocatalytic nanomaterials for benzyl alcohol photo-oxidation***".

Hypothesis 3

Benzaldehyde is widely utilized in food, perfumery and pharmaceutical industries, which can be derived from the selective oxidation of benzyl alcohol. Recently, selective photo-oxidation of benzyl alcohol to chlorine-free benzaldehyde has been reported using different catalysts with high selectivity, which is a promising alternative to the traditional syntheses-either by benzyl chloride hydrolysis or via toluene oxidation. The study on selective oxidation of benzyl alcohol might also contribute to the strategy development for lignin valorization, as it is a model molecule of the complex lignin.

TiO_2 (anatase phase) has excellent photocatalytic performance and different methods have been reported to overcome its main limitation of high band gap energy. Coupling TiO_2 with other materials is a common method that can effectively extend the light absorption capability and improve the separation of the photogenerated electron-hole pairs. In this regard, iron oxide is an ideal candidate that can not only achieve these purposes, but also endow the composite magnetic separable property due to the intrinsic superparamagnetic nature of iron oxide.

Objective 3

SBA-15 will be synthesized via hydrothermal method and then both titanium and iron precursors will be deposited on SBA-15 support simultaneously via mechanochemical method. Amount of titanium precursor will be varied in the synthesis to obtain samples with different TiO_2 loading. Various characterization techniques will be employed for the analysis of as-synthesized samples, including N_2 physisorption, SEM, TEM, XRD, XPS, UV-Vis, etc. Subsequently, as-synthesized materials will be employed in the selective photo-oxidation of benzyl alcohol to test their photocatalytic activity. As references, experiments with SBA-15, MAGSNC, commercial TiO_2 P25 and without catalyst will also be performed. The proposed research will be addressed in to work "***Mechanochemical synthesis of TiO_2 nanocomposites as photocatalysts for benzyl alcohol photo-oxidation***".

3. Results and Discussion


Contents lists available at ScienceDirect

Catalysis Today

journal homepage: www.elsevier.com/locate/cattod

3.1. Towards Industrial Furfural Conversion: Selectivity and Stability of Palladium and Platinum Catalysts under Continuous Flow Regime

Weiyi Ouyang*, Alfonso Yepez, Antonio A. Romero, Rafael Luque*

a Departamento de Quimica Organica, Universidad de Cordoba, Edificio Marie Curie(C-3), Ctra Nnal IV-A, Km 396, E14014 Córdoba, Spain

∗ *Corresponding authors. E-mail addresses: qo2ououw@uco.es (W. Ouyang), q62alsor@uco.es (R. Luque).*

Received 7 May 2017; Received in revised form 4 July 2017; Accepted 8 July 2017; Available online 10 July 2017

DOI: 10.1016/j.cattod.2017.07.011

Abstract

Furfural is an important biorefinery platform chemical, derived from hemicelluloses which represent an import fraction of lignocellulosic biomass feedstocks and waste streams originating

from them. Recently, promising results have been reported on the hydrogenation of furfural, although the selectivity still may be improved. Most of these studies dealt with batch hydrogenation, however, hydrogenation in continuous flow is preferable for industrial applications. In this work, we compare the conversion, selectivity and stability on-stream in continuous flow regime of lab-synthesized and commercial palladium and platinum catalysts.

Keywords: Furfural, Hydrogenation, Continuous flow, Selectivity, Stability

Graphical abstract

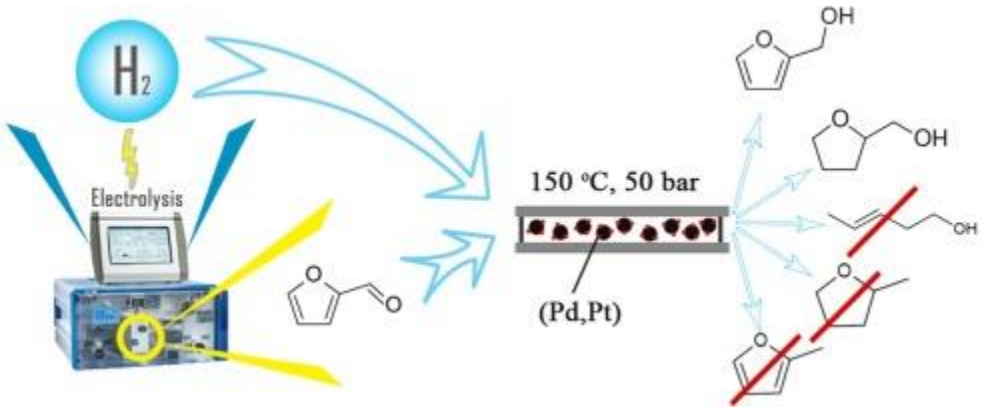

3.1.1. Introduction

The global population could reach and even exceed 9 billion by 2050 [1]. The use of sustainable feedstocks to meet the growing global energy demand and to reduce the use of fossil resources is now a highly imminent challenge for the research community, and a challenge to be adopted in currently existing industrial refineries or to be designed in future biorefinery plants. The largest part of the current fossil derived petroleum refining is used for fuels production. Still, an important part of petroleum is used for the production of bulk chemicals and materials. Today, the use of alternative biomass feedstocks (or waste streams derived from them) has become a

widely reported research area. Considering the complexity and the recalcitrance of biomass, many works focused on the transformation of biomass derived platform molecules to fuels and high-added value chemicals. For example, C5 sugars are key representative compounds of the hemicellulose fraction of lignocellulose, which can be converted to valuable platform molecules and subsequently valorized into high-added value products [2].

Furfural (F) is an important platform chemical, which can be obtained via dehydration under mild conditions from xylose, a typical C5 sugar. Furfural can undergo reactions typical for aldehydes like acetalization, acylation, aldol and Knoevenagel condensations, reduction to alcohols, reductive amination to amines, decarbonylation, oxidation to carboxylic acids and Grignard reactions. Besides, the furan ring can be subjected to alkylation, hydrogenation, oxidation, halogenations and nitration reactions. Due to the electron-withdrawing effect of the carbonyl group, the furan ring is less susceptible to hydrolytic ring cleavage and Diels-Alder cycloaddition reactions. Therefore, furfural is considered to be an attractive platform chemical for the production of a wide range of chemicals, e.g. solvents (tetrahydrofuran), plastics (in particular, polyamides), resins via furfuryl alcohol and fuel additives (methylfuran, methyl-tetrahydrofuran, valerate esters, ethylfurfuryl and ethyltetrahydrofurfuryl ethers and C10–C15 coupling products) [2]. Around 60–70% of the global furfural production is converted to furfuryl alcohol [2,3]. It is widely reported that furfural can be further transformed into various compounds by hydrogenation, such as furfuryl alcohol (FA), tetrahydrofurfuryl alcohol (THFA), 2-methylfuran (MF) and 2-methyltetrahydrofuran (MTHF). Most of these reactions were performed in batch conditions [4–8] with noble or transition metals-based catalysts, while only a few of them were performed in continuous flow [7,9]. Especially, these reactions were performed using only either lab-synthesized or commercial catalysts, with a simple comparison of existing results obtained under different conditions. Regarding to the advantages of flow chemistry, such as faster, safer reactions and easy scale-up, it would be interesting to give a comparison of catalytic performance of both lab synthesized and commercial catalysts under same reaction conditions in continuous flow system. Previous work from our group has provided insights into the reaction pathway comparing noble metal and transition metal catalysts (Scheme 1), showing favorable results for Pd based catalysts [9]. The mechanism of furfural conversion on palladium catalysts was also studied by other researchers based on density functional theory (DFT) [10].

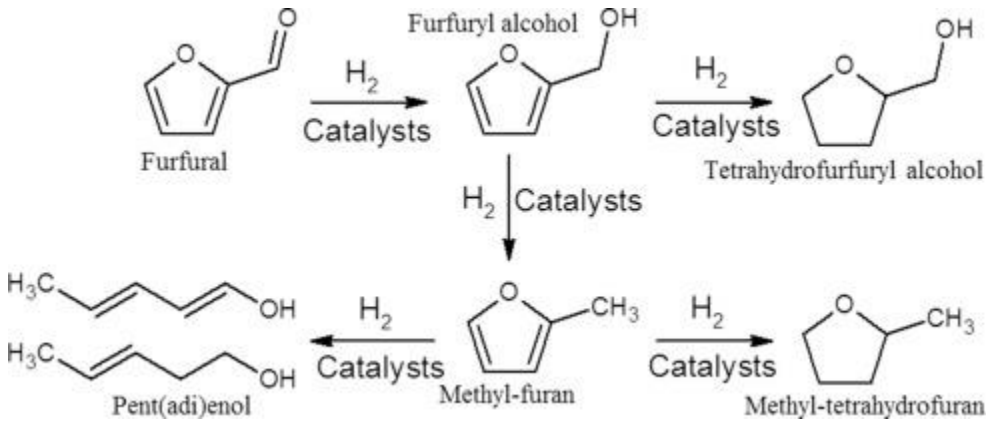

Scheme 1. Reaction pathway in the catalytic furfural hydrogenation using heterogeneous catalysts.

Despite the excellent conversion and selectivity of Pd catalysts, adding magnetic properties to the catalyst would be preferable for catalyst recovery through applying an external magnetic field, which would result in a more straightforward and cost-effective separation method as compared with conventional methods, as illustrated in previous reports [11–14]. Magnetically separable Pd based nanocomposite materials have shown good catalytic activities before in different organic synthesis, such as oxidation and C-C coupling [15–18]. Interestingly, temperature and pressure were reported to have significant positive effects to the reaction [19]. In previous work in our group on continuous flow furfural hydrogenation with hydrogen gas, relatively mild conditions were used (90 °C, 50 bar, 0.3 mL min^{-1}) [9]. In continuation of our previous work, we employ a lower catalyst loading, but at higher temperature and longer residence time, using both lab-synthesized and commercial catalysts to provide a comparison in terms of activity and stability. This study on hydroconversion of furfural attempts to further progress towards the industrial valorization of hemicellulose derived compounds in lignocellulosic biomass.

3.1.2. Experimental

3.1.2.1. Reagents

Chemicals were purchased from Sigma-Aldrich [Pluronic P123, tetraethyl orthosilicate, palladium (II) acetate, tetraammineplatinum (II) chloride hydrate, iron nitrate nanohydrate, furfural, furfuryl alcohol, tetrahydrofurfuryl alcohol, aluminum isopropoxide], Panreac [37% HCl, ethanol] and Merk [$Fe(NO_3)_3 \cdot 9H_2O$] respectively. All chemicals were used as purchased in the experiments without any further purification.

3.1.2.2. Synthesis of SBA-15 and Al-SBA-15

SBA-15 silica was prepared according to the procedure reported by Bonardet et al. [20]. More specific, Pluronic P123 surfactant (8.0 g) was dissolved into a solution of deionized water (260 mL) and HCl (12 M, 40 mL) under vigorous stirring at 40 °C for 2 h. Subsequently, 7 g of tetraethyl orthosilicate (TEOS) were added dropwise to the above solution. The mixture was stirred at 40 °C for 24 h, followed by hydrothermal treatment at 100 °C for 48 h in an oven. The liquid phase was removed by filtration and the obtained white solid was dried at 60 °C. The template was removed by calcination at 600 °C for 8 h. The Al-SBA support was synthesized using a modification of the protocol previously reported by our group [21]. After filtration and drying dried at RT, the solid was calcined under nitrogen atmosphere at 600 °C for 2 h and then in air for an additional 6 h.

3.1.2.3. Synthesis of Cu-Pd/Al-SBA-15

The continuous flow deposition of palladium oxide nanoparticles on Al-SBA-15 was performed under a series of conditions using a recently reported innovative continuous setup [22]. A stainless-steel reactor was packed with Al-SBA-15 support set between two plugs of quartz wool to prevent the solid support to move in the reactor upon pumping in the flow of the metal precursor feed solution. Separately, a 0.5 wt% Pd solution in ethanol was prepared using palladium (II) acetate as Pd precursor. The solution was filtered off prior to flow through the system to avoid the presence of any undissolved metal precursor. The system started with pumping

a solution of pure ethanol (0.5 mL min^{-1}, 5 min) through the catalyst bed to wet the support. The temperature of the reactor was then set to 150 °C and the feed was changed to the 0.5 wt% Pd solution. The incorporation was conducted under optimized flow rates (0.5 mL min^{-1}) and circulation time (15 min). At the end of the process, the feed was again switched to ethanol which was pumped through the Pd-incorporated catalyst to remove physisorbed/unreacted Pd species on the catalyst. The resulting Pd/Al-SBA-15 was recovered from the reactor and calcined at 400 °C for 4 h under air. Following, the Cu nanoparticles were supported on Pd/Al-SBA-15 material by a mechanochemical protocol using a planetary ball mill (Retsch 100) under previously reported optimized conditions (350 rpm, 10 min) [23] yielding the Cu-Pd/Al-SBA-15 bimetallic catalyst after calcination at 400 °C for 4 h in air.

3.1.2.4. Synthesis of (Pd,Pt)/SBA-15

Pd/SBA-15 and Pt/SBA-15 materials were synthesized following a previously reported mechanochemical protocol for the straightforward preparation of the supported metal nanoparticles on SBA–aluminosilicates [23]. The appropriate amount of Pd and Pt precursor (palladium (II) acetate and tetraammineplatinum (II) chloride hydrate, respectively) to reach the theoretical Pd and Pt contents of 2 wt% Pd and Pt, respectively. The pattern SBA-15 and precursor were milled together in a planetary ball mill (Retsch 100) under previously reported optimized conditions (350 rpm, 10 min) [23]. Upon incorporation of the metal, the sample was calcined at 400 °C (4 h, in air). The obtained materials were highly reproducible from batch to batch.

3.1.2.5. Synthesis of Pd/MAGSNC

5% Pd/MAGSNC was synthesized using a mechanochemical method according to the protocol reported previously by our group [24]. In detail, 0.5 g synthesized SBA-15 was grinded with 1.34 g $Fe(NO_3)_3 \cdot 9H_2O$, 0.25 mL propionic acid and an appropriate amount of the palladium precursor [$Pd(Ac)_2$] in a Retsch PM-100 planetary ball mill (18 10 mm stainless steel balls, 10 min, 350 rpm) to reach a theoretical 5 wt% Pd loading. The nanocomposite was slowly heated (1 °C min^{-1}) to 300 °C under air and kept at 300 °C for an additional 30 min.

3.1.2.6. Continuous flow hydrogenation

The hydrogenation of furfural was performed in a H-Cube Pro apparatus (ThalesNano, see Fig. S1 in the Supporting information (SI)). Both lab-synthesized and commercial catalysts (*ca.* 100 mg) were packed in CatCart cartridges, a stainless-steel tube with length of 70 mm and inner diameter 4 mm. The synthesized SBA catalysts based were swollen upon absorbing solvent; therefore, the SBA supported catalysts were first diluted with celite at 1:1 mass ratio prior to package. A feedstock solution of 0.2 M furfural in ethyl acetate (EA) was prepared as starting material. A filter was applied in the entrance of the pump to avoid undissolved compounds entering to the system. Prior to catalytic conversion experiments, EA was pumped through the continuous flow system. When reaching the desired reaction conditions in the reaction column (temperature, pressure and flow rate), the EA solvent feed was substituted by a 0.2 M furfural solution in EA. The flow rate and the hydrodynamic system pressure were set as 0.3 mL min^{-1} and 50 bar, identically as in the work reported previously reported by our group [9]. Full hydrogen mode was used in each reaction, which corresponds to a hydrogen production capacity of 60 mL/min in the H-Cube pro. The reactions took place upon contact of the catalyst with the mixture of feed solution and hydrogen in the CatCart column. After pumping the 0.2 M furfural feed, samples were taken from the product flow in the outlet at different time intervals. The time-on-stream was measured with the zero point at the moment that experimental reaction conditions were reached and after changing the feed from EA solvent to furfural solution in EA. The weight hourly space velocity (WHSV) was calculated by dividing the mass flow rate of the reagent with the catalyst mass. With the above described reaction conditions and catalyst loading, WHSV in the current work were between 3.3–4.6 h^{-1}. The WSHV values on metal weight basis were between 38 and 865 h^{-1}.

3.1.2.7. Product analysis and calculations

The product solution was analyzed by GC. Calibration curves (Fig. S2, see SI) were determined for furfural (F) and the two main products, furfuryl alcohol (FA) and tetrahydrofurfuryl alcohol (THFA). The other products, 2-methylfuran and/or pentenol, were only detected as traces. The calibration solutions and all collected samples were analyzed in an Agilent 6850 series II gas

chromatograph combined with an Agilent 5975C VL MSD system fitted with an HP-5MS-UI column (30 m × 0.25 mm × 0.25 μm i.d.). He in constant flow rate mode was used as carrier gas, which starting pressure was 0.88 bar. The initial temperature was 50 °C with 3 min hold time, then the temperature ramped to 200 °C in 3 min and stayed at 200 °C for another 3 min. Finally, the temperature was increased to 300 °C at 100 °C min^{-1} and held at 300 °C for 2 min. The conversion and selectivity were calculated as the following:

$$Furfural\ conversion\ (\%) = \frac{[C_{Initial} - C_{Final}]}{C_{Initial}} \times 100$$

$$Selectivity\ (\%) = \frac{C_{Product}}{[C_{F(Initial)} - C_{F(Final)}]}$$

Where C is the concentration of furfural or product (mmol mL^{-1}) as determined by GC.

3.1.2.8. Catalyst characterization

A VG Scientific photoelectron spectrometer ESCALAB-210 equipped with Mg Kα radiation (1486.6 eV) from an X-ray source was applied for the X-ray photoelectron spectroscopy (XPS) measurements, operated at 15 kV and 20 mA. Survey spectra in the energy range from 0 to 1350 eV were recorded using 0.4 eV steps for all the samples. High resolution spectra were recorded with 0.1 eV steps, 100 ms dwell time and 25 eV pass energy. A 90° take-off angle was set in all measurements. Curve fitting was carried out using the CasaXPS software, in which each component of the complex envelope is described as a Gaussian–Lorentzian sum function using a constant G/L ratio of 0.3 ± 0.05. The background was fitted using a nonlinear Shirley model. An aromatic carbon C 1 s peak at 284.5 eV was used as the reference of the binding energy.

Transmission electron microscopy (TEM) images of the selected samples were recorded using FEI Tecnai G2 equipment fitted with a CCD (Charge-coupled Device) camera for ease and speed of use at the SCAI (Research Support Service Center, University of Cordoba, Spain). The resolution of the equipment was around 0.4 nm. Prior to the recording, samples were suspended in ethanol assisted by sonication and followed by deposition on a copper grid.

Catalyst leaching was analyzed by ICP-MS in SCAI of University of Cordoba. The selected samples were transferred to 25 mL falcon tube and dried in oven to evaporate the organic compounds. Subsequently, 20 mL 2% HNO_3 and 0.5% HCl aqueous solution was used to digest the solid components. Samples were then immediately analyzed in an ICP/MS Perkin Elmer ELAN-DRC-e model equipped with an automatic diluting injecting system and ionization under Ar plasma followed by quadrupole ion detection with a DRC cell to remove potential interferences.

3.1.3. Results and discussion

In previously reported work on furfural conversion using a Cu-Fe catalyst reaction temperature and pressure showed significant effects on conversion and selectivity [19]. In the present study, we first tested the 5% Pd/MAGSNC at two different temperatures (90 and 150 °C). After 120 min streaming in continuous flow at 90 °C, the furfural conversion decreased from >99% to *ca.* 41%, while the selectivity also varied strongly, as shown in Figure 1. Meanwhile, the furfural conversion (95–99%) and the product selectivity (74–90% to FA) maintained relatively stable after streaming for 20 and 120 min at 150 °C. Remarkably, the catalytic performance of 5% Pd/MAGSNC was more stable at higher temperature (150 °C). Therefore, the temperature was set as 150 °C in the following catalytic tests.

Various lab-synthesized and commercial catalysts were tested for the hydrogenation of furfural in identical conditions. Interestingly, the major product in the reaction catalyzed by 10% Pd/C was THFA instead of pentenol in our previous work [9], showing the high impact of the reaction temperature and the WHSV on the product selectivity. The WHSV in the current work was 3.80 h^{-1} for 2% Pd/SBA-15, 5% Pd/MAGSNC and 10% Pd/C, respectively, which is much higher than the corresponding reported WSHV value of 1.73 h^{-1}[9]. All the Pd catalysts exhibited high catalytic activity in furfural conversion, except for the Cu-Pd/Al-SBA-15 catalyst, whereas the Pt catalysts were less active (Figure 2**a**). Apart from the catalytic activity, the Pd catalysts and Pt catalysts also showed difference in the product selectivity. While Pd catalysts supported on SBA-15 or carbon showed higher selectivity to THFA, 5% Pd/MAGSNC and Pt catalysts were more favorable in the formation of FA. Despite the Pd content, the main difference between 5%

Pd/MAGSNC and 2% Pd/SBA-15 was the introduction of Fe_2O_3 in the synthesis of the corresponding supports, which in turn influences for instance the dispersion of Pd particles on the support. The introduction of pure Fe into Pd catalysts has shown to increase its catalytic activity in hydrogenation of furfural drastically, at least in aqueous phase [25]. Upon furfural adsorption onto the Pd or Pt surface η^2-(C–O) surface species were formed, where the first H could attack the carbonyl O, forming hydroxyalkyl surface species which could be subsequently reduced to form furfuryl alcohol [10,26,27]. The difference in reaction activity between Pd catalysts and Pt catalysts could probably be attributed to the strong affinity and sorption of H_2 on the palladium surface [28]. Besides, Pd and Pt nanoparticles also behave differently in the affinity and sorption of furfural. In detail, Pt favors the sorption of C═O bonds [29] and has strong electron repulsive interaction between furan ring π-electrons and metal d-electrons, whereas Pd shows strong affinity to not only C═O bonds but also to the furan ring π-electrons [10,30,31]. Thus, Pt catalysts shows higher selectivity to FA while Pd catalysts has higher selectivity to THFA.

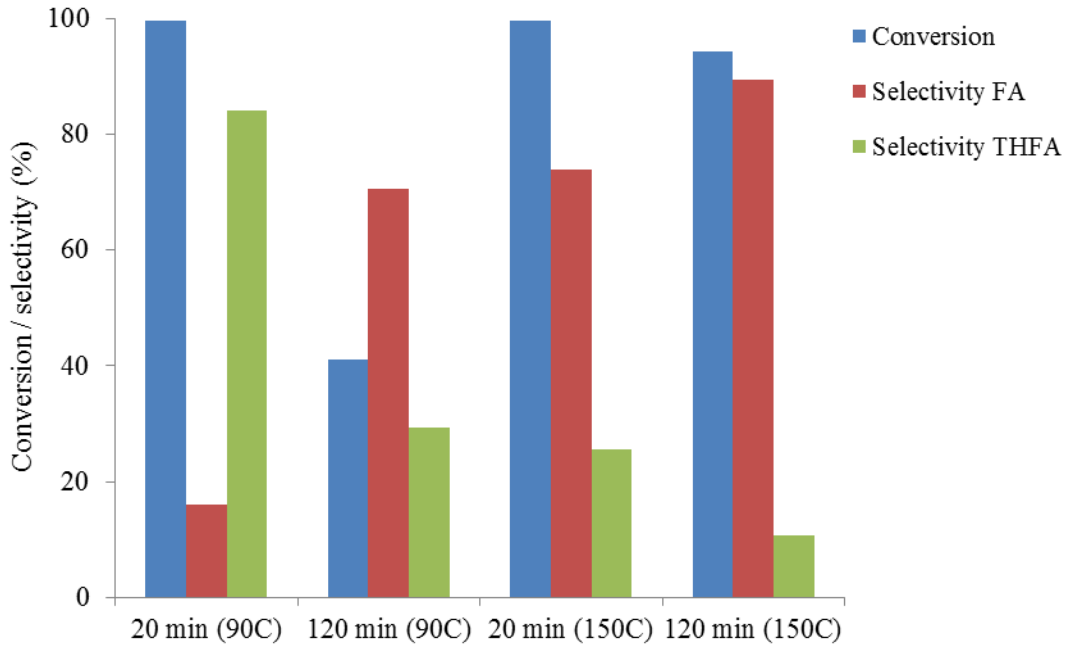

Figure 1. Performance of 5% Pd/MAGSNC for the conversion of furfural under continuous flow regime in function of time-on-stream and temperature. Reaction conditions: 0.2 M furfural, 0.3 mL min^{-1}, 50 bar.

After streaming for 120 min (Figure 2**b**), some of the catalysts maintained high activity for the conversion of furfural but with rather small differences in the product selectivity, including 5% Pd/MAGSNC, 2% Pd/SBA-15 and 10% Pd/C. The sharp drop of conversion for the 0.5% Pd/SBA-15 catalyst might be due to Pd leaching during the reaction, but no Pd in the sample was detected in the ICP-MS data (Table 1) which could be resulted from the low Pd content in the collected samples. Although the selectivity of the Pt catalysts remained consistent and high, the conversion of furfural was much lower than the three Pd catalysts mentioned before.

Table 1. Elemental analysis of collected samples using ICP-MS

Time-on-stream (min)	Element content in the sample (μg/L)					
	5% Pd/MAGSNC		2% Pd/SBA-15	0.5% Pd/SBA-15	10% Pd/C	5% Pt/C
	Fe	Pd	Pd	Pd	Pd	Pt
20	66	5	ND[1]	ND	ND	ND
120	16	ND	ND	ND	ND	ND
140	13	ND	ND	/[2]	ND	ND
240	44	ND	ND	/	ND	ND
360	/	/	13	/	ND	ND
480	60	ND	ND	/	ND	ND
720	/	/	ND	/	ND	ND
1560	/	/	/	/	ND	/

[1] ND represents not detected

[2] "/" represents no sample

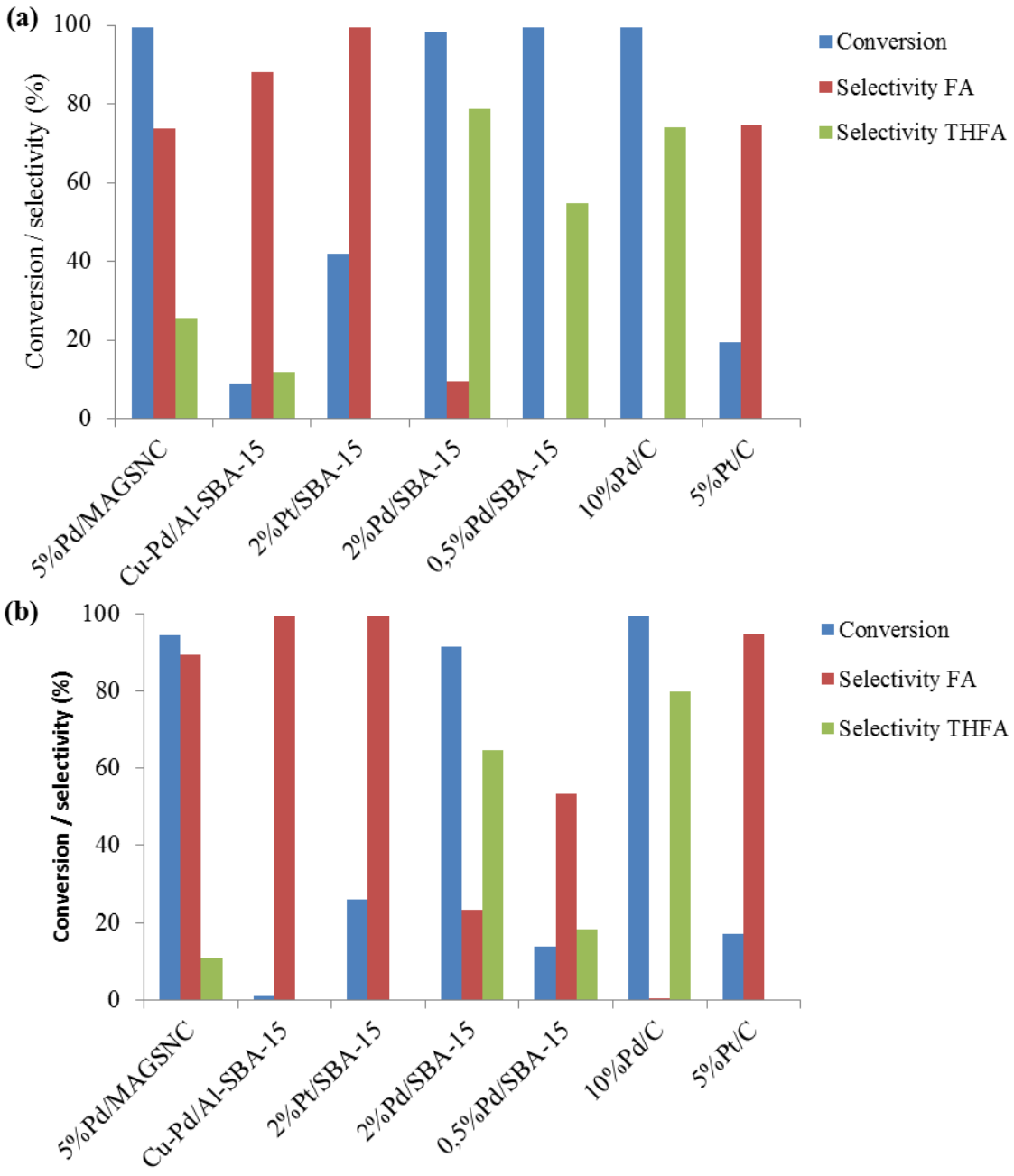

Figure 2. Performance of various Pd and Pt catalysts for the conversion of furfural under continuous flow regime after **(a)** 20 min time-on-stream and **(b)** 120 min time-on-stream. Reaction conditions: 0.2 M furfural, 0.3 mL min^{-1}, temperature = 150 °C, 50 bar.

Hence, the experiments were repeated with 5% Pd/MAGSNC, 2% Pd/SBA-15 and 10% Pd/C to investigate their long-term stability, with times-on-stream between 480 and 1560 min. (Figure

3). The furfural conversion using 5% Pd/MAGSNC and 2% Pd/C was reduced to *ca.* 50% after 480 and 600 min, respectively, but 5% Pd/MAGSNC showed higher stability in the selectivity. The conversion with the 10% Pd/C catalyst in turn remained over 98% after streaming for 1560 min while the selectivity to THFA decreased from 83 to 64%. It exhibited the highest stability among all the catalysts tested. Notably, lab-synthesized catalysts (5% Pd/MAGSNC and 2% Pd/SBA-15) with relatively low Pd content showed strong catalytic activity in the first a few hours as compared with the commercial 10% Pd/C, and even outperformed 5% Pt/C in the hydrogenation of furfural.

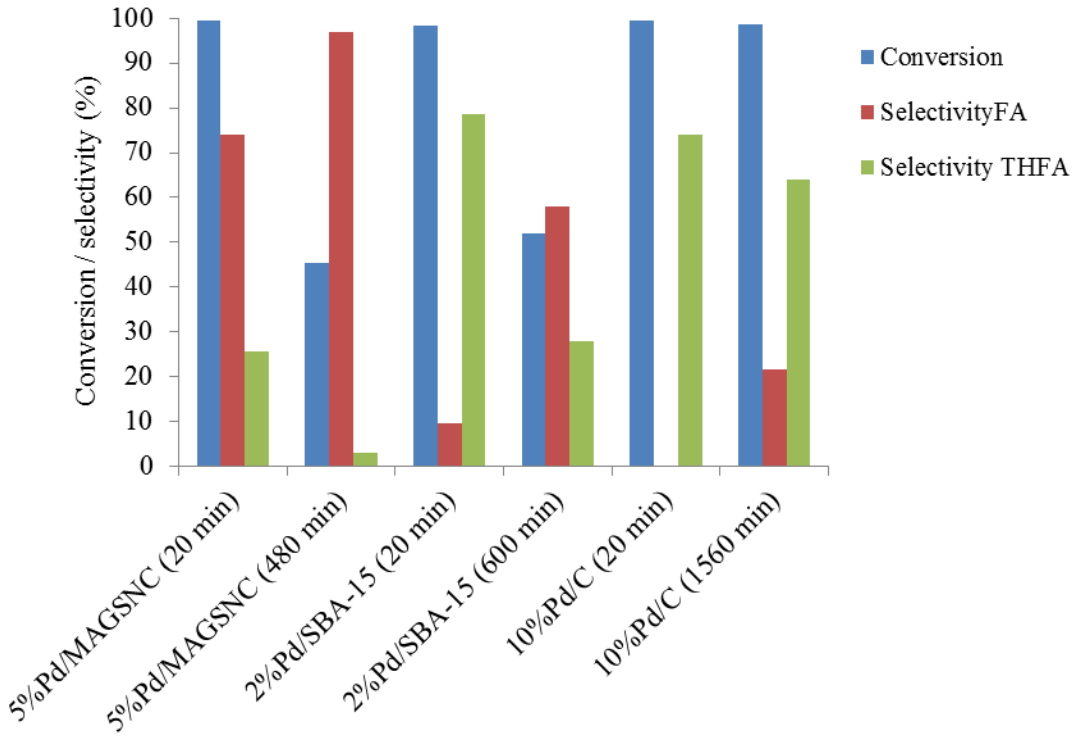

Figure 3. Long term stability of 5% Pd/MAGSNC, 2% Pd/SBA-15 and 10% Pd/C catalysts for the conversion of furfural under continuous flow regime. Reaction conditions: 0.2 M furfural, 0.3 mL min^{-1}, temperature = 150 °C, 50 bar.

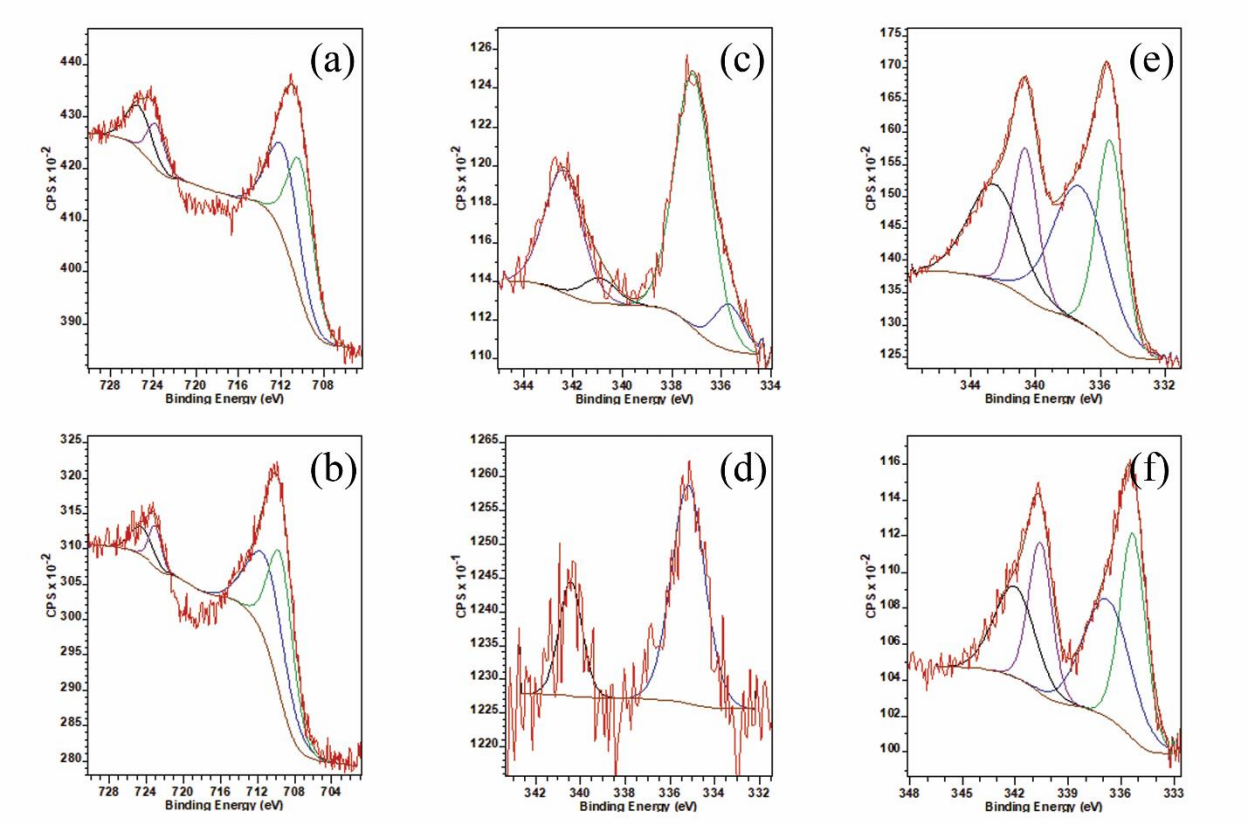

Figure 4. XPS spectra of Fe2p in **(a)** fresh and **(b)** spent 5% Pd/MAGSNC; Pd3d in **(c)** fresh and **(d)**spent 5% Pd/MAGSNC and Pd3d in **(e)** fresh 10% Pd/C and **(f)** spent 10% Pd/C.

To understand better the reaction mechanism, XPS spectra of the fresh and spent 5% Pd/MAGSNC and 10% Pd/C catalysts were recorded. The spectra of Fe2p confirmed the presence of Fe^{3+} on the catalysts surface before and after reaction (Figure 4**a**–**b**), consistent with the well-preserved magnetic property of the catalysts after long time streaming. This facilitates the separation of 5% Pd/MAGSNC from celite in order to attempt to reactivate the catalyst. The main peak (5/2 orbital) of Pd3d shifted from *ca.*337.1 to 335.7 eV (Figure 4**c**–**d**), indicating the reduction of Pd^{2+} species on the catalysts surface. This difference could be responsible for the change in catalytic performance of 5% Pd/MAGSNC during the time-on-stream. Although leaching of Pd also can be expected, the peak intensity in the spectrum of the spent catalyst was very similar as in the fresh catalyst. Elemental analysis could provide more reliable results to confirm any leaching effect. In comparison, the Pd3d spectra of the fresh and spent commercial 10% Pd/C catalysts did not show any peak shift, as the initial catalyst was already in the reduced

state (335.7 eV). The intensities of both the 5/2 and 3/2 peaks did decrease with respect to the intensities in the fresh catalyst, which indicates leaching of Pd from the carbon support. These results show that the evolution of the Pd oxidation state is the main factor to keep the catalytic activity high. Additionally, TEM micrographs of the 5% Pd/MAGSNC and 10% Pd/C catalysts (Figure 5) were recorded in which the structures of the catalysts were maintained well after long term stability tests.

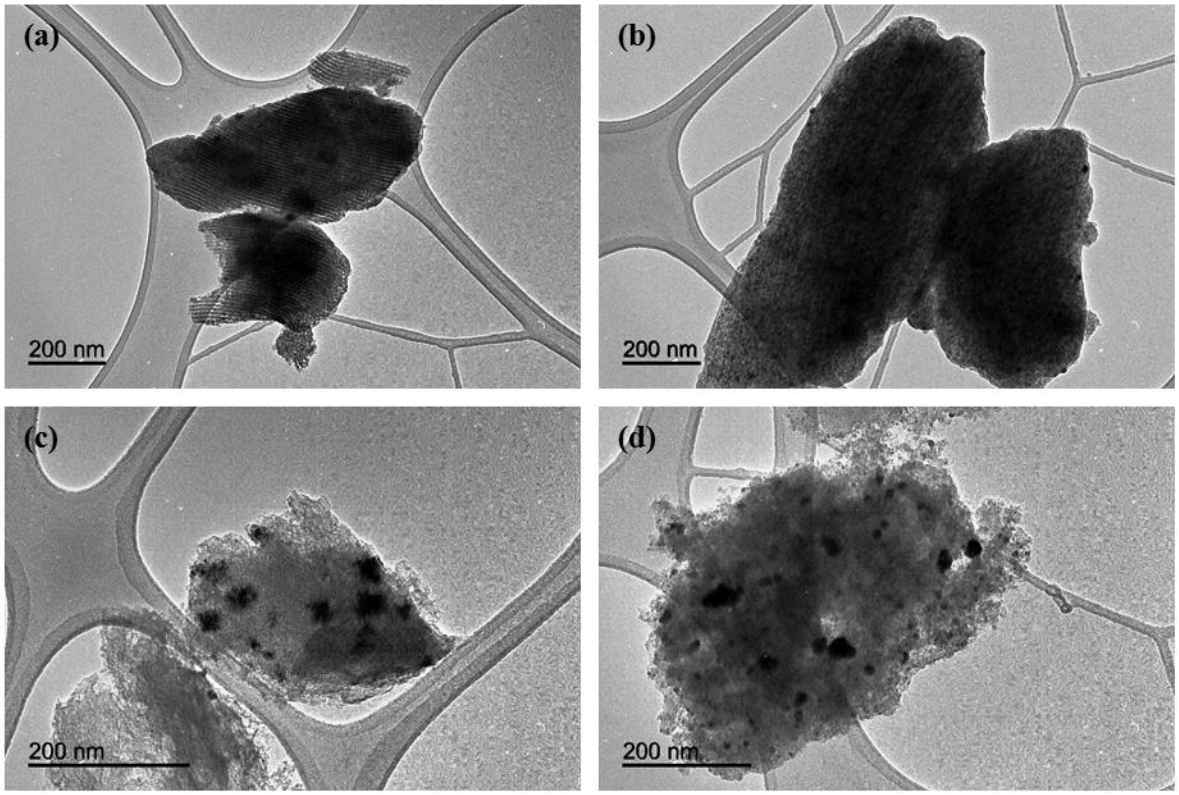

Figure 5. TEM images of **(a)** fresh and **(b)** spent 5% Pd/MAGSNC catalysts, and **(c)** fresh and **(d)**spent 10% Pd/C catalysts.

Catalyst leaching is a challenging issue in heterogeneous catalysis, which is difficult to avoid. Likewise, there was slight catalyst leaching in the hydrogenation of fufrfural, though it might not be detected by ICP-MS (Table 1). Continuously leaching of Fe content on 5% Pd/MAGSNC was observed, which might also contribute to the changes in the catalysts acvtivity because presence of Fe promotes the catalytic activity of Pd [25].

3.1.4. Conclusions

Continuous flow hydrogenation of furfural was performed with both lab-synthesized and commercial catalysts in the current work. Based on previous and present results, the temperature and the weight hourly space velocity (WHSV) were factors that affected the furfural conversion and product selectivity drastically. The lab-synthesized catalyst (5% Pd/MAGSNC) offered comparable performance to the 10% Pd/C within the first few hours. Furthermore, its well-preserved magnetic property offers a simple, efficient method for catalyst recovery from solid solution by applying a magnetic field, which is easier for catalyst reactivation. We do believe that findings in the current work offer a possibility for the valorization of biomass derived platform molecules in continuous flow system with easy recovered catalyst.

Acknowledgements

Rafael Luque gratefully acknowledges Consejeria de Ciencia e Innovacion, Junta de Andalucia for funding project P10-FQM-6711. Funding from Marie Curie Actions under ITN Project Photo4Future (H2020-MSCA-ITN-2014-641861), especially for funding WO Ph.D studies. We also greatly acknowledge ThalesNano Inc. for all supports, including the continuous flow reactor, H-Cube Pro, commercial catalysts and chemicals for the hydrogenation reactions.

References

[1] H. C. J. Godfray, J. R. Beddington, I. R. Crute, L. Haddad, D. Lawrence, J. F. Muir, J. Pretty, S. Robinson, S. M. Thomas, C. Toulmin, *Science (80-.).* **2010**, *327*, 812–818.

[2] J.-P. Lange, E. van der Heide, J. van Buijtenen, R. Price, *ChemSusChem* **2012**, *5*, 150–166.

[3] H. E. Hoydonckx, W. M. Van Rhijn, W. Van Rhijn, D. E. De Vos, P. A. Jacobs, H. E. Hoydonckx, W. M. Van Rhijn, W. Van Rhijn, D. E. De Vos, P. A. Jacobs, in *Ullmann's Encycl. Ind. Chem.*, Wiley-VCH Verlag GmbH & Co. KGaA, Weinheim, Germany, **2007**.

[4] P. Panagiotopoulou, D. G. Vlachos, *Appl. Catal. A Gen.* **2014**, *480*, 17–24.

[5] R. V. Sharma, U. Das, R. Sammynaiken, A. K. Dalai, *Appl. Catal. A Gen.* **2013**, *454*, 127–136.

[6] M. M. Villaverde, N. M. Bertero, T. F. Garetto, A. J. Marchi, *Catal. Today* **2013**, *213*, 87–92.

[7] N. S. Biradar, A. A. Hengne, S. N. Birajdar, R. Swami, C. V. Rode, *Org. Process Res. Dev.* **2014**, *18*, 1434–1442.

[8] K. Fulajtárova, T. Soták, M. Hronec, I. Vávra, E. Dobročka, M. Omastová, *Appl. Catal. A Gen.* **2015**, *502*, 78–85.

[9] A. J. Garcia-Olmo, A. Yepez, A. M. Balu, A. A. Romero, Y. Li, R. Luque, *Catal. Sci. Technol.* **2016**, *6*, 4705–4711.

[10] V. Vorotnikov, G. Mpourmpakis, D. G. Vlachos, *ACS Catal.* **2012**, *2*, 2496–2504.

[11] M. Ojeda, A. M. Balu, V. Barrón, A. Pineda, Á. G. Coleto, A. Á. Romero, R. Luque, *J. Mater. Chem. A* **2014**, *2*, 387.

[12] J. C. Colmenares, W. Ouyang, M. Ojeda, E. Kuna, O. Chernyayeva, D. Lisovytskiy, S. De, R. Luque, A. M. Balu, *Appl. Catal. B Environ.* **2016**, *183*, 107–112.

[13] C. Zhang, L. Qiu, F. Ke, Y. Zhu, Y. Yuan, G. Xu, X. Jiang, *J. Mater. Chem. A* **2013**, *1*, 14329.

[14] M. B. Gawande, P. S. Branco, I. D. Nogueira, C. A. A. Ghumman, N. Bundaleski, A. Santos, O. M. N. D. Teodoro, R. Luque, *Green Chem.* **2013**, *15*, 682.

[15] J. R. Dodson, E. C. Cooper, A. J. Hunt, A. Matharu, J. Cole, A. Minihan, J. H. Clark, D. J. Macquarrie, *Green Chem.* **2013**, *15*, 1203.

[16] J. Liu, X. Peng, W. Sun, Y. Zhao, C. Xia, *Org. Lett.* **2008**, *10*, 3933–3936.

[17] H. Wang, Y. Liu, M. Li, H. Huang, H. M. Xu, R. J. Hong, H. Shen, *Optoelectron. Adv. Mater. Rapid Commun.* **2010**, *4*, 1166–1169.

[18] S. Verma, D. Verma, A. K. Sinha, S. L. Jain, *Appl. Catal. A Gen.* **2015**, *489*, 17–23.

[19] K. Yan, J. Liao, X. Wu, X. Xie, *RSC Adv.* **2013**, *3*, 3853.

[20] B. Jarry, F. Launay, J. P. Nogier, V. Montouillout, L. Gengembre, J. L. Bonardet, *Appl. Catal. A Gen.* **2006**, *309*, 177–186.

[21] M. J. Gracia, E. Losada, R. Luque, J. M. Campelo, D. Luna, J. M. Marinas, A. A. Romero, *Appl. Catal. A Gen.* **2008**, *349*, 148–155.

[22] A. Yepez, F. L. Y. Lam, A. A. Romero, C. O. Kappe, R. Luque, *ChemCatChem* **2015**, *7*, 276–282.

[23] A. Pineda, A. M. Balu, J. M. Campelo, A. A. Romero, D. Carmona, F. Balas, J. Santamaria, R. Luque, *ChemSusChem* **2011**, *4*, 1561–1565.

[24] M. Ojeda, A. Pineda, A. a. Romero, V. Barrón, R. Luque, *ChemSusChem* **2014**, *7*, 1876–1880.

[25] J. Lee, Y. T. Kim, G. W. Huber, *Green Chem.* **2014**, *16*, 708.

[26] S. Sitthisa, T. Pham, T. Prasomsri, T. Sooknoi, R. G. Mallinson, D. E. Resasco, *J. Catal.* **2011**, *280*, 17–27.

[27] B. Liu, L. Cheng, L. Curtiss, J. Greeley, *Surf. Sci.* **2014**, *622*, 51–59.

[28] M. Yamauchi, R. Ikeda, H. Kitagawa, M. Takata, *J. Phys. Chem. C* **2008**, *112*, 3294–3299.

[29] F. Delbecq, P. Sautet, *J. Catal.* **2002**, *211*, 398–406.

[30] A. Giroir-Fendler, D. Richard, P. Gallezot, **1988**, pp. 171–178.

[31] S. Bhogeswararao, D. Srinivas, *J. Catal.* **2015**, *327*, 65–77.

Appendix A. Supplementary data

Contents lists available at ScienceDirect

Catalysis Today

journal homepage: www.elsevier.com/locate/cattod

Towards industrial furfural conversion: Selectivity and stability of palladium and platinum catalysts under continuous flow regime

Weiyi Ouyang*, Alfonso Yepez, Antonio A. Romero, Rafael Luque*

a Departamento de Quimica Organica, Universidad de Cordoba, Edificio Marie Curie(C-3), Ctra Nnal IV-A, Km 396, E14014 Córdoba, Spain

* *Corresponding authors. E-mail addresses: qo2ououw@uco.es (W. Ouyang), q62alsor@uco.es (R. Luque).*

Supporting Information

Figure S1 shows the continuous flow equipment used for the catalytic hydrogenation of furfural in ethyl acetate. **Figure S2** shows the calibration curve for furfural, furfuryl alcohol and tetrahydrofurfuryl alcohol.

Figure S21. H-Cube Pro apparatus (ThalesNano, Budapest, Hungary).

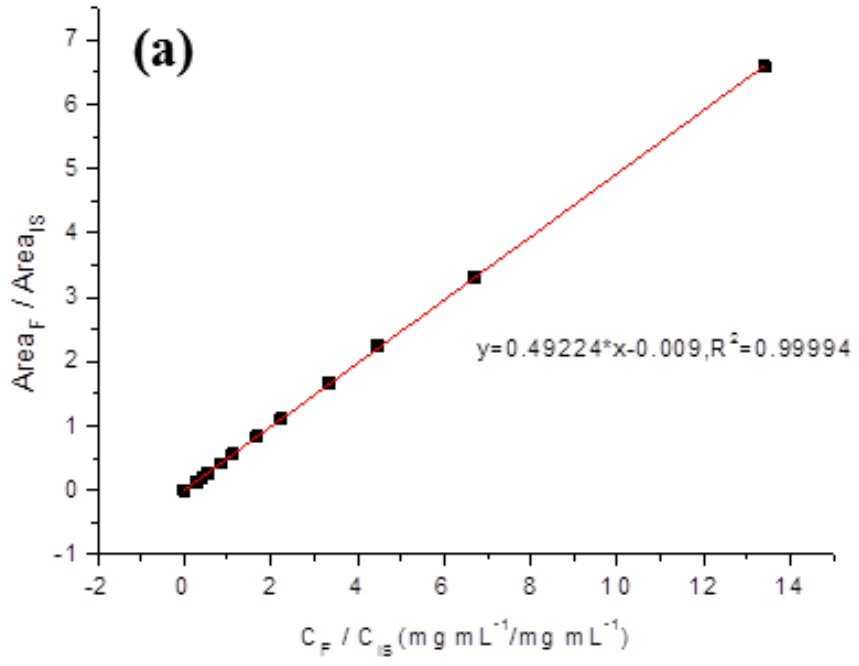

Figure S2. Calibration curve for furfural, furfuryl alcohol and tetrahydrofurfuryl alcohol

Contents lists available at ScienceDirect

Journal of Environmental Management

journal homepage: www.elsevier.com/locate/jenvman

3.2. Wheat Bran Valorization: Towards Photocatalytic Nanomaterials for Benzyl Alcohol Photo-Oxidation

Weiyi Ouyang[a], Jose M. Reina[a], Ewelina Kuna[b], Alfonso Yepez[a], Alina M. Balu[a], Antonio A. Romero[a], Juan Carlos Colmenares[b], Rafael Luque*[a]

[a]*Departamento de Quimica Organica, Universidad de Cordoba, Edificio Marie Curie(C-3), Ctra Nnal IV-A, Km 396, E14014 Córdoba, Spain, e-mail: q62alsor@uco.es*

[b]*Institute of Physical Chemistry PAS, Kasprzaka 44/52, 01-224 Warsaw (Poland)*

Article first published online: 1 December 2017

DOI: 10.1016/j.jenvman.2016.07.013

Abstract

In this work, we have successfully synthesized a set of titania photocatalytic nanocomposites by the incorporation of different TiO_2 content on wheat bran residues. The obtained catalysts were characterized by different techniques including UV-Vis spectroscopy, X-ray diffraction (XRD), X-ray photoelectron spectroscopy (XPS) and Transmission Electron Microscopy (TEM) while their photocatalytic activity was investigated in the oxidation of benzyl alcohol under UV light irradiation. Benzaldehyde yields were ca. 20%, with conversion in the systems of ca. 33% of benzyl alcohol by using 10%Ti-Bran catalyst, as compared to 33% yield to the target product

(quantitative conversion of benzyl alcohol) using commercial pure TiO_2 (P-25). The photocatalytic activity results indicate that designed waste-derived nanomaterials with low TiO_2 content can efficiently photocatalyze the conversion of benzyl alcohol with relative high selectivity towards benzaldehyde.

Keywords: waste valorization, wheat bran, photocatalysis, benzyl alcohol oxidation

3.2.1. Introduction

Environmentally friendly and energy-saving technologies are becoming increasingly advantageous with the increase of public awareness on environment protection and sustainable development, Since the discovery of photocatalytic splitting of water on TiO2 electrodes [1], semiconductor-based heterogeneous photocatalysis has received extensive attention and now is considered as one of the most relevant and environmentally friendly technologies with advantages including simplicity, environmental compatibility, low-cost and energy-saving.

To assess the photocatalytic activity of a semiconductor photocatalyst, several factors should be taken into consideration, including stability, efficiency, selectivity and the wavelength range response [2]. Among different semiconductor-based photocatalysts, TiO_2 is one of the most attractive photocatalyst owing to its outstanding photocatalytic activity, high thermal and chemical stability, non-toxicity, cost effectiveness and the strong oxidizing power of the photogenerated holes. Massive investigations on TiO_2 photocatalyst have been reported in different applications in the last decades, including chemicals and fuels production from CO_2 reduction [3–5], decontamination of water [6–9], organic synthesis [10–13] and production of H_2 from water splitting [14,15]. However, the use of pure TiO_2 photocatalyst is limited by its large band gap (3.2eV, anatase crystalline phase) which requires light with wavelength $\lambda<387$ nm for the excitation of electrons from the valence to the conduction band, resulting that only 5% of the solar irradiation can be utilized for the photocatalytic process. Modifications on TiO_2 are necessary to improve its photocatalytic properties under solar irradiation or artificial light source. Modifications

such as introductions of metals, dopants or combinations with other semiconductors are beneficial in suppressing the recombination of the photogenerated electron-hole pairs and thus increasing the quantum yield of the photocatalytic process [2]. Meanwhile, the new created heterojunctions can help the photocatalyst expand the wavelength range response into visible light region.

Many reported investigations have revealed that doping with non-metal atoms, such as C, N, F, P or S, can significantly improve the photocatalytic activity of TiO_2 under visible light. [7,16–22] Co-doping of C and N was investigated [8,23], and metal and non-metal atoms co doping was also reported to have high visible light response [21,24,25].

Selective oxidation of benzyl alcohol to benzaldehyde is an attractive research topic since benzaldehyde is extensively used in food, perfumery and pharmaceutical industries, as well as its use as precursor in various chemical industries. Moreover, the study of conversion of benzyl alcohol to benzaldehyde can potentially provide the reactivity and transformation strategies for the valorization of lignocellulose-based biomass. Photocatalytic oxidation of benzyl alcohol towards benzaldehyde with high selectivity has been reported in recent years [12,13,26–28], which provide a possible substitution to the traditional synthetic routes - either by benzyl chloride hydrolysis or through oxidation of toluene. A review on transformation of biomass-derived compounds with heterogeneous photocatalytic nanomaterials was also recently reported [29]. The target product (benzaldehyde) is a well-known specialty chemical with a large market value and important applications in the flavoring, fragrances and cosmetics industries, present in a wide range of commercial formulations.

In the present investigation, we have developed a novel, low cost TiO_2 photocatalytic nanocomposite (denoted as Ti-Bran) derived from the valorization of a widespread and highly abundant industrial waste such as wheat bran. Catalysts with different TiO_2 content on the wheat bran support were synthesized. The photocatalytic activity was tested by the oxidation of benzyl alcohol to benzaldehyde. Different techniques were applied in the characterization of the catalyst including Nitrogen physisorption, X-ray diffraction (XRD), X ray photoelectron spectroscopy (XPS), Transmission Electron Microscopy (TEM) and UV Vis spectroscopy.

3.2.2. Material and methods

Titanium isopropoxide (IV), Sigma-Aldrich 99%, wheat bran was kindly donated by a local company as by product of wheat refining for food products. All remaining reagents including benzyl alcohol and acetonitrile (99%, Sigma-Aldrich) and related others were used as purchased.

3.2.2.1. Catalyst synthesis

For the catalyst synthesis, several different nanomaterials were prepared an investigated with the same quantity of waste starting material (wheat bran, 5 g) and different quantities of titanium isopropoxide as illustrated on Table S1 to reach different theoretical contents of titanium (from 0.5 to 10 wt%) in the final material. In a typical synthesis, the respective mixtures containing wheat bran (5 g) and the different quantities of titanium precursor were milled in a planetary ball mill RETSCH PM 100 model under previously optimized conditions (350 rpm, 30 mins) (Francavilla et al. 2014). 18 stainless steel balls (1 cm diameter) were utilized in the stainless-steel milling chamber. After milling, the final powdery mixture was collected and subjected to calcination at 400 ºC for 5 h (heating ramp 3 ºC min^{-1}) to partially remove the organic matter from the wheat bran, leaving a nice brownish Ti-Bran final product. Only a 6-15% of the weight of the initial mixture was obtained after calcination, indicating that most of the wheat bran (organic material) was eliminated in the calcination step. The temperature used for calcination was 400 ºC because of the preferential formation of anatase phase at lower temperatures (450 ºC and below) as compared to the formation of a rutile poorly active phase in photocatalysis obtained at higher temperatures [29].

3.2.2.2. Materials characterization

Nitrogen porosimetry studies were conducted in a Micromeritics ASAP 2000 volumetric adsorption analyzer at 77 K. Samples were degassed at 100 ºC during 24 h under vaccuum ($p < 10^{-2}$ Pa) prior to analysis. The linear part of the BET equation (partial pressures in the 0.05 and 0.30 range) was used to determine the specific surface area. The pore size distribution was

calculated from the adsorption branch of the N_2 physisorption isotherms using the Barret-Joyner-Halenda (BJH) formula. The cumulative mesopore volume V_{BJH} was obtained from the PSD curve.

XRD patterns were obtained in a Bruker D8 DISCOVER A25 diffractometer equipped with a vertical goniometer under theta-theta geometry using Ni filtered Cu Kα (λ=1,5418 Å) radiation and operated at 40KeV and 40mA. Wide angle scanning patterns were collected from 10 to 80º with a step size of 0.01º and counting time of 500 seconds per step.

The light absorption properties of the photocatalysts were investigated through UV-Vis spectroscopy. UV–Vis diffuse reflectance spectra were recorded on UV/VIS/NIR spectrophotometer Jasco V-570 equipped with an integrating sphere. The baseline was recorded using Spectralon™ (poly(tetrafluoroethylene) as a reference material. The Kubelka-Munk method based on the diffuse reflectance spectra was applied to determine the band gap function. The E_g was calculated form $(f(R)h\nu)^{1/2}$ versus hν plots. The function f(R) was calculated from the following equation (1):

$$f(R) = \frac{(1-R)^2}{2R} \qquad (1)$$

XPS measurements were conducted at an ultrahigh vacuum (UHV) multipurpose surface analysis system (Specs™ model, Germany) at the SCAI in Universidad de Cordoba, operating at pressures $<10^{-14}$ MPa using a conventional X-Ray source (XR-50, Specs, Mg-Kα, 1253.6 eV) in a "stop-and-go" mode to reduce potential damage due to sample irradiation. The survey and detailed high-resolution spectra (pass energy 25 and 10 eV, step size 1 and 0.1 eV, respectively) were recorded at room temperature using a Phoibos 150-MCD energy analyzer. Powdered samples were deposited on a sample holder using double sided adhesive tape and subsequently evacuated under vacuum ($<10^{-6}$ Torr) overnight. Eventually, the sample holder containing the degassed sample was transferred to the analysis chamber for XPS studies. Binding energies were referenced to the C1s line at 284.6 eV from adventitious carbon.

Transmission Electron Microscopy (TEM) images for selected Ti-Bran nanocomposites were recorded in a FEI Tecnai G2 fitted with a CCD camera for ease and speed of use at the SCAI from

Universidad de Cordoba. The resolution is around 0.4 nm. Samples were suspended in ethanol and deposited straight away on a copper grid prior to analysis.

ICP-MS experiments were conducted at the SCAI of Universidad de Cordoba. Prior to analysis and metal quantification, samples were prepared by treating 0.05 g of nanocomposite material with 1 mL concentrated HF (till complete dissolution of the powder) in special recipients. In some cases, a few drops of HNO_3 and HCl were also added to ensure complete dissolution of the samples, which were subsequently topped with milli Q water to 25 mL total volume. Samples were then immediately analyzed in an ICP/MS Perkin Elmer ELAN-DRC-e model equipped with an automatic diluting injecting system and ionization under Ar plasma followed by quadrupole ion detection with a DRC cell to remove potential inferences.

3.2.2.3. Photocatalytic activity experiments

The photocatalytic activity of the synthesized Ti-Bran catalysts was tested in the oxidation of benzyl alcohol to benzaldehyde. All reactions were performed in a Pyrex cylindrical double-walled immersion well reactor equipped with medium pressure 125W mercury lamp (λ= 365 nm), supplied by Photochemical Reactors Ltd. UK (Model RQ 3010). A homogeneous suspension of the catalyst was obtained by means of magnetic stirring at 1100 rpm. Benzyl alcohol was prepared in acetonitrile medium with an initial concentration of 1.5 mM. The reaction temperature was set at 30 °C. Experiments were performed from 150 mL of the mother solution with catalyst loading of 1 g/L under UV light for 4 hours. Air bubbling was also applied with a flow rate at 25 mL/min. The reaction solution was put into dark environment for 30 min prior to the reaction in order to equilibrate the adsorption-desorption over the photocatalyst surface. At each sampling point, 1 mL sample was collected directly from the reactor and filtered (0.20, 20 µm, 25 mm, nylon filters). High performance liquid chromatography (HPLC, Waters Model 590 pump) equipped with a Dual Absorbance Detector (Waters 2487) and the SunFire™ C18 (3.5µm, 150 mm length, 4.6 mm inner diameter) column provided by Waters was applied to determine the concentration of the model compound. The mobile phase was Milli-Q water/acetonitrile/methanol in the volumetric ratio of

77.5: 20: 2.5 with 0.1% of H_3PO_4. The isocratic elution flow rate was 1 mL/min and the injection volume was 10 µL.

3.2.3. Results and discussion

The synthesized nanocomposites denoted as Ti-Bran were characterized using a number of analytical techniques. Nitrogen physisorption isotherms of Ti-containing nanocomposites indicated the presence of a certain interparticle macro/mesoporosity in the materials after the calcinations process, most probably due to the removal of some organics from the decomposition of wheat bran (Figure S1). Materials were essentially non-porous in nature, as expected from wheat bran, although the observed interparticle porosity was reflected in the observed not negligible surface areas (<20 m^2 g^{-1}, Table 1).

Table 1. Textural properties and Ti content of Ti-Bran nanocomposites

Sample	Surface area (m^2/g)	Pore size (nm)	Pore volume (cm^3/g)	Ti content[a] (wt%)	Titania nanoparticle size[b] (nm)
Bran	<5	-	-	-	-
0.5% Ti-Bran	10	27	0.07	8.1	4.6 (5)
1% Ti-Bran	12	32	0.09	14.0	5.7 (6)
2% Ti-Bran	15	35	0.1	24.6	5.2 (6)
5% Ti-Bran	13	25	0.1	36.5	6.2 (7)
10% Ti-Bran	20	30	0.1	41.4	7.8 (10)

a Ti content measured by ICP/MS

b nanoparticle sizes was calculated using the Scherrer equation as compared to average particle size by TEM (in brackets), respectively

XRD patterns compiled in Figure 1 pointed to the clear presence of a distinctive anatase phase in the materials, together with the presence of additional crystalline phases (not quantified) of a range of metal oxides in low quantities including Zn, Mn and related trace elements detected in

ICP/MS analysis (not quantified). All materials exhibited almost identical XRD patterns differing only in terms of the intensity of the main diffraction lines. The calculated titania nanoparticle size using the Scherrer equation from XRD patterns was of ca. 4.6-7.8 nm for all synthesized nanomaterials, slightly increasing at high Ti loadings in the materials (Table 1).

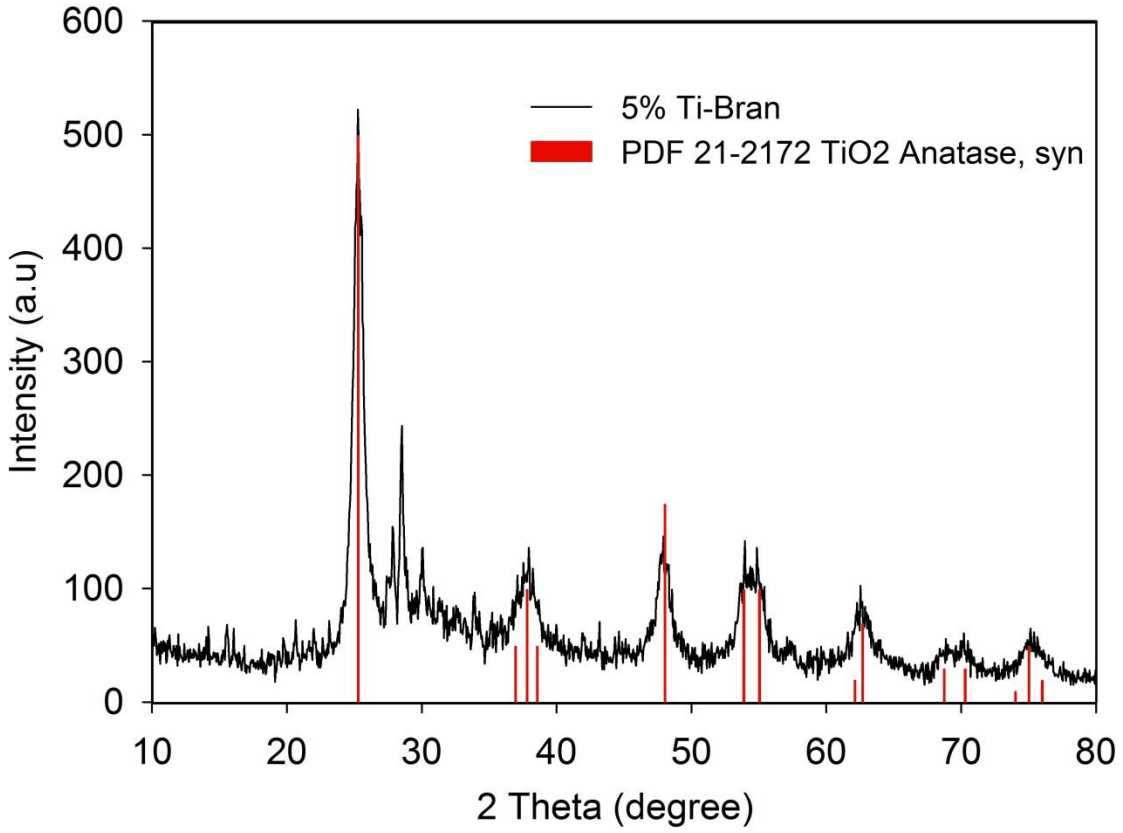

Figure 1. XRD pattern of 5% Ti-Bran nanocomposite as compared to the diffraction lines of the pure anatase phase (red vertical lines).

Further XPS characterization studies confirmed the presence of incorporated Ti^{4+} species (Ti2p3/2, 458.3 eV) in the materials as clearly illustrated in Figure 2. Interestingly, the fitting peak at ca. 454.5 eV in the Ti2p spectra of 0.5% Ti-Bran catalyst might be ascribed to the substitution of oxygen by carbon species in the TiO_2 lattice and formation of Ti-C bond which can also be observed in the C1s spectra from the peak at 282.2 eV [30, 31]. The difference in the fitting peak for Ti2p of 454.5 eV and 458.3 eV is potentially resulted from the presence of C-Ti-O bond in the TiO_2 lattice that the electronegativity of C (2.55) is lower than that of O (3.44) which results in more electron-rich in Ti-O bond and further affects the difference in binding energy. This may

also indicate the lattice distortion due to the presence of C atom [24], as similarly observed in the XPS spectra of other Ti-Bran catalysts. Ti content (Table 1) was also quantified via ICP/MS and was found to be in the range of 8 to 40 wt% of the final materials in the Ti-Bran samples after partial removal of the organics from wheat bran.

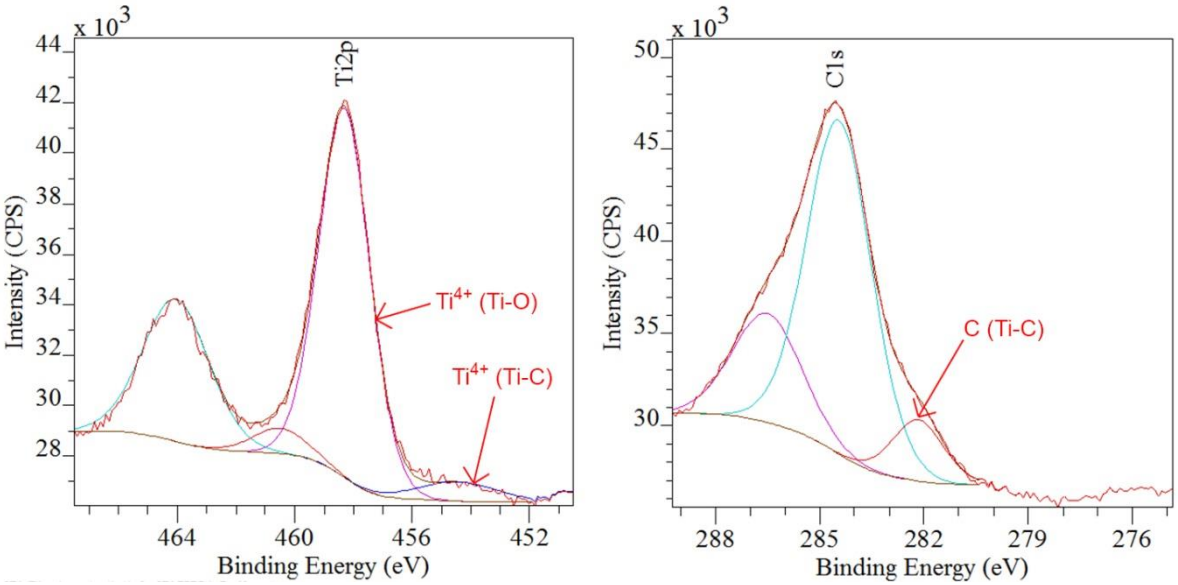

Figure 2. XPS spectra of 0.5% Ti-Bran: Ti2p (left), C1s (right).

Nevertheless, nanoparticle sizes could remain relatively small probably due to the mechanochemical process between the titania precursor and the wheat bran as well as to the partial (not complete) elimination of part of the organic phase from wheat bran in the calcinations. Indeed, these results were in good agreement with TEM images of the synthesized Ti-Bran nanocomposites which clearly depicted the presence of highly dispersed and homogeneously distributed titania nanoparticles (black dots) on the remnants of the wheat bran feedstock (Figure 3). The visualized nanoparticle sizes on TEM also correlated well with results of XRD patterns obtained using the Scherrer equation, with particle sizes around 10 nm (10% Ti-Bran) and even smaller (5-7 nm) for lower loaded Ti-Bran nanocomposites (Figure 3, top images). Some titania aggregates could also be observed in TEM images of the synthesized nanocomposites although these were clearly minor.

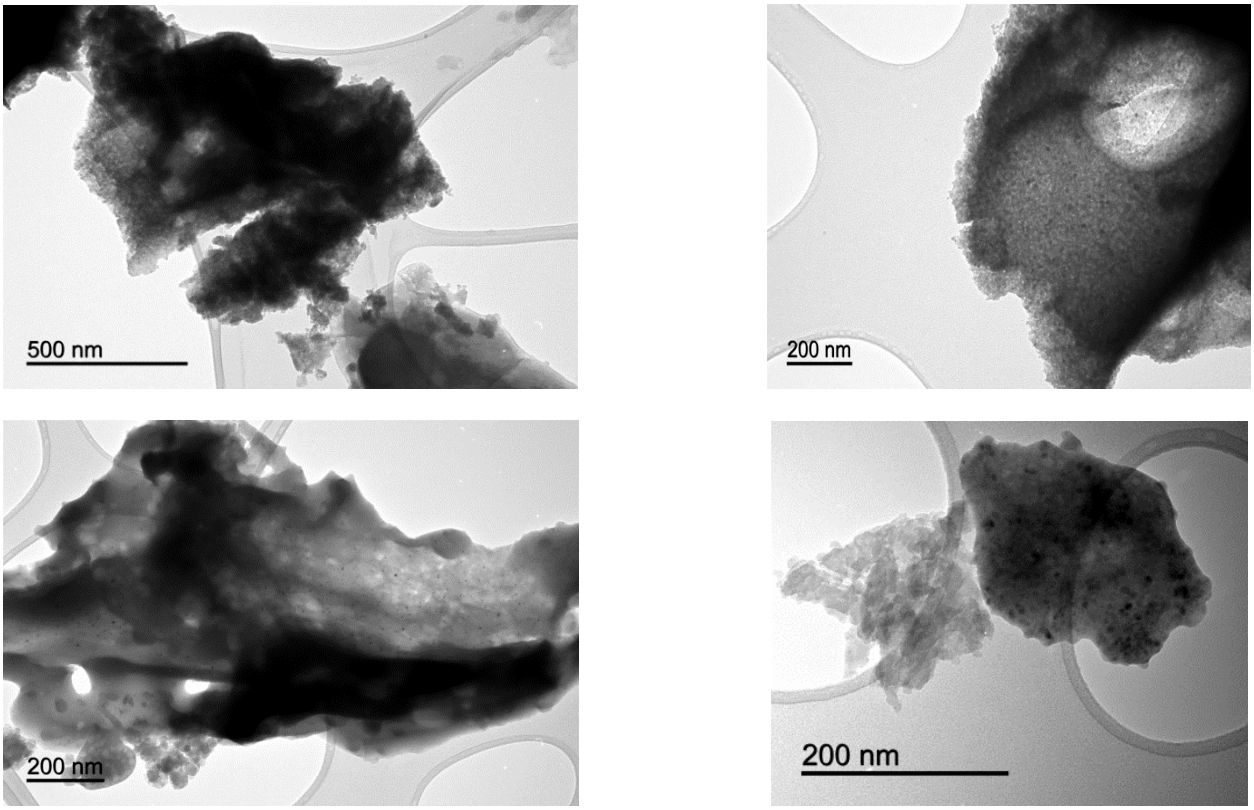

Figure 3. TEM micrographs of 0.5% Ti-Bran (top images) and 10% Ti-Bran (bottom images). Titania nanoparticles could be clearly visualized as black dots.

Optical absorption spectra of the synthesized photonanocomposites with different TiO_2 content are shown in Figure S2. As expected, the optical response of all the catalysts were extended into the visible light region with a slight enhancement of light absorption of all the samples achieved at a wavelength of around 400 nm as compared to that of pure anatase TiO_2 (< 387 nm). The promotion of the light response could be attributed to the presence of carbon and trace elements which act as photosensitizer [32] and probably the newly created heterojunctions between TiO_2 and the carbon support. The average band gap of the synthesized samples is ca. 3.0 eV, reduced as compared to pure anatase TiO_2 (3.2eV). Details about the band gap energy and absorption threshold can be seen in Table S2.

Table 2. Photocatalytic oxidation of benzyl alcohol using different photocatalysts

Catalyst	Conversion (%)	Selectivity[a] BHA[b] (%)	Yield BHA (%)	Selectivity BAC[c] (%)
Photolysis	<3	-	-	-
0.5% Ti-Bran	<5	73	<5	-
1% Ti-Bran	16	53	9	<5
2% Ti-Bran	20	63	12	<5
5% Ti-Bran	19	89	17	<5
10% Ti-Bran	33	66	20	<5
TiO_2 (P-25)	>99	32	33	6

a Apart from BHA and BAC, the remaining selectivity to 100 corresponds mostly to CO_2

b BHA: benzaldehyde

c BAC: benzoic acid

After careful materials characterization, the application of the synthesized photonanocomposites was subsequently investigated in the selective photo-oxidation of benzyl alcohol to benzaldehyde. A summary of photocatalytic activity experiments has been presented in Table 2, while the comparison of photocatalytic performance in oxidation of benzyl alcohol between 10% Ti-Bran and other reported TiO_2 based catalysts was listed in Table S3. The conversion of the controlled photolysis (blank reaction, in the absence of catalysts) was found to be negligible (<5%) after 4 h of illumination time, as well as the conversion with 0.5% Ti-Bran. Upon increasing Ti content, both conversion of starting material and yield of benzyl alcohol increased with the content of TiO_2 on the carbonaceous nanocomposite. The maximum yield of benzaldehyde (ca. 20% at 33% conversion of benzyl alcohol) was achieved for 10%Ti-Bran catalyst with a selectivity of over 60%. Comparatively, the P-25 Evonik titania photocatalyst provided a maximum of 33% yield, with quantitative conversion of starting material (mostly

mineralization of benzyl alcohol takes place under the investigated conditions).[13] Taking into account the titania content in both materials, we can conclude that the designed titania-wheat bran nanocomposites outperform commercial titania nanomaterials in the investigated selective photo-oxidation. The higher selectivity towards benzaldehyde for Ti-Bran nanocomposites (see Table 2) may be attributed to the incorporation of carbon atoms on the TiO_2 lattice. Additionally, researchers suggested that carbon acted as photosensitizer and the excited electrons could migrate to the conduction band of TiO_2 which would be transferred to surface-absorbed O_2 and forming superoxide anions. The superoxide anions could further convert to ·OH and initiate the reaction. [8] Over-oxidation products including benzoic acid were observed in the experiments using catalysts with TiO_2 content ≥1.0%, although these were obtained in relatively minor quantities.

3.2.4. Conclusions

This contribution was aimed to illustrate the potential of valorizing agroindustrial waste into a range of valuable materials, chemicals and fuels. The use of wheat bran, a residue with numerous available from the agricultural industry, as feedstock for the design of innovative photocatalytic nanocomposites for advanced applications in the selective conversion of benzyl alcohol to benzaldehyde, a well-known specialty chemical with important applications in the food, fragrances and cosmetics industries. The use of a simple, efficient and environmentally friendly technology (ball milling, mechanochemistry) provided the possibility to synthesizing titania-containing nanocomposites with promising textural and surface properties and useful photocatalytic activities in the selected photo-oxidation process. The optimum nanocomposite (10% Ti-Bran) provided a 20% yield of benzaldehyde at 33% conversion of benzyl alcohol, comparable to that of P25 Evonik commercial titania utilized under the same conditions for comparative purposes.

Acknowledgements

Rafael Luque gratefully acknowledges Consejeria de Ciencia e Innovacion, Junta de Andalucia for funding project P10-FQM-6711. Funding from Marie Curie Actions under ITN Project Photo4Future (H2020-MSCA-ITN-2014-641861), especially for funding WO Ph.D studies. JCC,

AMB and RL gratefully acknowledge support from COST Action FP1306 for networking and possibilities for meetings and future students exchange. Prof. Colmenares would like to thank the Institute of Physical Chemistry of the Polish Academy of Sciences for all support.

References

[1] A. Fujishima, K. Honda, *Nature* **1972**, *213*, 8656.

[2] A. L. Linsebigler, A. L. Linsebigler, J. T. Yates Jr, G. Lu, G. Lu, J. T. Yates, *Chem. Rev.* **1995**, *95*, 735–758.

[3] J. Yu, J. Low, W. Xiao, P. Zhou, M. Jaroniec, *J. Am. Chem. Soc.* **2014**, *136*, 8839–8842.

[4] K. Adachi, K. Ohta, T. Mizuno, *Sol. Energy* **1994**, *53*, 187–190.

[5] D. Chen, X. Zhang, A. F. Lee, *J. Mater. Chem. A* **2015**, *3*, 14487–14516.

[6] M. R. Hoffmann, M. R. Hoffmann, S. T. Martin, S. T. Martin, W. Choi, W. Choi, D. W. Bahnemannt, D. W. Bahnemannt, *Chem. Rev.* **1995**, *95*, 69–96.

[7] J. Virkutyte, B. Baruwati, R. S. Varma, *Nanoscale* **2010**, *2*, 1109–1111.

[8] X. Yang, C. Cao, L. Erickson, K. Hohn, R. Maghirang, K. Klabunde, *J. Catal.* **2008**, *260*, 128–133.

[9] J.-M. Herrmann, H. Tahiri, C. Guillard, P. Pichat, *Catal. Today* **1999**, *54*, 131–141.

[10] T. Ohno, K. Tokieda, S. Higashida, M. Matsumura, *Appl. Catal. A Gen.* **2003**, *244*, 383–391.

[11] C. Hubert, A. Denicourt-Nowicki, P. Beaunier, A. Roucoux, *Green Chem.* **2010**, *12*, 1167.

[12] S. Higashimoto, N. Kitao, N. Yoshida, T. Sakura, M. Azuma, H. Ohue, Y. Sakata, *J. Catal.* **2009**, *266*, 279–285.

[13] J. C. Colmenares, W. Ouyang, M. Ojeda, E. Kuna, O. Chernyayeva, D. Lisovytskiy, S. De, R. Luque, A. M. Balu, *Appl. Catal. B Environ.* **2016**, *183*, 107–112.

[14] X. Chen, S. Shen, L. Guo, S. S. Mao, *Chem. Rev.* **2010**, *110*, 6503–6570.

[15] M. Ni, M. K. H. Leung, D. Y. C. Leung, K. Sumathy, *Renew. Sust. Energy Rev.* **2007**, *11*, 401–425.

[16] T. Ohno, T. Mitsui, M. Matsumura, *Chem. Lett.* **2003**, *32*, 364–365.

[17] T. Ohno, M. Akiyoshi, T. Umebayashi, K. Asai, T. Mitsui, M. Matsumura, *Appl. Catal. A Gen.* **2004**, *265*, 115–121.

[18] J. T. Chang, Y. F. Lai, J. L. He, *Surf. Coatings Technol.* **2005**, *200*, 1640–1644.

[19] H. Irie, Y. Watanabe, K. Hashimoto, *J. Phys. Chem. B* **2003**, *107*, 5483–5486.

[20] G. Wu, T. Nishikawa, B. Ohtani, A. Chen, *Chem. Mater.* **2007**, *19*, 4530–4537.

[21] J. Virkutyte, R. S. Varma, *New J. Chem.* **2010**, *34*, 1094–1096.

[22] J. Sun, L. Qiao, S. Sun, G. Wang, *J. Hazard. Mater.* **2008**, *155*, 312–319.

[23] D. Chen, Z. Jiang, J. Geng, Q. Wang, D. Yang, *Ind. Eng. Chem. Res.* **2007**, *46*, 2741–2746.

[24] E. M. Neville, M. J. Mattle, D. Loughrey, B. Rajesh, M. Rahman, J. M. D. MacElroy, J. a. Sullivan, K. R. Thampi, *J. Phys. Chem. C* **2012**, *116*, 16511–16521.

[25] Y. Shen, T. Xiong, T. Li, K. Yang, *Appl. Catal. B Environ.* **2008**, *83*, 177–185.

[26] C.-J. Li, G.-R. Xu, B. Zhang, J. R. Gong, *Appl. Catal. B Environ.* **2012**, *115*, 201–208.

[27] D. Spasiano, L. del Pilar Prieto Rodriguez, J. C. Olleros, S. Malato, R. Marotta, R. Andreozzi, *Appl. Catal. B Environ.* **2013**, *136–137*, 56–63.

[28] R. Marotta, I. Di Somma, D. Spasiano, R. Andreozzi, V. Caprio, *Chem. Eng. J.* **2011**, *172*, 243–249.

[29] J. C. Colmenares, R. Luque, *Chem. Soc. Rev.* **2014**, *43*, 765–778.

[30] J. Liu, Q. Zhang, J. Yang, H. Ma, M. O. Tade, S. Wang, J. Liu, *Chem. Commun.* **2014**, *50*, 13971–13974.

[31] F. Sordello, G. Zeb, K. Hu, P. Calza, C. Minero, T. Szkopek, M. Cerruti, *Nanoscale* **2014**, *6*, 6710.

[32] C. Lettmann, K. Hildenbrand, H. Kisch, W. Macyk, W. F. Maier, *Appl. Catal. B Environ.* **2001**, *32*, 215–227.

[33] W. Ouyang, E. Kuna, A. Yepez, A. Balu, A. Romero, J. Colmenares, R. Luque, *Nanomaterials* **2016**, *6*, 93.

[34] A. Magdziarz, J. C. Colmenares, O. Chernyayeva, K. Kurzydłowski, J. Grzonka, *ChemCatChem* **2016**, *8*, 536–539.

[35] C. J. Li, G. R. Xu, B. Zhang, J. R. Gong, *Appl. Catal. B Environ.* **2012**, *115–116*, 201–208.

Appendix A. Supplementary data


Contents lists available at ScienceDirect

Journal of Environmental Management

journal homepage: www.elsevier.com/locate/jenvman

Wheat bran valorization: towards photocatalytic nanomaterials for benzyl alcohol photo-oxidation

Weiyi Ouyang[a], Jose M. Reina[a], Ewelina Kuna[b], Alfonso Yepez[a], Alina M. Balu[a], Antonio A. Romero[a], Juan Carlos Colmenares[b], Rafael Luque*[a]

[a]*Departamento de Quimica Organica, Universidad de Cordoba, Edificio Marie Curie(C-3), Ctra Nnal IV-A, Km 396, E14014 Córdoba, Spain, e-mail: q62alsor@uco.es*

[b]*Institute of Physical Chemistry PAS, Kasprzaka 44/52, 01-224 Warsaw (Poland)*

Table S1. Synthesized Ti-Bran nanomaterials using varying quantities of titanium isopropoxide

Material	Quantity of Titanium isopropoxide (μL)
0.5%Ti-Bran	157
1%Ti/Bran	307
2%Ti-Bran	615
5%Ti-Bran	1536
10%Ti-Bran	3072

Table S2. Band gap and light absorption threshold of different Ti-Bran catalysts

Catalyst	Band Gap (eV)	Absorption threshold (nm)
0.5%Ti-Bran	2.94	421
1%Ti-Bran	3.07	403
2% Ti-Bran	3.09	401
5% Ti-Bran	3.07	403
10% Ti-Bran	3.00	413

Table S3. Comparison of photocatalytic efficiency of catalysts in selective oxidation of benzyl alcohol

Catalyst	Catal. loading (g/L)	Solvent	Init. Conc. (mM)	Conv. (%)	Selec. BHA (%)	Yield BHA (%)	Reac. Cond.	Ref.
10% Ti-Bran	1	CH_3CN	1.5	33	66	20	125W Hg lamp, 4h, 30 ^{0}C	-
5% TiO_2-MAGSNC	1	CH_3CN	1.5	20	84	17	125W Hg lamp, 4h, 30 ^{0}C	[1]
TiO_2-MAGSNC	1	CH_3CN	1.5	50	90	47	125W Hg lamp, 4h, 30 ^{0}C	[2]
Fe/TiO_2/ZeSPD	3	CH_3CN	1.0	48	-	46	150 W Xe lamp, 8h, 35 ^{0}C	[3]
Fe-TiO_2/ZeUI	3	CH_3CN	1.0	10	-	9	150 W Xe lamp, 8h, 35 ^{0}C	[3]
TiO_2	5	CH_3CN	5	>99	-	>99	$1.8*10^4$ lux, blue LED lamp, 4h, 25 ^{0}C	[4]
TiO_2 (rutile)	5	CH_3CN	9.66	-	-	26	300 W Xe lamp, 12h, -	[5]

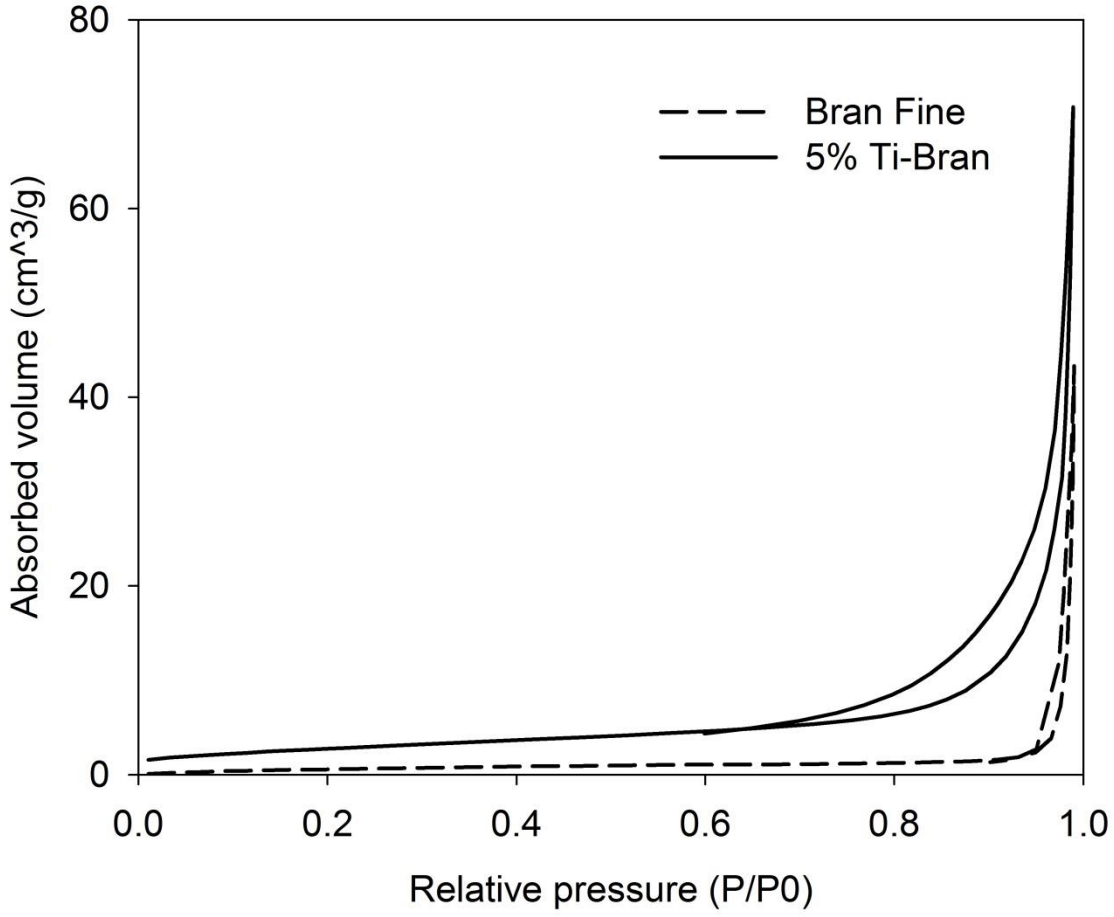

Figure S1. Nitrogen physisorption isotherms of 5%Ti-Bran as compared to the parent wheat bran (BranFine).

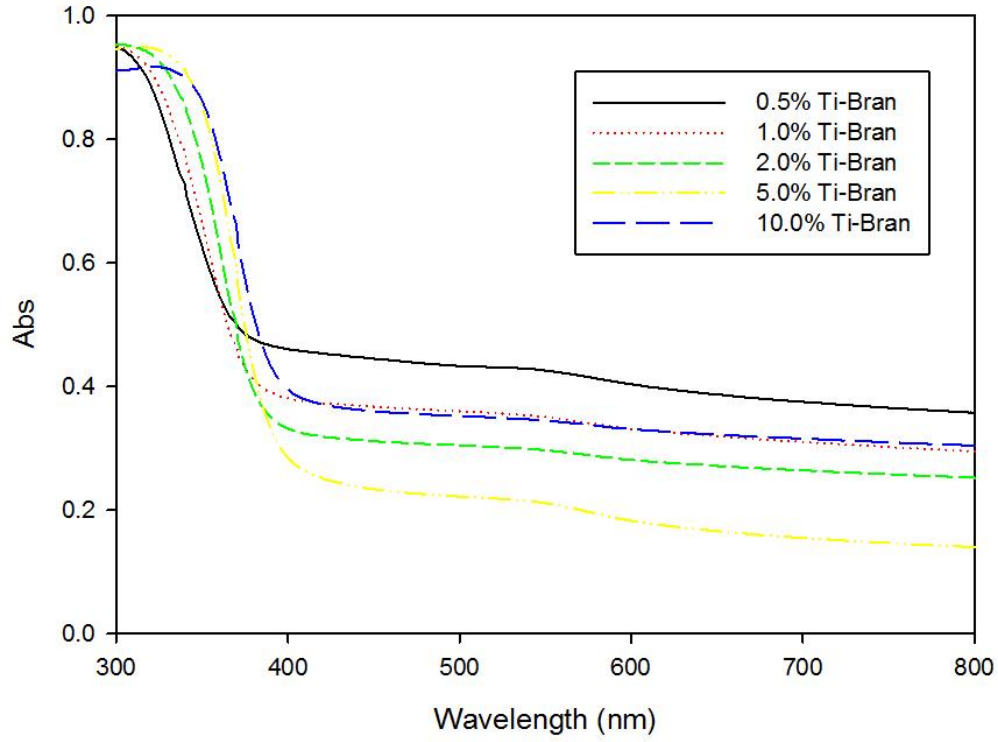

Figure S2. UV-Vis absorption spectra of different Ti-Bran catalysts

References

[1] W. Ouyang, E. Kuna, A. Yepez, A. Balu, A. Romero, J. Colmenares, R. Luque, *Nanomaterials*, **2016**, *6*, 93.

[2] J. C. Colmenares, W. Ouyang, M. Ojeda, E. Kuna, O. Chernyayeva, D. Lisovytskiy, S. De, R. Luque, A. M. Balu, *Appl. Catal. B Environ.* **2016**, *183*, 107–112.

[3] A. Magdziarz, J. C. Colmenares, O. Chernyayeva, K. Kurzydłowski, J. Grzonka, *ChemCatChem*, **2016**, *8*, 536–539.

[4] S. Higashimoto, N. Kitao, N. Yoshida, T. Sakura, M. Azuma, H. Ohue, Y. Sakata, *J. Catal.* **2009**, *266*, 279–285.

[5] C. J. Li, G. R. Xu, B. Zhang, J. R. Gong, *Appl. Catal. B Environ.* **2012**, 115–116, 201–208.

OPEN ACCESS

nanomaterials

MDPI

3.3. Mechanochemical Synthesis of TiO_2 Nanocomposites as Photocatalysts for Benzyl Alcohol Photo-Oxidation

Weiyi Ouyang [1], Ewelina Kuna [2], Alfonso Yepez [1], Alina M. Balu [1], Antonio A. Romero [1], Juan Carlos Colmenares [2] and Rafael Luque [1,*]

1 Department of Organic Chemistry, University of Cordoba, Edificio Marie Curie(C-3), Ctra Nnal IV-A, Km 396, Cordoba E14014, Spain; qo2ououw@uco.es (W.O.); z22yegaa@uco.es (A.Y.); qo2balua@uco.es (A.M.B.); qo1rorea@uco.es (A.A.R.)

2 Institute of Physical Chemistry Polish Academy of Sciences (PAS), Kasprzaka 44/52, Warsaw 01-224, Poland; ekuna@ichf.edu.pl (E.K.); jcarloscolmenares@ichf.edu.pl (J.C.C.)

***** *Correspondence: q62alsor@uco.es; Tel.: +34-957211050*

Received: 3 March 2016; Accepted: 7 May 2016; Published: 18 May 2016

DOI: 10.3390/nano6050093

Abstract

TiO_2 (anatase phase) has excellent photocatalytic performance and different methods have been reported to overcome its main limitation of high band gap energy. In this work, TiO_2-magnetically-separable nanocomposites (MAGSNC) photocatalysts with different TiO_2 loading were synthesized using a simple one-pot mechanochemical method. Photocatalysts were characterized

by a number of techniques and their photocatalytic activity was tested in the selective oxidation of benzyl alcohol to benzaldehyde. Extension of light absorption into the visible region was achieved upon titania incorporation. Results indicated that the photocatalytic activity increased with TiO_2 loading on the catalysts, with moderate conversion (20%) at high benzaldehyde selectivity (84%) achieved for 5% TiO_2-MAGSNC. These findings pointed out a potential strategy for the valorization of lignocellulosic-based biomass under visible light irradiation using designer photocatalytic nanomaterials.

Keywords: TiO_2; magnetically separable photocatalysts; selective photo-oxidation; mechanochemical synthesis; ball mill

3.3.1. Introduction

Photocatalysis has been considered as one of the most environmentally friendly and promising technologies owing to advantages such as being clean, efficient, cost-effective, and energy-saving [1–3] Typical applications of photocatalysis are conversion of CO_2 to fuels and chemicals [4–8], self-cleaning surfaces [9,10], disinfection of water [11,12], oxidation of organic compounds [13–15], and production of hydrogen from water splitting [16–19]. In this regard, different types of heterogeneous photocatalysts have been extensively reported, including metal oxide nanoparticles, composite nanomaterials, metal-organic frameworks, plasmonic photocatalysts, and polymeric graphitic carbon nitride [3,4].

Among these different types of photocatalysts, TiO_2 has been extensively investigated and is one of the most widely used in the aforementioned applications due to its excellent photocatalytic activity, high thermal and chemical stability, low cost, and non-toxicity [20,21]. However, in spite of its advantages, the main drawback of TiO_2 in photocatalysis relates to the large band gap (3.2 eV) for its anatase crystalline phase which restricts its utilization to ultraviolet (UV) irradiation ($\lambda < 387$ nm), with UV irradiation comprising less than 5% of the solar energy. Therefore, it is very important to extend the photocatalytic activity of TiO_2 nanocatalysts under visible light to profit

from abundant solar energy. Various approaches have been developed to improve the photoactivity of TiO_2 by lowering the band-gap energy and delaying the recombination of the excited electron-hole pairs, i.e., cationic [22,23] and anionic [20,24,25] doping, dye photosensitization, deposition of noble metals. Photocatalysts doped with noble metals can improve their photoactivities, but with limitations for large scale applications. Importantly, the design of photocatalysts featuring magnetic separation has not been considered to a large extent despite the obvious advantages of separation and recycling for magnetically-separable heterogeneous photocatalysts [26]. Conventional methods for heterogeneous catalyst recovery, such as filtration, centrifugation, etc., are either time consuming or costly, while the enhanced magnetically-separable properties of the heterogeneous catalyst can exceed these limitations. In recent years, photocatalysts with TiO_2 coated on magnetic particles have been reported by many researchers [27–29], which showed enhanced photocatalytic activities and feasible separation by applying external magnetic field. Ojeda et al. reported a maghemite/silica nanocomposite, which were also magnetically separable [30], followed by a report on the incorporation of TiO_2 on maghemite/silica nanocomposites under ultrasounds which exhibited excellent photocatalytic performance in the selective oxidation of benzyl alcohol [31].

The selective oxidation of alcohols to the corresponding carbonyl compounds accounts for one of the most significant transformations in organic chemistry. Particularly, the conversion of benzyl alcohol (BA) to benzaldehyde (BHA) has attracted extensive attention, since benzaldehyde is widely applied in food, pharmaceutical, and perfumery industries and as building block in other chemical industries. Recently, the photocatalytic oxidation of benzyl alcohol to benzaldehyde has been reported using different catalysts and chlorine-free benzaldehyde with high selectivity, with respect to the traditional syntheses-either by benzyl chloride hydrolysis or via toluene oxidation [15,26,32].

In continuation with research efforts from the group related to the design of advanced nanomaterials for (photo)catalytic processes, we aimed to synthesize an advanced magnetically-separable nanophotocatalyst (TiO_2-MAGSNC) using a simple one-pot mechanochemical method under ball mill. A widely-reported porous support (SBA-15) was utilized as support, together with an iron precursor and propionic acid to obtain a magnetic phase able to provide magnetically-separable features to the catalyst. A high-energy ball milling process was applied in this work

which could provide small nanoparticle sizes as well as a highly homogeneous crystalline structure and morphology. TiO_2-MAGSNC catalysts were found to be photoactive with a high selectivity in the selective oxidation of benzyl alcohol to benzaldehyde.

3.3.2. Experimental

3.3.2.1. Synthesis of TiO_2/MAGSNC Photocatalysts

SBA-15 silica was prepared using the procedure reported by Bonardet *et al.* [33] Different amounts of titanium precursor were used to obtain various contents of TiO_2 (0.5, 1.0, 2.0, 5.0 wt %) on the catalysts. Titanium incorporation was subsequently achieved by a simple mechanochemical method in a planetary ball mill under previous optimized conditions [34]. In detail, Pluronic P123 surfactant (Sigma-Aldrich Inc., St. Louis, MO, USA) (8.0 g) was dissolved in deionized water (260 mL) and HCl (Panreac Química S.L.U., Barcelona, Catalonia, Spain) (12 M, 40 mL) under vigorous stirring, at 40 °C for 2 h. Upon complete dissolution, 7 g of tetraethyl orthosilicate (TEOS) (Sigma-Aldrich Inc., St. Louis, MO, USA) were added dropwise to the above solution. The mixture was stirred at 40 °C for 24 h, followed by hydrothermal treatment at 100 °C for 48 h in an oven. The white solid was separated from the solution by filtration and dried at 60 °C. The template was removed by calcination at 600 °C for 8 h. Different amounts (13, 59, 188 and 661 μL) of titanium isopropoxide (Sigma-Aldrich Inc., St. Louis, MO, USA), 1.34 g $Fe(NO_3)_3 \cdot 9H_2O$ (Merck, Darmstadt, Hesse, Germany), 0.5 g SBA-15 and 0.25 mL propionic acid (Panreac Química S.L.U., Barcelona, Catalonia, Spain) were added to a 125 mL reaction chamber with eighteen 10 mm stainless steel balls and then ground in a Retsch PM-100 planetary ball mill (350 rpm, 10 min) (Retsch GmbH, Haan, North Rhine-Westphalia, Germany). Materials calcination was performed at 400 °C (heating rate 3 °C/min) for 5 h in a furnace under an oxygen deficient atmosphere (static air). MAGSNC sample was synthesized under same conditions without adding titanium isopropoxide. All chemicals were used as received.

3.3.2.2. Characterization of the TiO_2-MAGSNC Photocatalysts

The crystal phase structures of TiO_2-MAGSNC samples were examined by powder X-ray diffraction (XRD) measurements performed in a Bruker D8 DISCOVER A25 diffractometer (Bruker Corporation, Billerica, MA, USA) equipped with a vertical goniometer under theta-theta geometry using Ni filtered Cu Kα (λ = 1.5418 Å) radiation and operated at 40 KeV and 40 mA. Wide angle scanning patterns were collected from 10° to 80° with a step size of 0.01° and counting time of 500 s per step.

Textural properties of the samples were determined by N_2 physisorption using a Micromeritics ASAP 2020 automated system (Micromeritics Instrument Corporation, Norcross, GA, USA) with the Brunauer-Emmet-Teller (BET) and the Barret-Joyner-Halenda (BJH) methods. Prior to adsorption measurements, samples were degassed under vacuum (0.1 Pa) for 4 h at 300 °C.

A UV/VIS/NIR spectrophotometer Jasco V-570 (JASCO international Co., Ltd., Hachioji, Tokyo, Japan) equipped with an integrating sphere was used to record Ultraviolet-Visible (UV-VIS) diffuse reflectance spectra. The baseline was obtained with SpectralonTM (poly(tetrafluoroethylene) as a reference material. The Kubelka-Munk method was utilized (from diffuse reflectance spectra) to determine the band gap function. Function $f(R)$ was calculated from the following equation:

$$f(R) = \frac{(1-R)^2}{2R} \quad (1)$$

while E_g was calculated from $(f(R)h\nu)^{1/2}$ *versus* hν plots.

X-ray photoelectron spectroscopy (XPS) measurements were carried out with a VG Scientific photoelectron spectrometer ESCALAB-210 (Thermo Scientific, Waltham, MA, USA) with Al Kα radiation (1486.6 eV) from an X-ray source, operating at 15 kV and 20 mA. Survey spectra in the energy range from 0 to 1350 eV with 0.4 eV step were recorded for all the samples. High resolution spectra were recorded with 0.1 eV step, 100 ms dwell time and 25 eV pass energy. A ninety degree take-off angle was employed in all measurements. Curve fitting was carried out using the CasaXPS software (Casa Software Ltd., Cheshire, England, UK), which each component of the complex

envelope is described as a Gaussian–Lorentzian sum function; a constant 0.3 (±0.05) G/L ratio was used. The background was fitted using a nonlinear Shirley model. Measured transmission function and Scofield sensitivity factors have been employed for quantification purposes. An aromatic carbon C 1s peak at 284.5 eV was used as the reference of binding energy.

Scanning electron microscopy images were recorded with a JEOL JSM-6300 scanning microscope (JEOL Ltd., Akishima, Tokyo, Japan) equipped with Energy-dispersive X-ray spectroscopy (EDX) at 20 kV. An Au/Pd coating was employed to analyze samples on a high-resolution sputtering SC7640 instrument (Quorum Technologies Ltd., Lewes, England, UK) (up to 7 nm thickness) at a sputtering rate of 1.5 kV per minute.

FEI Tecnai G2 (FEI Tecnai, Hillsboro, OR, USA) fitted with a Charge-coupled Device (CCD) camera for ease and speed of use was applied to record the transmission electron microscopy (TEM) images of the synthesized TiO_2-MAGSNC samples at the Research Support Service Center (SCAI) from Universidad de Cordoba. The resolution of the equipment is around 0.4 nm. Prior to the recording, samples were prepared by suspension in ethanol, assisted by sonication and followed by deposition on a copper grid.

The magnetic susceptibility was measured at low frequency (470 Hz) using a Bartington MS-2 (Bartington Instruments Ltd., Witney, England, UK), at room temperature.

3.3.2.3. Photocatalytic experiments

A Pyrex cylindrical double-wall immersion well reactor equipped with medium pressure 125 W mercury lamp ($\lambda = 365$ nm), which was supplied by Photochemical Reactors Ltd. UK (Model RQ 3010), (Reading, UK) was used in all the catalytic reactions (Figure 1). The distance between the light source and reaction media was *ca.* (*ca.*: abbreviation of circa) 10 nm and irradiance of the light source reached 1845.6 W/m^2. Magnetic stirring with a speed of 1100 rpm was utilized in the batch reactor to obtain a homogenous suspension of the TiO_2-MAGSNC photocatalysts. The reaction temperature was established at 30 °C. 1.5 mM benzyl alcohol (Sigma-Aldrich Inc., St. Louis, MO, USA) was prepared in acetonitrile (Sigma-Aldrich Inc., St. Louis, MO, USA) medium.

Experiments were performed from 150 mL of the mother solution and 1 g/L of catalyst concentration for 4 h under UV light and air bubbling conditions (25 mL/min). In order to equilibrate the adsorption-desorption over the photocatalyst surface, the reaction solution was left in the dark for 30 min before each reaction. Samples were periodically withdrawn (*ca.* 1 mL) from the photoreactor at different times and filtered off (0.20 µm, 25 mm, nylon filters). The concentration of model compound was determined by a high-performance liquid chromatography (HPLC, Waters Model 590 pump) (Waters Limited, Hertfordshire, UK) equipped with a dual absorbance detector (Waters 2487) and the SunFire™ C18 (3.5 µm, 150 mm length, 4.6 mm inner diameter) column provided by Waters. The mobile phase was Milli-Q water/acetonitrile/methanol in the volumetric ratio of 77.5:20:2.5 with 0.1% of H_3PO_4 (Sigma-Aldrich Inc., St. Louis, MO, USA). We used isocratic elution at a flow rate of 1 mL/min. The injection volume was 10 µL. TiO_2 P25 (approx. 80% anatase and 20% rutile) is a commercial catalyst purchased from Evonik Industries (Evonik Industries AG, Essen, Germany) and used as comparison here.

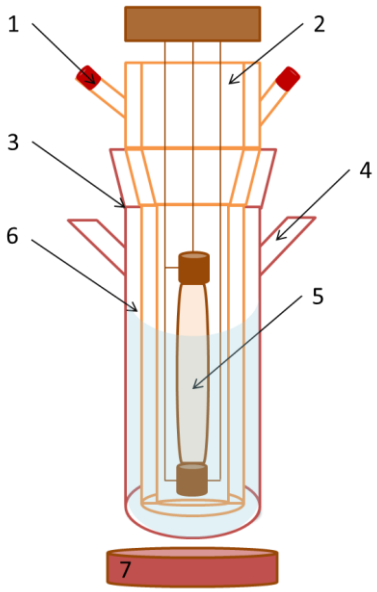

Figure 1. Reaction system: (1) lamp cooling system; (2) double-walled immersion well reactor; (3) photoreactor; (4) port for taking samples; (5) 125 W ultraviolet (UV) lamp; (6) mother solution; and (7) magnetic stirrer.

3.3.3. Results and discussion

XRD analysis was performed to investigate the crystal phase of the synthesized TiO_2-MAGSNC nanocomposites. The XRD pattern of a representative sample (5% TiO_2-MAGSNC) is shown in Figure 2 The mean observed peaks ($2\theta = 35.6°$) could be assigned to the presence of a magnetic phase (in principle γ-Fe_2O_3, although the presence of a magnetite phase cannot be completely ruled out) while titania peaks were not obvious due to the low titanium loading on the supports; hence, particle size could not be worked out from these data. By applying the Scherrer equation, iron oxide nanoparticle sizes can be calculated to be *ca.* 14 nm. Results from XRD pattern also suggested that our simple mechanochemical protocol can successfully lead to the formation of magnetically-separable nanocomposites, as further supported with subsequent characterization techniques.

N_2 absorption-desorption isotherms were used to evaluate the textural properties of the TiO_2-MAGSNC samples with different content of TiO_2. The isotherms (Figure 3) matched the characteristic type IV isotherm profile indicating these samples are essentially mesoporous in nature. In comparison to commercial titanium oxide (59 $m^2 \cdot g^{-1}$) our materials possess significantly higher surface area (generally 400–500 $m^2 \cdot g^{-1}$), without any significant changes in terms of textural properties with respect to those of the parent MAGSNC, probably due to the low titania loading. These could also be observed in TEM images. Pore volumes in the 0.40–0.45 mLg^{-1} range and diameters typical of the parent SBA-15 material (*ca.* 6 nm) were also obtained.

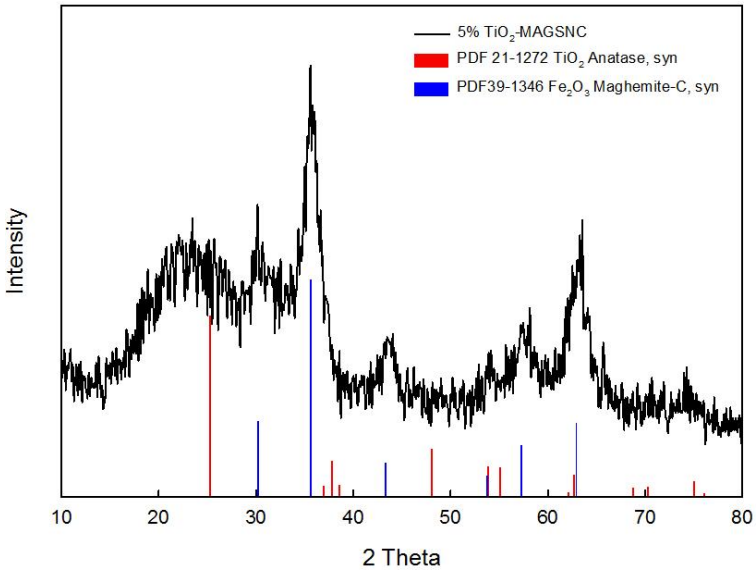

Figure 2. X-ray diffraction (XRD) pattern of 5% TiO_2- MAGSNC photocatalysts. (PDF 21-1272 and PDF 39-1346 are the card numbers for the crystalline structures in the data base, while Anatase, syn and Maghemite-C, syn are the corresponding structure names.)

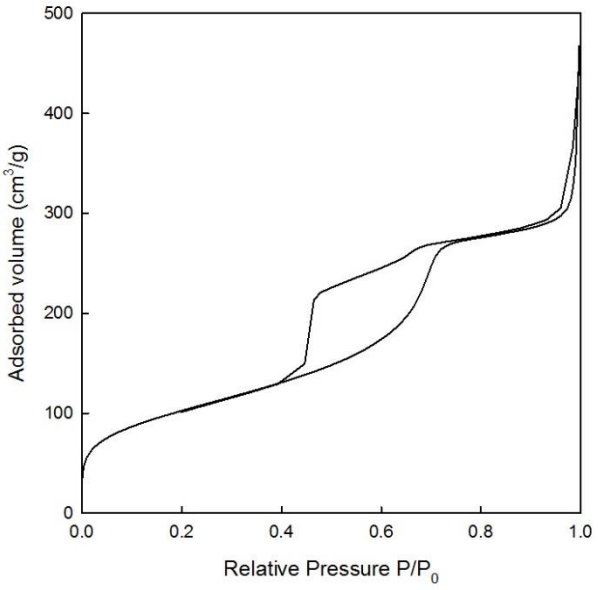

Figure 3. N_2 absorption-desorption isotherm of 5% TiO_2-MAGSNC photocatalysts. P: partial vapor pressure of adsorbate gas in equilibrium with the surface at 77.4 K; P_0: saturated pressure of adsorbate gas.

Diffuse reflectance (DR) UV-VIS spectroscopy was used to record the optical properties of the samples. UV-VIS adsorption spectra of TiO_2-MAGSNC samples are shown in Figure 4, which showed extensions of absorption band into the visible region for all catalysts. Significant enhancement of light absorption of all samples was achieved at a wavelength of around 700 nm, when comparing to those of pure commercial TiO_2 (P25, 386 nm). The extension of light absorption of the synthesized catalysts into the visible range was probably resulting from the presence of the photocatalytic composite, iron oxide phase, on the MAGSNC supports. As a result of the extension of light absorption into the visible light range, better utilization of the abundant solar energy might be possible.

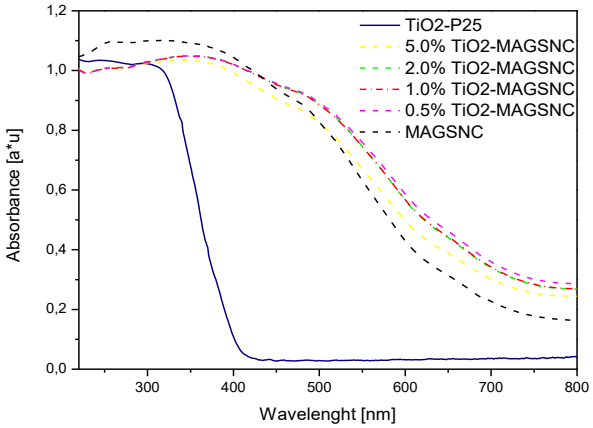

Figure 4. Diffuse reflectance (DR) Ultraviolet-Visible (UV-VIS) absorption spectra of different TiO_2-MAGSNC photocatalysts. P25: pure commercial TiO_2 from Evonik Industries.

The band gaps of synthesized TiO_2-MAGSNC were calculated, based on the Kubelka-Munk function (Table 1), to be in the 1.62 to 1.67 eV range. These extraordinary low values are derived from the iron oxide phase formed during ball mill in the synthetic stage as a result of the mechanochemical process [30,34], which only slightly decrease upon titanium incorporation. With Fe^{3+} radius (0.64 Å) close to that of Ti^{4+} (0.68 Å), the incorporation of Fe^{3+} into the TiO_2 crystal lattice during synthesis may also take place [35]. The proposed one-pot synthesis procedure might facilitate the incorporation of Fe^{3+} and formation of heterojunctions between TiO_2 and iron oxide phases during the transformation of titanium precursor to TiO_2 which might favor the charge separation in the catalysts and further improve the photocatalytic activity.

Table 1. Optical properties of synthesized TiO_2-MAGSNC photocatalysts. P25: pure commercial TiO_2 from Evonik Industries.

Materials	Band Gap [eV]	Absorption Threshold [nm]
TiO_2-P25	3.21	386
MAGSNC	1.75	705
0.5% TiO_2-MAGSNC	1.62	765
1.0% TiO_2-MAGSNC	1.63	761
2.0% TiO_2-MAGSNC	1.65	751
5.0% TiO_2-MAGSNC	1.67	740

In order to analyze the chemical states of the prepared samples, XPS spectra were also recorded. Figure 5a depicts binding energies (BEs) of *ca.* 463.3 and 457.5 eV for Ti 2p3/2 and Ti 2p1/2, respectively, characteristic of the Ti^{4+} cation with a 5.8 eV spin orbit splitting. The fitting peak with higher binding energy arises from the Ti^{4+} species in a Ti–O–Fe structure. Electrons can be induced by transfer from Ti^{4+} to Fe^{3+} in the Ti–O–Fe bond due to the electronegativity difference between Ti^{4+} (1.54) and Fe^{3+} (1.83), which makes Ti^{4+} species potentially less electron-rich (and Fe^{3+} more electron-rich), resulting in the increase of BE for Ti^{4+} species and decrease of BE for Fe^{3+} [36]. Peaks at a binding energy of 723.8 (Fe 2p1/2) and 710.2 eV (Fe 2p3/2) also correlated well to typical signals of Fe^{3+} from Fe 2p in Figure 5b, which confirmed the presence of such species in the nanocomposites, in good agreement with XRD results. Despite the stability of the hematite phase (as most thermodynamically stable at temperature over 300 °C), the magnetic phase was still well preserved after calcination at 400 °C. Most importantly, the absence of any Fe^{2+} species on the external surface in all catalysts can be confirmed from XPS spectra (Figure 5).

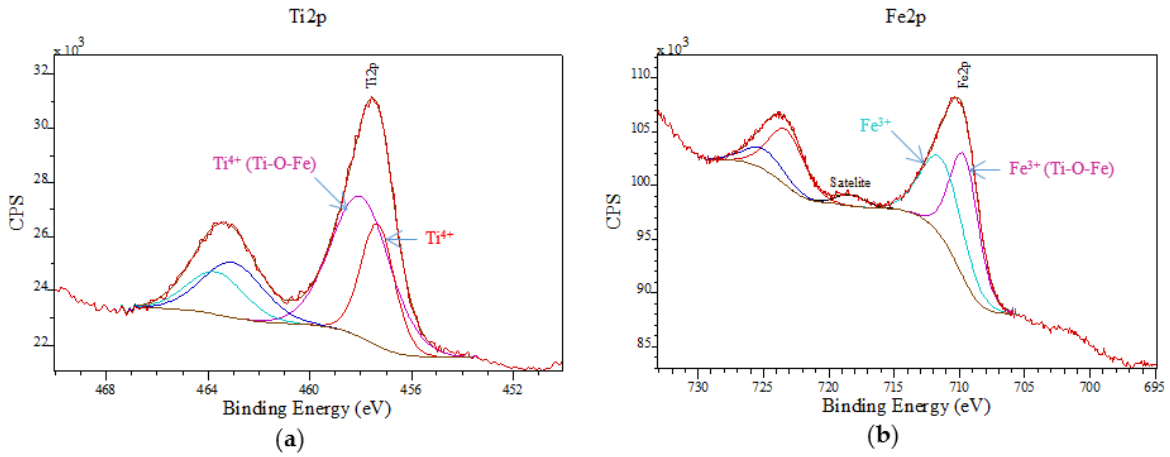

Figure 5. X-ray photoelectron spectroscopy (XPS) spectra of 5% TiO_2-MAGSNC photocatalysts: (**a**) Ti 2p; and (**b**) Fe 2p.

Both scanning electron microscopy (SEM) and TEM images of the catalysts were in good agreement with the textural properties and characterization results of the mesoporous nanocomposites (Figures 6 and 7). Element mapping illustrated for 2% TiO_2-MAGSNC pointed out that both Ti^{4+} and Fe^{3+} were homogeneously distributed on the supports, in line with analogous observations for the other catalysts. Particularly, the fully preserved SBA-15 structure could be visualized in TEM micrographs of the final photocatalytic nanomaterials, with small nanoparticles (*ca.* average nanoparticle size 10 nm), in good agreement with XRD results. Titania nanoparticles could not be distinguished from TEM images, in line with XRD data, which may again relate to a very high dispersion of TiO_2 in the nanocomposites at such low loadings. Results of EDX analysis have been summarized on Table 2, showing a good agreement in terms of Ti content on the catalysts with respect to the theoretical Ti content selected. These findings confirm the excellent incorporation of Ti provided by the proposed mechanochemical approach.

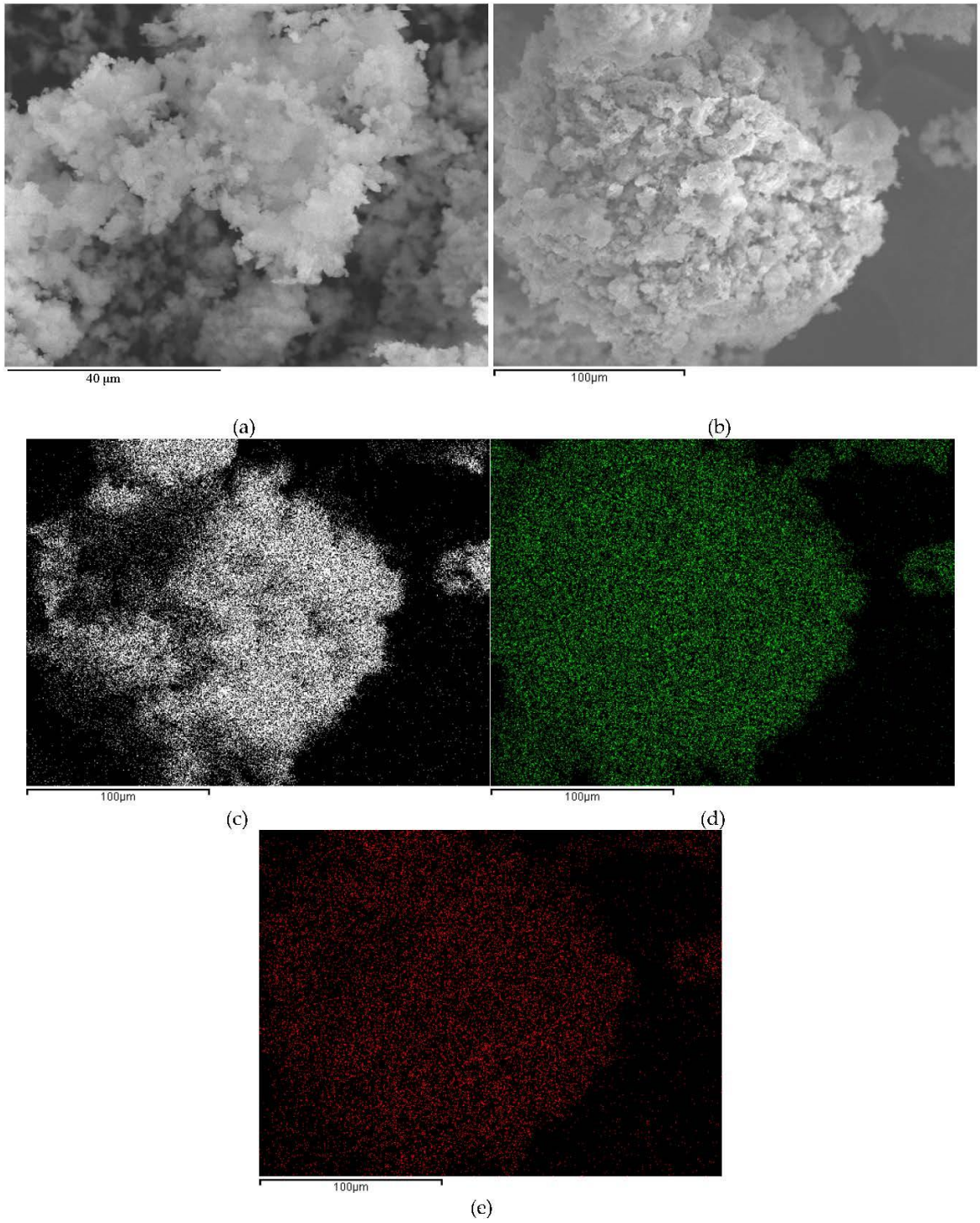

Figure 6. Scanning electron microscopy (SEM) images: (**a**) 5% TiO_2-MAGSNC photocatalysts; (**b**) 2% TiO_2-MAGSNC nanocomposites; and elements mapping of 2% TiO_2-MAGSNC photocatalysts: (**c**) Si; (**d**) Fe; (**e**) Ti.

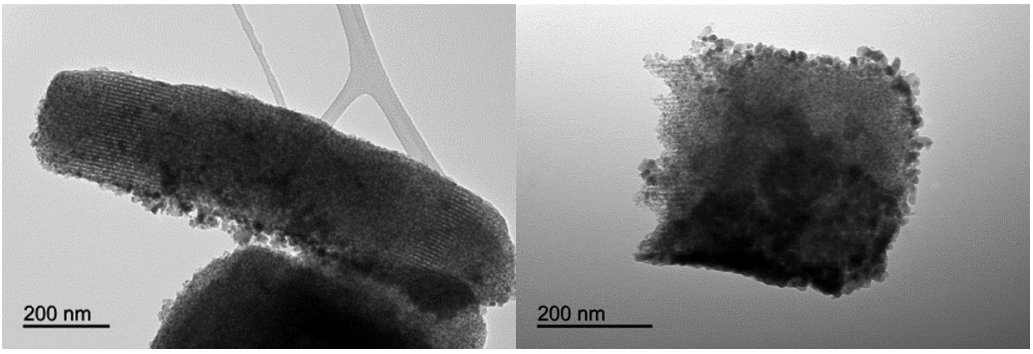

Figure 7. Transmission electron microscopy (TEM) images of 5% TiO_2-MAGSNC photocatalysts.

Table 2. Ti and Fe content on TiO_2-MAGSNC photocatalysts (obtained from energy-dispersive X-ray spectroscopy (EDX) analysis).

Sample ID	Ti (wt %)	Fe (wt %)
0.5% TiO_2-MAGSNC	0.2	19.2
1.0% TiO_2-MAGSNC	1.0	24.4
2.0% TiO_2-MAGSNC	1.7	16.2
5.0% TiO_2-MAGSNC	4.7	9.6

The magnetic susceptibility of the TiO_2-MAGSNC photocatalysts were summarized in Table 3, showing that the obtained catalysts all possessed relatively strong ferromagnetism and could be easily separated from the reaction mixture using a simple magnet.

Table 3. The magnetic susceptibility of the TiO_2-MAGSNC photocatalysts.

Sample ID	Magnetic Susceptibility ($\times 10^{-6}$ $m^3 \cdot kg^{-1}$)
0.5% TiO_2-MAGSNC	116.7
1.0% TiO_2-MAGSNC	179.1
2.0% TiO_2-MAGSNC	117.7
5.0% TiO_2-MAGSNC	130.0

After characterization, the effectiveness of TiO_2-MAGSNC photocatalysts with different TiO_2 content was subsequently studied in the photo-oxidation of benzyl alcohol. Photocatalytic activity experiment results have been summarized on Table 4. With illumination time of 4 h, the reaction using TiO_2-MAGSNC photocatalysts with low TiO_2 loading (≤1.0 wt %) provided negligible (<5%) photoconversion of benzyl alcohol to benzaldehyde, with conversion only increasing with TiO_2 loading. The magnetically-separable support (MAGSNC) or SBA-15 itself did not provide any photoactivity under otherwise identical reaction conditions. Bare iron oxides can promote the recombination of photogenerated electron-hole pairs, resulting in inactive materials. Interestingly, a titania loading as low as 5% onto MAGSNC containing the iron oxide phase could significantly decrease the band gap of the TiO_2 as well as improve the photoconversion of benzyl alcohol (up to 20% in this work) with a remarkable 84% selectivity to the target product. No over-oxidation products, such as benzoic acid and/or CO_2 from mineralization, were observed in the photo-oxidation of benzyl alcohol photocatalyzed by TiO_2-MAGSNC. Under the same photocatalytic conditions, the photoconversion of P25 Evonik was obviously quantitative but with an extremely low selectivity to benzaldehyde (32%, over 65% to mineralization), almost comparable in terms of product yield. The enhancement of the photocatalytic properties of the TiO_2-MAGSNC catalysts, especially in terms of selectivity, makes very attractive this type of magnetically separable nanocomposite containing low titania content, as compared to pure P25 commercial photocatalysts.

Table 4. Photocatalytic oxidation of benzyl alcohol to benzaldehyde [1].

Catalyst	Conversion [%]	Selectivity BHA [2][%]	Yield BHA [3][%]
Blank (no catalyst)	-	-	-
SBA-15	-	-	-
MAGSNC	-	-	-
0.5% TiO_2-MAGSNC	<5	94	-
1.0% TiO_2-MAGSNC	<5	80	-
2.0% TiO_2-MAGSNC	<10	73	-
5.0% TiO_2-MAGSNC	20	84	17
P25 Evonik	>95	32	30

[1] Reaction conditions: C_o benzyl alcohol = 1.5 mM, 125 W lamp, loading: 1 g/L. (solvent: acetonitrile, air flow: 25 mL/min, temperature: 30 °C, reaction time: 4 h). [2] BHA: benzaldehyde. [3] The selectivity of a reaction was estimated as the ratio of the required product to the undesirable

product formed during reaction. Yields were calculated as the ratio of the desired product formed to the total stoichiometric amount. Amount of substance (in mol) were determined using high performance liquid chromatography (HPLC) analysis.

3.3.4. Conclusions

Magnetically-separable catalysts with different content of TiO_2 were synthesized in a one-pot mechanochemical approach. The synthesized TiO_2-MAGSNC photocatalysts showed great improvement in light absorption into the visible light range (around 700 nm), with an interesting performance in the photocatalytic conversion of benzyl alcohol to benzaldehyde, particularly at higher loadings (5% Ti). The proposed systems will pave the way to further investigations currently ongoing in our group to the design of photoactive nanomaterials for selective oxidations, which will be reported in due course.

Acknowledgements

Rafael Luque gratefully acknowledges Consejeria de Ciencia e Innovacion, Junta de Andalucia for funding project P10-FQM-6711. Funding from Marie Curie Actions under Innovative Training Networks Project Photo4Future (H2020-MSCA-ITN-2014-641861), especially for funding Weiyi Ouyang Ph.D studies. Juan Carlos Colmenares, Alina M. Balu and Rafael Luque gratefully acknowledge support from COST Action FP1306 for networking and possibilities for meetings and future students exchange. Juan Carlos Colmenares would like to thank for the support from the National Science Centre (Poland) within the project Sonata Bis Nr. 2015/18/E/ST5/00306.

Author Contributions: Weiyi Ouyang was responsible for the synthesis and characterization of the catalysts, also writing and revising the manuscript; Ewelina Kuna was in charge of the photocatalytic activity test; Alfonso Yepez offered his help in the material synthesis and

characterization; Alina M. Balu and Antonio A. Romero supervised the work and lead the discussion while Juan Carlos Colmenares supervised the work in Poland and offered information on the photocatalytic experiments; Rafa Luque provided to project concept and was in charge of completing and revising the manuscript from submission to acceptance.

Conflicts of Interest: The authors declare no conflict of interest.

Abbreviations

The following abbreviations are used in this manuscript:

BA	Benzyl alcohol
BE	Binding energy
BHA	Benzaldehyde
ca.	Circa
EDX	Energy-dispersive X-ray spectroscopy
MAGSNC	Magnetically separable nanocomposites
P	Partial vapor pressure of adsorbate gas in equilibrium with the surface at 77.4 K
P_0	Saturated pressure of adsorbate gas
P25	Pure commercial TiO_2 from Evonik Industries
SEM	Scanning electron microscopy
TEM	Transmission electron microscopy
UV- Vis	Ultraviolet- Visible
XPS	X-ray photoelectron spectroscopy
XRD	Powder X-ray diffraction

References

[1] J. Herrmann, *Catal. Today* **1999**, *53*, 115–129.

[2] J. C. Colmenares, R. Luque, *Chem. Soc. Rev.* **2014**, *43*, 765–778.

[3] X. Lang, X. Chen, J. Zhao, *Chem. Soc. Rev.* **2014**, *43*, 473–486.

[4] D. Chen, X. Zhang, A. F. Lee, *J. Mater. Chem. A* **2015**, *3*, 14487–14516.

[5] K. Adachi, K. Ohta, T. Mizuno, *Sol. Energy* **1994**, *53*, 187–190.

[6] Y. Fu, D. Sun, Y. Chen, R. Huang, Z. Ding, X. Fu, Z. Li, *Angew. Chem. Int. Ed.* **2012**, *51*, 3364–3367.

[7] S. C. Roy, O. K. Varghese, M. Paulose, C. a Grimes, *ACS Nano* **2010**, *4*, 1259–1278.

[8] J. Yu, J. Low, W. Xiao, P. Zhou, M. Jaroniec, *J. Am. Chem. Soc.* **2014**, *136*, 8839–8842.

[9] I. P. Parkin, R. G. Palgrave, *J. Mater. Chem.* **2005**, *15*, 1689–1689.

[10] R. Blossey, *Nat. Mater.* **2003**, *2*, 301–306.

[11] S. Sakthivel, B. Neppolian, M. V. Shankar, B. Arabindoo, M. Palanichamy, V. Murugesan, *Sol. Energy Mater. Sol. Cells* **2003**, *77*, 65–82.

[12] M. R. Hoffmann, M. R. Hoffmann, S. T. Martin, S. T. Martin, W. Choi, W. Choi, D. W. Bahnemannt, D. W. Bahnemannt, *Chem. Rev.* **1995**, *95*, 69–96.

[13] J. Peral, D. F. Ollis, *J. Catal.* **1992**, *136*, 554–565.

[14] T. Ohno, K. Tokieda, S. Higashida, M. Matsumura, *Appl. Catal. A Gen.* **2003**, *244*, 383–391.

[15] S. Higashimoto, N. Kitao, N. Yoshida, T. Sakura, M. Azuma, H. Ohue, Y. Sakata, *J. Catal.* **2009**, *266*, 279–285.

[16] M. Ni, M. K. H. Leung, D. Y. C. Leung, K. Sumathy, *Renew. Sust. Energy Rev.* **2007**, *11*, 401–425.

[17] A. Kudo, Y. Miseki, *Chem. Soc. Rev.* **2009**, *38*, 253–278.

[18] X. Chen, S. Shen, L. Guo, S. S. Mao, *Chem. Rev.* **2010**, *110*, 6503–6570.

[19] K. Maeda, K. Teramura, D. Lu, T. Takata, N. Saito, Y. Inoue, K. Domen, *Nature* **2006**, *440*, 295.

[20] X. Yang, C. Cao, L. Erickson, K. Hohn, R. Maghirang, K. Klabunde, *J. Catal.* **2008**, *260*, 128–133.

[21] C. Han, R. Luque, D. D. Dionysiou, *Chem. Commun.* **2012**, *48*, 1860–1862.

[22] J. Zhu, F. Chen, J. Zhang, H. Chen, M. Anpo, *J. Photochem. Photobiol. A Chem.* **2006**, *180*, 196–204.

[23] X. H. Wang, J. G. Li, H. Kamiyama, Y. Moriyoshi, T. Ishigaki, *J. Phys. Chem. B* **2006**, *110*, 6804–6809.

[24] T. Ohno, T. Mitsui, M. Matsumura, *Chem. Lett.* **2003**, *32*, 364–365.

[25] J. Virkutyte, B. Baruwati, R. S. Varma, *Nanoscale* **2010**, *2*, 1109–1111.

[26] T. Shishido, T. Miyatake, K. Teramura, Y. Hitomi, H. Yamashita, T. Tanaka, *J. Phys. Chem.* **2009**, *113*, 18713–18718.

[27] J. Liu, S. Yang, W. Wu, Q. Tian, S. Cui, Z. Dai, F. Ren, X. Xiao, C. Jiang, *ACS Sust. Chem. Eng.* **2015**, *3*, 2975–2984.

[28] H. Cui, Y. Liu, W. Ren, *Adv. Powder Technol.* **2013**, *24*, 93–97.

[29] W. Li, J. Yang, Z. Wu, J. Wang, B. Li, S. Feng, Y. Deng, F. Zhang, D. Zhao, *J. Am. Chem. Soc.* **2012**, *134*, 11864–11867.

[30] M. Ojeda, A. Pineda, A. a. Romero, V. Barrón, R. Luque, *ChemSusChem* **2014**, *7*, 1876–1880.

[31] J. C. Colmenares, W. Ouyang, M. Ojeda, E. Kuna, O. Chernyayeva, D. Lisovytskiy, S. De, R. Luque, A. M. Balu, *Appl. Catal. B Environ.* **2016**, *183*, 107–112.

[32] M. Zhang, C. Chen, W. Ma, J. Zhao, *Angew. Chem. Int. Ed.* **2008**, *120*, 9876–9879.

[33] B. Jarry, F. Launay, J. P. Nogier, V. Montouillout, L. Gengembre, J. L. Bonardet, *Appl. Catal. A Gen.* **2006**, *309*, 177–186.

[34] M. Ojeda, A. M. Balu, V. Barrón, A. Pineda, Á. G. Coleto, A. Á. Romero, R. Luque, *J. Mater. Chem. A* **2014**, *2*, 387.

[35] K. Qi, B. Fei, J. H. Xin, *Thin Solid Films* **2011**, *519*, 2438–2444.

[36] M.-H. Pham, C.-T. Dinh, G.-T. Vuong, N.-D. Ta, T.-O. Do, *Phys. Chem. Chem. Phys.* **2014**, *16*, 5937–41.

4.Conclusions

According to the elaborated results in the previous part from the research works conducted in the thesis, conclusions can be drawn as below:

1. Hydrothermal method has been employed in the synthesis of mesoporous silicas (SBA-15, Al-SBA-15), which were subsequently functionalized by deposition of various metal (Cu, Pd, Pt or metal oxide (Fe_2O_3 or/and TiO_2) by post-synthetic methods, either mechanochemical method (ball milling) or flow deposition.
2. Starting from wheat bran, a largely abundant residue from the agricultural industry, innovative Titania-containing photocatalytic nanocomposites with promising textural and surface properties has been successfully synthesized by a simple, efficient and environmentally friendly technology mechanical ball milling.
3. All synthesized catalysts were carefully characterized with various techniques to understand their natures, such as N_2 physisorption, XRD, XPS, UV-Vis, SEM, TEM, ICP-MS.
4. Continuous flow hydrogenation of furfural was performed with both lab-synthesized mesoporous silica-based catalysts and commercial catalysts in a continuous flow reactor. Reaction temperature and the weight hourly space velocity (WHSV) have significant effects on the furfural conversion and product selectivity. In general cases, Pd catalysts have higher selectivity to tetrahydrofurfuryl alcohol, while Pt catalysts favor the formation of furfuryl alcohol, which is resulted from the strong affinity between Pd and the furan ring. Presence of Fe_2O_3 can affect the dispersion of Pd particles on the support, causing change in the product selectivity. The lab-synthesized catalyst, 5% Pd/MAGSNC, offered comparable performance to the 10% Pd/C within the first few hours.
5. The innovative nanocomposites, Ti-Brans, are active in the photocatalytic oxidation of benzyl alcohol to benzaldehyde, among which 10% Ti-Bran provided a 20% yield of benzaldehyde at 33% conversion of benzyl alcohol, comparable to the yield from P25 Evonik commercial titania, but the selectivity of the former material is much higher. The excellent photocatalytic performance 10% Ti-Bran might be attributed to the carbon support for the effective charge carrier separation.

6. The presence of Fe_2O_3 in TiO_2-MAGSNC dramatically extended the light absorption of nanocomposite materials into the visible light range (around 700 nm). Without the presence of TiO_2, the support and Fe_2O_3 were not active in the photocatalytic conversion of benzyl alcohol. TiO_2-MAGSNC nanocomposites were highly selective in production of benzaldehyde and higher TiO_2 loading on the catalysts resulted in higher conversion of benzyl alcohol, which could be attributed to the increase of catalytic active species (TiO_2).
7. The novel designed catalysts in the current thesis exhibited effective catalytic performance in upgrading platform molecules (furfural, benzyl alcohol) derived from lignocellulosic biomass to valuable chemicals using the modern technologies: flow chemistry and photochemistry. In general, works presented in this thesis are paving the way for the valorization of lignocellulosic biomass and seeking for solutions to produce sustainable fuels, chemicals and materials.

5. Resumen

Los trabajos de investigación que se recogen dentro de esta Memoria de Tesis Doctoral se han realizado dentro del grupo de investigación FQM-383, Nanoquímica y Valorización de Biomasa y Residuos (NANOVAL), al que he tenido el privilegio de pertenecer como becario Marie Curie. Las líneas de trabajo llevadas a cabo por el grupo de investigación NANOVAL se centran en el desarrollo de nuevos nanomateriales para la transformación catalítica de biomasa y residuos en compuestos de alto valor añadido mediante herramientas avanzadas como la química en flujo y la fotocatálisis. El proyecto de esta Tesis Doctoral se corresponde con los principales objetivos del grupo de investigación FQM-383, entre los que destacan el diseño de nuevos nanocatalizadores y su aplicación en la valorización de moléculas derivadas de la biomasa lignocelulósica bien mediante sistemas de reacción en flujo continuo o bien mediante fotocatálisis. Los principales resultados obtenidos de los trabajos de investigación llevados a cabo en esta Tesis Doctoral han sido publicados como artículos de investigación en diferentes revistas científicas, los cuales han sido incluidos en la Sección3 y se resumen a continuación.

En el primer trabajo, "***Towards industrial furfural conversion: Selectivity and stability of palladium and platinum catalysts under continuous flow regime***", se han preparado silicatos mesoporosos (SBA-15 y Al-SBA-15) siguiendo un procedimiento hidrotermal y, posteriormente, se han funcionalizado con metal(es) (Cu, Pd, Pt) y/o Fe_2O_3 mediante un procedimiento mecanoquímico o por deposición en flujo. Los materiales sintetizados, así como otros materiales comerciales fueron empleados en la hidrogenación del furfural en un reactor de flujo continuo. La conversión de furfural (95-99 %) y la selectividad hacia el producto (74-90% a alcohol furfurílico) se mantuvieron relativamente estables tras tiempos en corriente entre 20 y 120 minutos a una temperatura de reacción de 150 ºC, obteniéndose un mayor rendimiento y más estable con el tiempo para el material 5%Pd/MAGSNC. Sin embargo, la actividad catalítica de los restantes catalizadores sintetizados decrecía con el tiempo de reacción. Los catalizadores de paladio poseen una mayor selectividad hacia alcohol tetrahidrofurfurilico debido a una mayor afinidad entre el Pd y el anillo furánico y el grupo carbonilo, mientras que el Pt favorece la formación de alcohol furfurílico debido a la baja afinidad que este muestra por los anillos furánicos. Por otro lado, la presencia de Fe_2O_3 puede afectar la dispersión de las partículas de Pt sobre el soporte, provocando un cambio en la selectividad a los productos. Los resultados de actividad catalítica sugirieron que

la naturaleza del catalizador, la temperatura de reacción y la velocidad espacial (WHSV) eran factores importantes que afectaban drásticamente a la conversión del furfural y a la selectividad a los productos. El catalizador 5%Pd/MAGSNC, sintetizado en el laboratorio, mostró una actividad catalítica similar al material comercial 10%Pd/C durante las primeras horas de reacción. Además, el material 5%Pd/MAGSNC conservó el carácter magnético, lo cual le permite ser aislado de la mezcla de reacción simplemente mediante la aplicación de un campo magnético, facilitando así su reactivación.

A continuación, en el trabajo titulado "***Wheat bran valorization: towards photocatalytic nanomaterials for benzyl alcohol photo-oxidation***", se sintetizaron composites Ti-Bran, para ser utilizado como fotocatalizador, empleando como soporte el salvado de trigo, que es un residuo agrícola bastante abundante. La síntesis se llevó a cabo mediante la adición de diferentes cantidades de los precursores de Ti al salvado de trigo, seguido de un proceso de molienda empleando un molino planetario de bolas. La presencia de TiO_2 en fase anatasa en los nanocompositos sintetizados fue confirmada mediante la Difracción de Rayos-X (XRD), con tamaños de partícula cuyos valores oscilaron entre 4,6 y 7,8 nm, los cuales fueron obtenidos empleando la ecuación de Scherrer. El ajuste de la curva a 454,5 eV, aproximadamente, en la región Ti2p del espectro de Espectroscopía Fotoelectrónica de Rayos-X (XPS) de alta resolución en el catalizador 0,5Ti-Bran podría ser adscrita a la sustitución de oxígeno por átomos de carbono en la red TiO_2 y a la formación de enlaces Ti-C. La mejora en la capacidad de absorción de luz podría deberse, potencialmente, a la presencia de átomos de C en el óxido de titanio y a la heterounión entre TiO_2 y los soportes. Cuando el soporte empleado era únicamente carbón, este se mostraba inactivo en la fotooxidación del alcohol bencílico, mientras que cuando aumentaba el contenido de TiO_2 sobre el soporte carbonoso aumentaban a su vez la conversión del alcohol bencílico, así como el rendimiento hacia el benzaldehído. El máximo rendimiento hacia benzaldehído obtenido fue obtenido 20% aproximadamente, obtenido por el catalizador 10%Ti-Bran, con una conversión de alcohol bencílico entorno al 33%, mientras que mediante el empleo del catalizador comercial P-25 Evonik se conseguía una conversión de alcohol bencílico >99%, con un rendimiento hacia benzaldehído de solamente un 33%. Por tanto, considerando el menor contenido de TiO_2 en los catalizadores Ti-Bran, se puede concluir que los nanocomposites TiO_2-salvado de trigo mejoran los resultados obtenidos por el catalizador comercial de óxido de titanio

en la fotooxidación selectiva de alcohol bencílico. La mayor selectividad hacia benzaldehído en los nanocomposites Ti-Bran podría ser debida a la potencial incorporación de átomos de carbono en la red de TiO_2 y a la heterounión entre TiO_2 y los soportes, actuando el carbono como fotosensibilizador y así los electrones excitados podrían migrar a la banda de conducción del TiO_2.

Finalmente, en el trabajo "***Mechanochemical Synthesis of TiO_2 Nanocomposites as Photocatalysts for Benzyl Alcohol Photo-Oxidation***", se llevó a cabo la síntesis en un paso de nanocomposites de TiO_2 magnéticamente separables empleando un método mecanoquímico y SBA-15 como soporte. Para llevar a cabo dicha síntesis, ambos precursores metálicos, tanto el de titanio como el de hierro, fueron añadidos al recipiente de molienda junto con el material SBA-15 empleado como soporte y sometidos conjuntamente al proceso de molienda, siendo finalmente calcinados. El patrón de difracción de rayos-X mostró una señal a $2\theta=35,6^{o}$ que se corresponde a la fase magnética, en principio γ-Fe_2O_3, mientras que no se observaron las líneas de difracción correspondientes al Ti debido a su bajo contenido en el material sintetizado. El incremento de absorción de luz en el rango del visible para el catalizador sintetizado fue, probablemente, debido a la presencia del óxido de hierro. El protocolo de síntesis en un paso puede favorecer la heterounión entre Fe_2O_3 y TiO_2, la cual, otorga a la luz visible la capacidad de activación electrónica y facilita la separación espacial de los pares electrón-hueco. En los espectros XPS de alta resolución en la región del Ti2p, la curva se ajusta con energías de enlace mayores como consecuencia de la presencia de especies Ti^{4+} en la estructura Ti-O-Fe, en las cuales se podría inducirse una transferencia electrónica desde el Ti^{4+} hacia el Fe^{3+} en el enlace Ti–O–Fe debido a la diferencia de electronegatividad entre el Ti^{4+} (1.54) y el Fe^{3+} (1.83), resultando en un incremento de energía de enlace para especies Ti^{4+} y un descenso de esta para especies Fe^{3+}. La actividad fotocatalítica de los materiales sintetizados fue evaluada en la oxidación selectiva del alcohol bencílico. Tanto el soporte como el Fe_2O_3 no eran activos en la conversión fotocatalítica del alcohol bencílico en ausencia de TiO_2, lo que indica que el TiO_2 es el centro fotocatalítico activo. Los nanocomposites de TiO_2-MAGSNC se mostraron altamente efectivos en la producción de benzaldehído y cuanto mayor contenido en TiO_2 en el catalizador daba lugar a una mayor conversión de alcohol bencílico, la cual podría atribuirse a un incremento de centros activos (TiO_2).

6. Index of Quality

Type	Journal article
Title	Towards industrial furfural conversion: Selectivity and stability of palladium and platinum catalysts under continuous flow regime
Authors	**Weiyi Ouyang**, Alfonso Yepez, Antonio A. Romero, Rafael Luque
Journal	Catalysis Today
Year, volume, page	2018, 308, 32-37
Publisher	Elsevier
Journal included in Journal Citation Reports	Yes SCI database
Impact factor	4.636 (2016)
Category	Chemistry, Applied
Ranking in the category	6/72
Quartile	Q1

Type	Journal article
Title	Wheat bran valorisation: Towards photocatalytic nanomaterials for benzyl alcohol photo-oxidation
Authors	**Weiyi Ouyang**, Jose M. Reina, Ewelina Kuna, Alfonso Yepez, Alina M. Balu, Antonio A. Romero, Juan Carlos Colmenares, Rafael Luque
Journal	Journal of Environmental Management
Year, volume, page	2017, 203, 768-773
Publisher	Elsevier
Journal included in Journal Citation Reports	Yes SCI database
Impact factor	4.010 (2016)
Category	Environmental sciences
Ranking in the category	39/299
Quartile	Q1

Type	Journal article
Title	Mechanochemical synthesis of TiO_2 nanocomposites as photocatalysts for benzyl alcohol photo-oxidation
Authors	**Weiyi Ouyang**, Ewelina Kuna, Alfonso Yepez, Alina M. Balu, Antonio A. Romero, Juan Carlos Colmenares, Rafael Luque
Journal	Nanomaterials
Year, volume, page	2016, 6, 93
Publisher	MDPI
Journal included in Journal Citation Reports	Yes SCI database
Impact factor	3.553 (2016)
Category	Materials science, Multidisciplinary
Ranking in the category	59/275
Quartile	Q1

7. Other scientific achievements

During my Ph.D study, I have accomplished other scientific achievements which are not included in the current thesis, including research articles and conference abstracts

Other scientific achievements as publication **not included** in the thesis:

1. Xu, C.[#], **Ouyang, W.** [#]*****, Muñoz-Batista, M. J., Fernandez-Garcia, M., Luque, R.* (2018). Highly active catalytic Ru/TiO_2 nanomaterials for continuous production of γ-valerolactone. *ChemSusChem*, accepted, DOI: 10.1002/cssc.201800667. (#: equal contribution, **IF: 7.226**)

2. **Ouyang, W.**, Zhao, D., Wang, Y., Balu, A. M., Len, C., Luque, R.* (2018). Continuous flow conversion of biomass-derived methyl levulinate into gamma valerolactone using functional metal organic frameworks. *ACS Sustainable Chemistry & Engineering*, 6, 6746-6752. (**IF: 5.951**)

3. Colmenares, J. C.*, **Ouyang, W.**, Ojeda, M., Kuna, E., Chernyayeva, O., Lisovytskiy, D., De, S., Luque, R., & Balu, A. M.* (2016). Mild ultrasound-assisted synthesis of TiO_2 supported on magnetic nanocomposites for selective photo-oxidation of benzyl alcohol. *Applied Catalysis B: Environmental*, *183*, 107-112. (**IF: 9.446, citations: 36**)

4. Cerdan, K., **Ouyang, W.,** Colmenares, J. C., Muñoz-Batista, M. J., Luque, R., Balu, A. M.* (2018). Facile mechanochemical modification of g-C_3N_4 for selective photo-oxidation of benzyl alcohol. *Chemical Engineering Science*, DOI: 10.1016/j.ces.2018.04.001. (**IF: 2.895**)

5. Zhao, D., Prinsen, P., Wang, Y., **Ouyang, W.**, Delbecq, F., Len, C*., Luque, R*. (2018). Continuous flow alcoholysis of furfuryl alcohol to alkyl levulinates and angelica lactones using zeolites. *ACS Sustainable Chemistry & Engineering*, 6, 6901-6909.

6. Ziarati, A., Badiei A.*, Luque R.*, **Ouyang, W.** (2018). Designer hydrogenated wrinkled Yolk@Shell TiO_2 architectures: towards advanced room temperature visible light selective photocatalysts. Journal of Materials Chemistry A, 2018,**6**, 8962-8968. (**IF: 8.867**)

Other scientific achievements as conference abstracts (oral communication & poster):

1. I Doctoral Seminar on Renewable Energies, Jaen, Spain, May 9-11, 2018. Poster, "**Catalytic transformation of biomass-derived methyl levulinate into gamma valerolactone in continuous flow by functionalized metal organic frameworks**"

2. **Ouyang, W.**, Muñoz-Batista M.J., Fernandez-Garcia, M., and Luque, R.*, Oral communication, "**Catalytic performance of Ru/TiO_2 in the conversion of methyl levulinate biowaste**", FP1306 COST Action Forth Workshop & Fifth MC Meeting, Thessaloniki, Greece, March 12-14, 2018.

3. **Ouyang, W.**, Muñoz-Batista M.J., Balu, A.M., Romero, A.A., Fernandez-Garcia, M., and Luque, R.*, Flash communication, "**A novel mixed-metal organic framework and its possible applications**", The 4th International Symposium on Green Chemistry 2017, La Rochelle, France, May 16-19, 2017

4. **Ouyang, W.**, Wang, B., Kuna, E., Balu, A.M., Romero, A.A., Colmenares,J.C., Luque, R.*, Oral communication, "**Novel Photoactive Mixed-metal Organic Framework and Its Possible Application in Selective Photo-oxidation of Benzyl Alcohol**", FP1306 COST Action Third Workshop & Fourth MC Meeting, Torremolinos, Spain, March 27-28, 2017.

5. **Ouyang, W.**, Kuna, E., Yepez, A., Balu,A.M., Romero, A.A., Colmenares,J.C., Luque, R.*, Poster, "**Mechanochemical Synthesis of TiO_2 Magnetically-separable Nanocomposites (TiO_2-MAGSNC) as Photocatalysts for Benzyl Alcohol Photo-Oxidation**", 17th Plenary Scientific Meeting of Inorganic Chemistry and 11th Plenary Scientific Meeting of Solid State Chemistry, Malaga, Spain, June 19-22, 2016.

6. **Ouyang, W.**, Reina J.M., Kuna, E., Balu, A. Yepez, A.M., Romero, A.A., Colmenares,J.C., Luque, R.*, Flash communication, "**Wheat Bran Valorization: towards Photocatalytic Nanomaterials for Benzyl Alcohol Photo-oxidation**", FP1306 COST Action Second Workshop & Third MC Meeting, Dubrovnik, Croatia, April 4-6, 2016.

8. Appendices

8.1. Appendix 1 Towards Industrial Furfural Conversion: Selectivity and Stability of Palladium and Platinum Catalysts under Continuous Flow Regime

ARTICLE IN PRESS

Catalysis Today xxx (xxxx) xxx–xxx

Contents lists available at ScienceDirect

Catalysis Today

journal homepage: www.elsevier.com/locate/cattod

Towards industrial furfural conversion: Selectivity and stability of palladium and platinum catalysts under continuous flow regime

Weiyi Ouyang*, Alfonso Yepez, Antonio A. Romero, Rafael Luque*

Departamento de Quimica Organica, Universidad de Cordoba, Campus de Rabanales, Edificio Marie Curie, CtraNnal IV, Km. 396, E-14014, Cordoba, Spain

ARTICLE INFO

Keywords:
Furfural
Hydrogenation
Continuous flow
Selectivity
Stability

ABSTRACT

Furfural is an important biorefinery platform chemical, derived from hemicelluloses which represent an import fraction of lignocellulosic biomass feedstocks and waste streams originating from them. Recently, promising results have been reported on the hydrogenation of furfural, although the selectivity still may be improved. Most of these studies dealt with batch hydrogenation, however, hydrogenation in continuous flow is preferable for industrial applications. In this work, we compare the conversion, selectivity and stability on-stream in continuous flow regime of lab-synthesized and commercial palladium and platinum catalysts.

1. Introduction

The global population could reach and even exceed 9 billion by 2050 [1]. The use of sustainable feedstocks to meet the growing global energy demand and to reduce the use of fossil resources is now a highly imminent challenge for the research community, and a challenge to be adopted in currently existing industrial refineries or to be designed in future biorefinery plants. The largest part of the current fossil derived petroleum refining is used for fuels production. Still, an important part of petroleum is used for the production of bulk chemicals and materials. Today, the use of alternative biomass feedstocks (or waste streams derived from them) has become a widely reported research area. Considering the complexity and the recalcitrance of biomass, many works focused on the transformation of biomass derived platform molecules to fuels and high-added value chemicals. For example, C5 sugars are key representative compounds of the hemicellulose fraction of lignocellulose, which can be converted to valuable platform molecules and subsequently valorized into high-added value products [2]. Furfural (F) is an important platform chemical, which can be obtained via dehydration under mild conditions from xylose, a typical C5 sugar.

Furfural can undergo reactions typical for aldehydes like acetalization, acylation, aldol and Knoevenagel condensations, reduction to alcohols, reductive amination to amines, decarbonylation, oxidation to carboxylic acids and Grignard reactions. Besides, the furan ring can be subjected to alkylation, hydrogenation, oxidation, halogenations and nitration reactions. Due to the electron-withdrawing effect of the carbonyl group, the furan ring is less susceptible to hydrolytic ring cleavage and Diels-Alder cycloaddition reactions. Therefore, furfural is considered to be an attractive platform chemical for the production of a wide range of chemicals, e.g. solvents (tetrahydrofuran), plastics (in particular, polyamides), resins via furfuryl alcohol and fuel additives (methylfuran, methyl-tetrahydrofuran, valerate esters, ethylfurfuryl and ethyltetrahydrofurfuryl ethers and C10–C15 coupling products) [2]. Around 60–70% of the global furfural production is converted to furfuryl alcohol [2,3]. It is widely reported that furfural can be further transformed into various compounds by hydrogenation, such as furfuryl alcohol (FA), tetrahydrofurfuryl alcohol (THFA), 2-methylfuran (MF) and 2-methyltetrahydrofuran (MTHF). Most of these reactions were performed in batch conditions [4–8] with noble or transition metals based catalysts, while only a few of them were performed in continuous flow [7,9]. Especially, these reactions were performed using only either lab-synthesized or commercial catalysts, with a simple comparison of existing results obtained under different conditions. Regarding to the advantages of flow chemistry, such as faster, safer reactions and easy scale-up, it would be interesting to give a comparison of catalytic performance of both lab-synthesized and commercial catalysts under same reaction conditions in continuous flow system. Previous work from our group has provided insights into the reaction pathway comparing noble metal and transition metal catalysts (Scheme 1), showing favorable results for Pd based catalysts [9]. The mechanism of furfural conversion on palladium catalysts was also studied by other researchers based on density functional theory (DFT) [10].

Despite the excellent conversion and selectivity of Pd catalysts, adding magnetic properties to the catalyst would be preferable for catalyst recovery through applying an external magnetic field, which would result in a more straightforward and cost-effective separation method as compared with conventional methods, as illustrated in previous reports [11–14]. Magnetically separable Pd based nanocomposite

* Corresponding authors.
E-mail addresses: qo2ououw@uco.es (W. Ouyang), q62alsor@uco.es (R. Luque).

http://dx.doi.org/10.1016/j.cattod.2017.07.011
Received 7 May 2017; Received in revised form 4 July 2017; Accepted 8 July 2017

Please cite this article as: Ouyang, W., Catalysis Today (2017), http://dx.doi.org/10.1016/j.cattod.2017.07.011

Acknowledgements

Rafael Luque gratefully acknowledges Consejeria de Ciencia e Innovacion, Junta de Andalucia for funding project P10-FQM-6711. Funding from Marie Curie Actions under ITN Project Photo4Future (H2020-MSCA-ITN-2014-641861), especially for funding WO Ph.D studies. We also greatly acknowledge ThalesNano Inc. for all supports, including the continuous flow reactor, H-Cube Pro, commercial catalysts and chemicals for the hydrogenation reactions.

Appendix A. Supplementary data

Supplementary data associated with this article can be found, in the online version, at http://dx.doi.org/10.1016/j.cattod.2017.07.011.

References

[1] H.C.J. Godfray, J.R. Beddington, I.R. Crute, L. Haddad, D. Lawrence, J.F. Muir, J. Pretty, S. Robinson, S.M. Thomas, C. Toulmin, Food security: the challenge of feeding 9 billion people, Science (80-.) 327 (2010) 812–818, http://dx.doi.org/10.1126/science.1185383.

[2] J.-P. Lange, E. van der Heide, J. van Buijtenen, R. Price, Furfural-A promising platform for lignocellulosic biofuels, ChemSusChem 5 (2012) 150–166, http://dx.doi.org/10.1002/cssc.201100648.

[3] H.E. Hoydonckx, W.M. Van Rhijn, W. Van Rhijn, D.E. De Vos, P.A. Jacobs, H.E. Hoydonckx, W.M. Van Rhijn, W. Van Rhijn, D.E. De Vos, P.A. Jacobs, Furfural and derivatives, Ullmann's Encycl. Ind. Chem. Wiley-VCH Verlag GmbH & Co. KGaA, Weinheim, Germany, 2007, http://dx.doi.org/10.1002/14356007.a12_119.pub2.

[4] P. Panagiotopoulou, D.G. Vlachos, Liquid phase catalytic transfer hydrogenation of furfural over a Ru/C catalyst, Appl. Catal. A Gen. 480 (2014) 17–24, http://dx.doi.org/10.1016/j.apcata.2014.04.018.

[5] R.V. Sharma, U. Das, R. Sammynaiken, A.K. Dalai, Liquid phase chemo-selective catalytic hydrogenation of furfural to furfuryl alcohol, Appl. Catal. A Gen. 454 (2013) 127–136, http://dx.doi.org/10.1016/j.apcata.2012.12.010.

[6] M.M. Villaverde, N.M. Bertero, T.F. Garetto, A.J. Marchi, Selective liquid-phase hydrogenation of furfural to furfuryl alcohol over Cu-based catalysts, Catal. Today 213 (2013) 87–92, http://dx.doi.org/10.1016/j.cattod.2013.02.031.

[7] N.S. Biradar, A.A. Hengne, S.N. Birajdar, R. Swami, C.V. Rode, Tailoring the product distribution with batch and continuous process options in catalytic hydrogenation of furfural, Org. Process Res. Dev. 18 (2014) 1434–1442, http://dx.doi.org/10.1021/op500196x.

[8] K. Fulajtárova, T. Soták, M. Hronec, I. Vávra, E. Dobročka, M. Omastová, Aqueous phase hydrogenation of furfural to furfuryl alcohol over Pd-Cu catalysts, Appl. Catal. A Gen. 502 (2015) 78–85, http://dx.doi.org/10.1016/j.apcata.2015.05.031.

[9] A.J. Garcia-Olmo, A. Yepez, A.M. Balu, A.A. Romero, Y. Li, R. Luque, Insights into the activity, selectivity and stability of heterogeneous catalysts in the continuous flow hydroconversion of furfural, Catal. Sci. Technol. 6 (2016) 4705–4711, http://dx.doi.org/10.1039/C6CY00249H.

[10] V. Vorotnikov, G. Mpourmpakis, D.G. Vlachos, DFT study of furfural conversion to furan, furfuryl alcohol, and 2-methylfuran on Pd(111), ACS Catal. 2 (2012) 2496–2504, http://dx.doi.org/10.1021/cs300395a.

[11] M. Ojeda, A.M. Balu, V. Barrón, A. Pineda, Á.G. Coleto, A.Á. Romero, R. Luque, Solventless mechanochemical synthesis of magnetic functionalized catalytically active mesoporous SBA-15 nanocomposites, J. Mater. Chem. A 2 (2014) 387, http://dx.doi.org/10.1039/c3ta13564k.

[12] J.C. Colmenares, W. Ouyang, M. Ojeda, E. Kuna, O. Chernyayeva, D. Lisovytskiy, S. De, R. Luque, A.M. Balu, Mild ultrasound-assisted synthesis of TiO2 supported on magnetic nanocomposites for selective photo-oxidation of benzyl alcohol, Appl. Catal. B Environ. 183 (2016) 107–112, http://dx.doi.org/10.1016/j.apcatb.2015.10.034.

[13] C. Zhang, L. Qiu, F. Ke, Y. Zhu, Y. Yuan, G. Xu, X. Jiang, A novel magnetic recyclable photocatalyst based on a core–shell metal–organic framework Fe3O4@MIL-100(Fe) for the decolorization of methylene blue dye, J. Mater. Chem. A 1 (2013) 14329, http://dx.doi.org/10.1039/c3ta13030d.

[14] M.B. Gawande, P.S. Branco, I.D. Nogueira, C.A.A. Ghumman, N. Bundaleski, A. Santos, O.M.N.D. Teodoro, R. Luque, Catalytic applications of a versatile magnetically separable Fe–Mo (Nanocat-Fe–Mo) nanocatalyst, Green Chem. 15 (2013) 682, http://dx.doi.org/10.1039/c3gc36844k.

[15] J.R. Dodson, E.C. Cooper, A.J. Hunt, A. Matharu, J. Cole, A. Minihan, J.H. Clark, D.J. Macquarrie, Alkali silicates and structured mesoporous silicas from biomass power station wastes: the emergence of bio-MCMs, Green Chem. 15 (2013) 1203, http://dx.doi.org/10.1039/c3gc40324f.

[16] J. Liu, X. Peng, W. Sun, Y. Zhao, C. Xia, Magnetically separable Pd catalyst for carbonylative sonogashira coupling reactions for the synthesis of α,β-alkynyl ketones, Org. Lett. 10 (2008) 3933–3936, http://dx.doi.org/10.1021/ol801478y.

[17] H. Wang, Y. Liu, M. Li, H. Huang, H.M. Xu, R.J. Hong, H. Shen, Multifunctional TiO2 nanowires-modified nanoparticles bilayer film for 3D dye-sensitized solar cells, Optoelectron. Adv. Mater. Rapid Commun. 4 (2010) 1166–1169, http://dx.doi.org/10.1039/b000000x.

[18] S. Verma, D. Verma, A.K. Sinha, S.L. Jain, Palladium complex immobilized on graphene oxide-magnetic nanoparticle composites for ester synthesis by aerobic oxidative esterification of alcohols, Appl. Catal. A Gen. 489 (2015) 17–23, http://dx.doi.org/10.1016/j.apcata.2014.10.004.

[19] K. Yan, J. Liao, X. Wu, X. Xie, A noble-metal free Cu-catalyst derived from hydrotalcite for highly efficient hydrogenation of biomass-derived furfural and levulinic acid, RSC Adv. 3 (2013) 3853, http://dx.doi.org/10.1039/c3ra22158j.

[20] B. Jarry, F. Launay, J.P. Nogier, V. Montouillout, L. Gengembre, J.L. Bonardet, Characterisation, acidity and catalytic activity of Ga-SBA-15 materials prepared following different synthesis procedures, Appl. Catal. A Gen. 309 (2006) 177–186, http://dx.doi.org/10.1016/j.apcata.2006.04.044.

[21] M.J. Gracia, E. Losada, R. Luque, J.M. Campelo, D. Luna, J.M. Marinas, A.A. Romero, Activity of gallium and aluminum SBA-15 materials in the Friedel-Crafts alkylation of toluene with benzyl chloride and benzyl alcohol, Appl. Catal. A Gen. 349 (2008) 148–155, http://dx.doi.org/10.1016/j.apcata.2008.07.023.

[22] A. Yepez, F.L.Y. Lam, A.A. Romero, C.O. Kappe, R. Luque, Continuous flow preparation of iron oxide nanoparticles supported on porous silicates, ChemCatChem 7 (2015) 276–282, http://dx.doi.org/10.1002/cctc.201402802.

[23] A. Pineda, A.M. Balu, J.M. Campelo, A.A. Romero, D. Carmona, F. Balas, J. Santamaria, R. Luque, A dry milling approach for the synthesis of highly active nanoparticles supported on porous materials, ChemSusChem 4 (2011) 1561–1565, http://dx.doi.org/10.1002/cssc.201100265.

[24] M. Ojeda, A. Pineda, A.a. Romero, V. Barrón, R. Luque, Mechanochemical synthesis of maghemite/silica nanocomposites: advanced materials for aqueous room-temperature catalysis, ChemSusChem 7 (2014) 1876–1880, http://dx.doi.org/10.1002/cssc.201400055.

[25] J. Lee, Y.T. Kim, G.W. Huber, Aqueous-phase hydrogenation and hydrodeoxygenation of biomass-derived oxygenates with bimetallic catalysts, Green Chem. 16 (2014) 708, http://dx.doi.org/10.1039/c3gc41071d.

[26] S. Sitthisa, T. Pham, T. Prasomsri, T. Sooknoi, R.G. Mallinson, D.E. Resasco, Conversion of furfural and 2-methylpentanal on Pd/SiO2 and Pd–Cu/SiO2 catalysts, J. Catal. 280 (2011) 17–27, http://dx.doi.org/10.1016/j.jcat.2011.02.006.

[27] B. Liu, L. Cheng, L. Curtiss, J. Greeley, Effects of van der Waals density functional corrections on trends in furfural adsorption and hydrogenation on close-packed transition metal surfaces, Surf. Sci. 622 (2014) 51–59, http://dx.doi.org/10.1016/j.susc.2013.12.001.

[28] M. Yamauchi, R. Ikeda, H. Kitagawa, M. Takata, Nanosize effects on hydrogen storage in palladium, J. Phys. Chem. C 112 (2008) 3294–3299, http://dx.doi.org/10.1021/jp710447j.

[29] F. Delbecq, P. Sautet, A density functional study of adsorption structures of unsaturated aldehydes on Pt(111): a key factor for hydrogenation selectivity, J. Catal. 211 (2002) 398–406, http://dx.doi.org/10.1006/jcat.2002.3744.

[30] A. Giroir-Fendler, D. Richard, P. Gallezot, Selectivity in Cinnamaldehyde Hydrogenation of Group-VIII Metals Supported on Graphite and Carbon, (1988), pp. 171–178, http://dx.doi.org/10.1016/S0167-2991(09)60812-0.

[31] S. Bhogeswararao, D. Srinivas, Catalytic conversion of furfural to industrial chemicals over supported Pt and Pd catalysts, J. Catal. 327 (2015) 65–77, http://dx.doi.org/10.1016/j.jcat.2015.04.018.

8.2. Appendix 2 Wheat Bran Valorisation: Towards Photocatalytic Nanomaterials for Benzyl Alcohol Photo-Oxidation

Journal of Environmental Management 203 (2017) 768–773

Contents lists available at ScienceDirect

Journal of Environmental Management

journal homepage: www.elsevier.com/locate/jenvman

Research article

Wheat bran valorisation: Towards photocatalytic nanomaterials for benzyl alcohol photo-oxidation

Weiyi Ouyang [a], Jose M. Reina [a], Ewelina Kuna [b], Alfonso Yepez [a], Alina M. Balu [a], Antonio A. Romero [a], Juan Carlos Colmenares [b], Rafael Luque [a, *]

[a] Departamento de Quimica Organica, Universidad de Cordoba, Edificio Marie Curie(C-3), Ctra Nnal IV-A, Km 396, E14014 Córdoba, Spain
[b] Institute of Physical Chemistry PAS, Kasprzaka 44/52, 01-224 Warsaw, Poland

ARTICLE INFO

Article history:
Received 3 February 2016
Received in revised form
3 July 2016
Accepted 4 July 2016
Available online 15 July 2016

Keywords:
Waste valorization
Wheat bran
Photocatalysis
Benzyl alcohol oxidation

ABSTRACT

In this work, we have successfully synthesized a set of titania photocatalytic nanocomposites by the incorporation of different TiO_2 content on wheat bran residues. The obtained catalysts were characterized by different techniques including UV–Vis spectroscopy, X-ray diffraction (XRD), X-ray photoelectron spectroscopy (XPS) and Transmission Electron Microscopy (TEM) while their photocatalytic activity was investigated in the oxidation of benzyl alcohol under UV light irradiation. Benzaldehyde yields were ca. 20%, with conversion in the systems of ca. 33% of benzyl alcohol by using 10%Ti-Bran catalyst, as compared to 33% yield to the target product (quantitative conversion of benzyl alcohol) using commercial pure TiO_2 (P-25). The photocatalytic activity results indicate that designed waste-derived nanomaterials with low TiO_2 content can efficiently photocatalyze the conversion of benzyl alcohol with relative high selectivity towards benzaldehyde.

1. Introduction

Environmentally friendly and energy-saving technologies are becoming increasingly advantageous with the increase of public awareness on environment protection and sustainable development. Since the discovery of photocatalytic splitting of water on TiO_2 electrodes (Fujishima and Honda, 1972), semiconductor-based heterogeneous photocatalysis has received extensive attention and now is considered to be one of the most relevant and environmentally friendly technologies with advantages including simplicity, environmental compatibility, low-cost and energy-saving.

To assess the photocatalytic activity of a semiconductor photocatalyst, several factors should be taken into consideration, including its stability, efficiency, selectivity and wavelength range response (Linsebigler et al., 1995). Among various semiconductor-based photocatalysts, TiO_2 is one of the most attractive photocatalysts owing to its outstanding photocatalytic activity, high thermal and chemical stability, non-toxicity, cost effectiveness and the strong oxidizing power of the photogenerated holes. Massive investigations related to TiO_2 photocatalysts have been reported in different applications in the last decades, including chemicals and fuels production from CO_2 reduction (Adachi et al., 1994; Chen et al., 2015; Yu et al., 2014), decontamination of water (Herrmann et al., 1999; Hoffmann et al., 1995; Virkutyte et al., 2010; Yang et al., 2008), organic synthesis (Colmenares et al., 2016; Higashimoto et al., 2009; Hubert et al., 2010; Ohno et al., 2003b) and production of H_2 from water splitting (Chen et al., 2010; Ni et al., 2007). However, the use of pure TiO_2 photocatalyst is limited by its large band gap (3.2eV, anatase crystalline phase) which requires light with wavelength $\lambda < 387$ nm for the excitation of electrons from the valence to the conduction band, resulting that only 5% of the solar irradiation can be utilized for the photocatalytic process. Modifications on TiO_2 are necessary to improve its photocatalytic properties under solar irradiation or artificial light source. Modifications such as introductions of metals, dopants or combinations with other semiconductors are beneficial because they suppress the recombination of the photogenerated electron-hole pairs and thus increase the quantum yield of the photocatalytic process (Linsebigler et al., 1995). Meanwhile, the newly created heterojunctions can help the photocatalyst expand the wavelength range response into visible light region.

Many reported investigations have revealed that doping with non-metal atoms, such as C, N, F, P or S, can significantly improve

* Corresponding author.
E-mail address: q62alsor@uco.es (R. Luque).

http://dx.doi.org/10.1016/j.jenvman.2016.07.013
0301-4797/

Higashimoto, S., Kitao, N., Yoshida, N., Sakura, T., Azuma, M., Ohue, H., Sakata, Y., 2009. Selective photocatalytic oxidation of benzyl alcohol and its derivatives into corresponding aldehydes by molecular oxygen on titanium dioxide under visible light irradiation. J. Catal. 266, 279–285. http://dx.doi.org/10.1016/j.jcat.2009.06.018.

Hoffmann, M.R., Hoffmann, M.R., Martin, S.T., Martin, S.T., Choi, W., Choi, W., Bahnemannt, D.W., Bahnemannt, D.W., 1995. Environmental applications of semiconductor photocatalysis. Chem. Rev. 95, 69–96. http://dx.doi.org/10.1021/cr00033a004.

Hubert, C., Denicourt-Nowicki, A., Beaunier, P., Roucoux, A., 2010. TiO_2-supported Rh nanoparticles: from green catalyst preparation to application in arene hydrogenation in neat water. Green Chem. 12, 1167. http://dx.doi.org/10.1039/c004079g.

Irie, H., Watanabe, Y., Hashimoto, K., 2003. Nitrogen-concentration dependence on photocatalytic activity of TiO_2-xNx powders. J. Phys. Chem. B 107, 5483–5486. http://dx.doi.org/10.1021/jp030133h.

Lettmann, C., Hildenbrand, K., Kisch, H., Macyk, W., Maier, W.F., 2001. Visible light photodegradation of 4-chlorophenol with a coke-containing titanium dioxide photocatalyst. Appl. Catal. B Environ. 32, 215–227. http://dx.doi.org/10.1016/S0926-3373(01)00141-2.

Li, C.-J., Xu, G.-R., Zhang, B., Gong, J.R., 2012. High selectivity in visible-light-driven partial photocatalytic oxidation of benzyl alcohol into benzaldehyde over single-crystalline rutile TiO_2 nanorods. Appl. Catal. B Environ. 115, 201–208. http://dx.doi.org/10.1016/j.apcatb.2011.12.003.

Linsebigler, A.L., Linsebigler, A.L., Yates Jr., J.T., Lu, G., Lu, G., Yates, J.T., 1995. Photocatalysis on TiO_2 surfaces: principles, mechanisms, and selected results. Chem. Rev. 95, 735–758. http://dx.doi.org/10.1021/cr00035a013.

Liu, J., Zhang, Q., Yang, J., Ma, H., Tade, M.O., Wang, S., Liu, J., 2014. Facile synthesis of carbon-doped mesoporous anatase TiO_2 for the enhanced visible-light driven photocatalysis. Chem. Commun. 50, 13971–13974. http://dx.doi.org/10.1039/C4CC05544F.

Marotta, R., Di Somma, I., Spasiano, D., Andreozzi, R., Caprio, V., 2011. Selective oxidation of benzyl alcohol to benzaldehyde in water by TiO_2/Cu(II)/UV solar system. Chem. Eng. J. 172, 243–249. http://dx.doi.org/10.1016/j.cej.2011.05.097.

Neville, E.M., Mattle, M.J., Loughrey, D., Rajesh, B., Rahman, M., MacElroy, J.M.D., Sullivan, J.A., Thampi, K.R., 2012. Carbon-doped TiO_2 and carbon, tungsten-codoped TiO_2 through sol–gel processes in the presence of melamine borate: reflections through photocatalysis. J. Phys. Chem. C 116, 16511–16521. http://dx.doi.org/10.1021/jp303645p.

Ni, M., Leung, M.K.H., Leung, D.Y.C., Sumathy, K., 2007. A review and recent developments in photocatalytic water-splitting using TiO_2 for hydrogen production. Renew. Sustain. Energy Rev. 11, 401–425. http://dx.doi.org/10.1016/j.rser.2005.01.009.

Ohno, T., Akiyoshi, M., Umebayashi, T., Asai, K., Mitsui, T., Matsumura, M., 2004. Preparation of S-doped TiO_2 photocatalysts and their photocatalytic activities under visible light. Appl. Catal. A Gen. 265, 115–121. http://dx.doi.org/10.1016/j.apcata.2004.01.007.

Ohno, T., Mitsui, T., Matsumura, M., 2003a. Photocatalytic activity of S-doped TiO_2 photocatalyst under visible light. Chem. Lett. 32, 364–365. http://dx.doi.org/10.1246/cl.2003.364.

Ohno, T., Tokieda, K., Higashida, S., Matsumura, M., 2003b. Synergism between rutile and anatase TiO_2 particles in photocatalytic oxidation of naphthalene. Appl. Catal. A Gen. 244, 383–391. http://dx.doi.org/10.1016/S0926-860X(02)00610-5.

Shen, Y., Xiong, T., Li, T., Yang, K., 2008. Tungsten and nitrogen co-doped TiO_2 nanopowders with strong visible light response. Appl. Catal. B Environ. 83, 177–185. http://dx.doi.org/10.1016/j.apcatb.2008.01.037.

Sordello, F., Zeb, G., Hu, K., Calza, P., Minero, C., Szkopek, T., Cerruti, M., 2014. Tuning TiO_2 nanoparticle morphology in graphene–TiO_2 hybrids by graphene surface modification. Nanoscale 6, 6710. http://dx.doi.org/10.1039/c4nr01322k.

Spasiano, D., del Pilar Prieto Rodriguez, L., Olleros, J.C., Malato, S., Marotta, R., Andreozzi, R., 2013. TiO_2/Cu(II) photocatalytic production of benzaldehyde from benzyl alcohol in solar pilot plant reactor. Appl. Catal. B Environ. 136–137, 56–63. http://dx.doi.org/10.1016/j.apcatb.2013.01.055.

Sun, J., Qiao, L., Sun, S., Wang, G., 2008. Photocatalytic degradation of Orange G on nitrogen-doped TiO_2 catalysts under visible light and sunlight irradiation. J. Hazard. Mater 155, 312–319. http://dx.doi.org/10.1016/j.jhazmat.2007.11.062.

Virkutyte, J., Baruwati, B., Varma, R.S., 2010. Visible light induced photobleaching of methylene blue over melamine-doped TiO_2 nanocatalyst. Nanoscale 2, 1109–1111. http://dx.doi.org/10.1039/c0nr00089b.

Virkutyte, J., Varma, R.S., 2010. Fabrication and visible light photocatalytic activity of a novel Ag/TiO_2–xNx nanocatalyst. New J. Chem. 34, 1094–1096. http://dx.doi.org/10.1039/c0nj00268b.

Wu, G., Nishikawa, T., Ohtani, B., Chen, A., 2007. Synthesis and characterization of carbon-doped TiO_2 nanostructures with enhanced visible light response. Chem. Mater 19, 4530–4537. http://dx.doi.org/10.1021/cm071244m.

Yang, X., Cao, C., Erickson, L., Hohn, K., Maghirang, R., Klabunde, K., 2008. Synthesis of visible-light-active TiO_2-based photocatalysts by carbon and nitrogen doping. J. Catal. 260, 128–133. http://dx.doi.org/10.1016/j.jcat.2008.09.016.

Yu, J., Low, J., Xiao, W., Zhou, P., Jaroniec, M., 2014. Enhanced photocatalytic CO_2-reduction activity of anatase TiO_2 by coexposed {001} and {101} facets. J. Am. Chem. Soc. 136, 8839–8842. http://dx.doi.org/10.1021/ja5044787.

8.3. Appendix 3 Mechanochemical Synthesis of TiO_2 Nanocomposites as Photocatalysts for Benzyl Alcohol Photo-Oxidation

nanomaterials

MDPI

Article

Mechanochemical Synthesis of TiO_2 Nanocomposites as Photocatalysts for Benzyl Alcohol Photo-Oxidation

Weiyi Ouyang [1], Ewelina Kuna [2], Alfonso Yepez [1], Alina M. Balu [1], Antonio A. Romero [1], Juan Carlos Colmenares [2] and Rafael Luque [1,*]

[1] Department of Organic Chemistry, University of Cordoba, Edificio Marie Curie(C-3), Ctra Nnal IV-A, Km 396, Cordoba E14014, Spain; qo2ououw@uco.es (W.O.); z22yegaa@uco.es (A.Y.); qo2balua@uco.es (A.M.B.); qo1rorea@uco.es (A.A.R.)

[2] Institute of Physical Chemistry Polish Academy of Sciences (PAS), Kasprzaka 44/52, Warsaw 01-224, Poland; ekuna@ichf.edu.pl (E.K.); jcarloscolmenares@ichf.edu.pl (J.C.C.)

* Correspondence: q62alsor@uco.es; Tel.: +34-957211050

Academic Editors: Hermenegildo García and Sergio Navalón
Received: 3 March 2016; Accepted: 7 May 2016; Published: 18 May 2016

Abstract: TiO_2 (anatase phase) has excellent photocatalytic performance and different methods have been reported to overcome its main limitation of high band gap energy. In this work, TiO_2-magnetically-separable nanocomposites (MAGSNC) photocatalysts with different TiO_2 loading were synthesized using a simple one-pot mechanochemical method. Photocatalysts were characterized by a number of techniques and their photocatalytic activity was tested in the selective oxidation of benzyl alcohol to benzaldehyde. Extension of light absorption into the visible region was achieved upon titania incorporation. Results indicated that the photocatalytic activity increased with TiO_2 loading on the catalysts, with moderate conversion (20%) at high benzaldehyde selectivity (84%) achieved for 5% TiO_2-MAGSNC. These findings pointed out a potential strategy for the valorization of lignocellulosic-based biomass under visible light irradiation using designer photocatalytic nanomaterials.

Keywords: TiO_2; magnetically separable photocatalysts; selective photo-oxidation; mechanochemical synthesis; ball mill

1. Introduction

Photocatalysis has been considered as one of the most environmentally friendly and promising technologies owing to advantages such as being clean, efficient, cost-effective, and energy-saving [1–3] Typical applications of photocatalysis are conversion of CO_2 to fuels and chemicals [4–8], self-cleaning surfaces [9,10], disinfection of water [11,12], oxidation of organic compounds [13–15], and production of hydrogen from water splitting [16–19]. In this regard, different types of heterogeneous photocatalysts have been extensively reported, including metal oxide nanoparticles, composite nanomaterials, metal-organic frameworks, plasmonic photocatalysts, and polymeric graphitic carbon nitride [3,4].

Among these different types of photocatalysts, TiO_2 has been extensively investigated and is one of the most widely used in the aforementioned applications due to its excellent photocatalytic activity, high thermal and chemical stability, low cost, and non-toxicity [20,21]. However, in spite of its advantages, the main drawback of TiO_2 in photocatalysis relates to the large band gap (3.2 eV) for its anatase crystalline phase which restricts its utilization to ultraviolet (UV) irradiation ($\lambda < 387$ nm), with UV irradiation comprising less than 5% of the solar energy. Therefore, it is very important to extend the photocatalytic activity of TiO_2 nanocatalysts under visible light to profit from abundant solar energy. Various approaches have been developed to improve the photoactivity of TiO_2 by lowering the band-gap energy and delaying the recombination of the excited electron-hole pairs, *i.e.*,

32. Zhang, M.; Chen, C.; Ma, W.; Zhao, J. Visible-Light-Induced Aerobic Oxidation of Alcohols in a Coupled Photocatalytic System of Dye-Sensitized TiO_2 and TEMPO. *Angew. Chem. Int. Ed. Engl.* **2008**, *120*, 9876–9879. [CrossRef]
33. Jarry, B.; Launay, F.; Nogier, J.P.; Montouillout, V.; Gengembre, L.; Bonardet, J.L. Characterisation, acidity and catalytic activity of Ga-SBA-15 materials prepared following different synthesis procedures. *Appl. Catal. A* **2006**, *309*, 177–186. [CrossRef]
34. Ojeda, M.; Balu, A.M.; Barrón, V.; Pineda, A.; Coleto, Á.G.; Romero, A.Á.; Luque, R. Solventless mechanochemical synthesis of magnetic functionalized catalytically active mesoporous SBA-15 nanocomposites. *J. Mater. Chem. A* **2014**, *2*, 387–393. [CrossRef]
35. Qi, K.; Fei, B.; Xin, J.H. Visible light-active iron-doped anatase nanocrystallites and their self-cleaning property. *Thin Solid Films* **2011**, *519*, 2438–2444. [CrossRef]
36. Pham, M.H.; Dinh, C.T.; Vuong, G.T.; Ta, N.D.; Do, T.O. Visible light induced hydrogen generation using a hollow photocatalyst with two cocatalysts separated on two surface sides. *Phys. Chem. Chem. Phys.* **2014**, *16*, 5937–5941. [CrossRef] [PubMed]

8.4. Appendix 4 Highly Active Catalytic Ru/TiO_2 Nanomaterials for Continuous Production of γ-Valerolactone

WILEY-VCH

FULL PAPER

Highly active catalytic Ru/TiO_2 nanomaterials for continuous production of γ-valerolactone

Chunping Xu[a]¥, Weiyi Ouyang,[b]¥* Mario J. Muñoz-Batista,[b] Marcos Fernández-García,[c] and Rafael Luque*[b][d]

Abstract: Green energy production from renewable sources is an attractive but challenging topic to face the likely energy crisis scenario in the future. In the current work, a series of versatile Ru/TiO_2 catalysts were simply synthesized and employed in continuous flow catalytic transfer hydrogenation of industrially derived methyl levulinate biowaste (from Avantium Chemicals B.V.) to γ-valerolactone. Different analytical techniques were applied in the characterization of the as-synthesized catalysts, including XRD, SEM, EDX, TEM and XPS etc. The effects of various reaction conditions (e.g. temperature, concentration and flow rate) were investigated. Results suggested that optimum dispersion and distribution of Ru on the TiO_2 surface could efficiently promote production of γ-valerolactone, with 5% Ru/TiO_2 catalyst providing excelling catalytic performance and stability as compared to commercial Ru catalysts.

Introduction

With the raising of public awareness on environmental protection and climate change, development of green energy, or renewable energy, as alternative to the fossil energy to reduce the carbon emission has drawn intensive attention and become a key issue in the recent decades. In this aspect, relevant research efforts have been devoted to the transformation of tremendous biomass into biofuels[1–5] and photocatalytic fuel generations[6–10]. Due to the complexity and recalcitrant of the abundant lignocellulosic biomass, direct transformation of these feedstocks into valuable products (fuels, chemicals and materials) has emerged a bottleneck[11,12], while valorization of carbohydrates derived from lignocellulosic biomass with different strategies has been widely reported[13–22]. Levulinic acid (LA) is one of the most promising primary building block and platform molecules from biomass refinery, which is selected as one of top 12 sugar-derived building blocks[23] and the top 10 chemical opportunities from biorefinery carbohydrates[24] by US Department of Energy (DOE). Therefore, there is great potential to valorize LA and its ester derivatives, alkyl levulinates into more valuable products such as γ-valerolatone (GVL).

GVL is considered as one of the most outstanding molecules which can be used as fuel additive, solvent, liquid fuel, and ideal precursor for production of valuable chemicals.[25–29] Notably, hydrogenation of alkyl levulinates to GVL is more preferable because alkyl levulinates have higher production from lignocellulose and are easier for separation when compared to LA.[22,30] Heterogeneous catalysts have been reported to play a key role in the hydrogenation process, most of which are carbon, zeolite and metal oxide supports decorated by transition metals (Au, Co, Cu, Ir, Ni, Pd, Pt, Re, Rh, Ru).[28–39] Especially, Ru catalysts is one of the most widely reported catalyst for hydrogenation of LA and alkyl levulinates because of its outstanding catalytic performance and efficiency because it is one of the most active catalyst for aliphatic carbonyl compounds hydrogenation.[34,40,41] For example, Ru/TiO_2 was reported to be highly efficient in hydrogenation of LA to GVL.[41] However, most of the reported works were performed in batch conditions, and only a few of them were in flow for the hydrogenation of LA instead of alkyl levulinates.[42–47] Considering the advantages of flow reactions (efficient energy utilization, easy scale-up, purification and etc.), it could provide closer view into practical production in industry by mimicking large-scale production on the laboratory scale.[48,49]

The catalytic transformation of alkyl levulinates to GVL via Meerwein–Ponndorf–Verley (MPV) reduction using alcohol as hydrogen donor is highly selective for reducing carbonyl group to alcoholic hydroxyl group.[50–54] Hence, such catalytic transfer hydrogenation (CTH) process offers a simple, efficient and safe option for the valorization of biomass derived molecules using abundant and inexpensive alcohols as hydrogen source and solvent as compared to formic acid and H_2.[51,52,55] For example, 2-propanol was reported to be an active hydrogen donor in the transformation of alkyl levulinates providing good conversion and selectivity.[51,55,56]

In the present work, we reported highly active, selective and stable Ru/TiO_2 catalysts for the continuous flow conversion of biowaste derived methyl levulinate from industrial activities of the company Avantium. TiO_2 was synthesized with reversed micro-emulsion method, while deposition of different Ru content (1, 2, 3, 5 wt.%) was performed using $NaBH_4$ as reducing agent under N_2 bubble production, while the obtained catalysts were denoted as 1% Ru/TiO_2, 2% Ru/TiO_2, 3% Ru/TiO_2 and 5% Ru/TiO_2 accordingly. The catalytic performance of the synthesized materials was tested by catalytic transfer hydrogenation of methyl levulinate (ML) in Phoenix reactor from ThalesNano.

Results and Discussion

[a] Prof. C. Xu
School of Food and Biological Engineering, Zhengzhou University of Light Industry, Dongfeng Road 5, Zhengzhou, Henan, 450002, P.R.China.
[b] W. Ouyang, Dr. M.J. Munoz-Batista, Prof. R. Luque
Departamento de Química Orgánica
Universidad de Córdoba, Edif. Marie Curie, Ctra Nnal IV-A Km 396, E14014, Córdoba (Spain)
E-mail: g62alsor@uco.es
[c] Dr. M. Fernández-García
Instituto de Catálisis y Petroleoquímica
CSIC, Marie Curie 2, 28049 Madrid, Spain
Email: mfg@icp.csic.es
[d] Peoples Friendship University of Russia (RUDN University), 6 Miklukho-Maklaya street, Moscow, 117198, Russia
¥ Equal contribution status

31.

[73] H. Li, Z. Fang, S. Yang, *ACS Sustain. Chem. Eng.* **2016**, *4*, 236–246.

[74] B. Cai, X.-C. Zhou, Y.-C. Miao, J.-Y. Luo, H. Pan, Y.-B. Huang, *ACS Sustain. Chem. Eng.* **2017**, *5*, 1322–1331.

[75] Z. Xiao, H. Zhou, J. Hao, H. Hong, Y. Song, R. He, K. Zhi, Q. Liu, *Fuel* **2017**, *193*, 322–330.

[76] C.-B. Chen, M.-Y. Chen, B. Zada, Y.-J. Ma, L. Yan, Q. Xu, W.-Z. Li, Q.-X. Guo, Y. Fu, *RSC Adv.* **2016**, *6*, 112477–112485.

[77] X. Tang, Z. Li, X. Zeng, Y. Jiang, S. Liu, T. Lei, Y. Sun, L. Lin, *ChemSusChem* **2015**, *8*, 1601–1607.

[78] M. J. Muñoz-Batista, A. Kubacka, M. Fernández-García, *ACS Catal.* **2014**, *4*, 4277–4288.

8.5. Appendix 5 Continuous Flow Conversion of Biomass-Derived Methyl Levulinate into γ-Valerolactone Using Functional Metal Organic Frameworks

ACS Sustainable Chemistry & Engineering

Research Article

Cite This: ACS Sustainable Chem. Eng. 2018, 6, 6746−6752

pubs.acs.org/journal/ascecg

Continuous Flow Conversion of Biomass-Derived Methyl Levulinate into γ-Valerolactone Using Functional Metal Organic Frameworks

Weiyi Ouyang,*[,†] Deyang Zhao,[‡] Yantao Wang,[‡] Alina M. Balu,[†] Christophe Len,[‡,§] and Rafael Luque*[,†,∥]

[†]Departamento de Química Orgánica, Universidad de Córdoba, Edif. Marie Curie, Ctra Nnal IV-A, Km 396, E14014 Córdoba, Spain

[‡]Sorbonne Universités, Université de Technologie de Compiègne (UTC), CS 60319, 60203 Cedex Compiègne, France

[§]Institut de Recherche de Chimie, Paris, PSL Research University, Chimie Paris Tech, CNRS, 11 rue Pierre et Marie Curie, F-75231 Cedex 05 Paris, France

[∥]Peoples Friendship University of Russia (RUDN University), 6 Miklukho-Maklaya street, Moscow 117198, Russia

ABSTRACT: The zirconium-based metal organic framework, UiO-66 (Zr), was successfully synthesized via solvothermal method, followed by various characterization including XRD, thermal analysis, N_2 physisorption, and TEM. As-synthesized UiO-66 (Zr) was employed in the transformation of methyl levulinate (ML) to γ-valerolactone (GVL) via catalytic transfer hydrogenation (CTH) under continuous flow and various reaction conditions, which gave superior catalytic performance and efficiency as compared to reported catalysts. The obtained results show great potential of applying UiO-66 (Zr) in upgrading biomass derivatives to useful biofuel/chemical products, paving the way for green energy production from renewable resources.

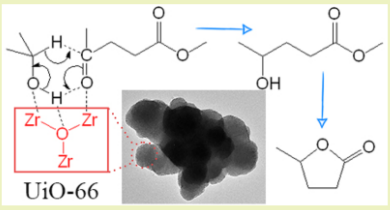

KEYWORDS: *Biomass valorization, Methyl levulinate, γ-Valerolactone, Continuous flow, Catalytic transfer hydrogenation (CTH), Metal organic framework, UiO-66 (Zr)*

INTRODUCTION

Because of the limited reserve of fossil fuels and the rising awareness on sustainable development, low-carbon-economy has been proposed and is being implementing globally, which is urging the expansion of renewable and sustainable energy. In this regard, valorization of enormous and low-cost lignocellulosic biomass into biofuels and platform molecules is of vital importance and has attracted massive attention in the last few decades. A wide range of catalytic strategies have been developed for the transformation of lignocellulosic biomass into a wide range of chemicals, among which levulinic acid (LA) is listed as one of the top 12 prospective building blocks derived from sugars,[1] indicating the great possibility in the valorization of levulinic acid and alkyl levulinates into valuable products. γ-Valerolactone (GVL) is one of the promising platform molecules derived from lignocellulosic biomass via hydrogenation of levulinic acid and alkyl levulinates, which can be used as solvent, fuel additive, and liquid fuel, as well as precursor for valuable chemicals (e.g., olefins, polymers, 5-nanonone).[2−5]

Catalysts, either homogeneous or heterogeneous, have key effects on the transformation of levulinic acid and its ester derivates to γ-valerolactone, including (supported) transition/noble metals, metal hydroxides, metal oxides, and metal salts.[6] A cobalt catalyst generated by reducing commercial Co_3O_4 was reported to be very efficient in solvent-free transformations of ethyl levulinate (EL) to GVL under mild conditions.[7] $Ca_5(PO_4)_3(OH)$ (HAP) incorporated with metals (Pd, Pt, Ru, Cu, Ni) was employed in the vapor-phase hydrogenation of levulinic acid, in which 2Ru/HAP catalyst gave the most efficient GVL production with TOF_{GVL} of 2.9 s^{-1} as compared to catalysts decorated with other metals. Apart from metal catalysts, metal hydroxides such as $Ru(OH)_x/TiO_2$[8] and $Zr(OH)_4$ were also reported to be active in this transformation while giving good conversion with excellent selectivity.[9] Considering the environmental impacts, metal hydroxides (homogeneous catalysts) are less preferable for separation/recycling issues while the high cost of noble metals will also limit their large-scale application at certain contents. In this aspect, metal oxides or supported metal oxides as catalysts offered an alternative to noble metal catalysts in the production of GVL from LA or its esters in high yields such as ZrO_2,[10,11] Cu/ZrO_2,[12] $ZrFeO_x$,[13] ZrO_2/SBA-15,[14] SnO_2/SBA-15,[15] etc.

Generally, there are two pathways for the catalytic hydrogenation upgrading of LA and its esters: (1) direct hydrogenation of the carbonyl group using molecular H_2; and (2) catalytic transfer hydrogenation (CTH) of the carbonyl group using organic molecules (e.g., alcohols and formic acid) as hydrogen donors. Subsequently, the reaction intermediates will be transformed into GVL via intramolecular (trans)esterification. Because of the low solubility of molecular H_2 in most solvents,

Received: February 2, 2018
Revised: April 9, 2018
Published: April 17, 2018

DOI: 10.1021/acssuschemeng.8b00549
ACS Sustainable Chem. Eng. 2018, 6, 6746−6752

the vapour phase at atmospheric pressure. *RSC Adv.* **2016**, *6* (24), 20230−20239.
(15) Xu, S.; Yu, D.; Ye, T.; Tian, P. Catalytic transfer hydrogenation of levulinic acid to γ-valerolactone over a bifunctional tin catalyst. *RSC Adv.* **2017**, *7* (2), 1026−1031.
(16) Gilkey, M. J.; Xu, B. Heterogeneous Catalytic Transfer Hydrogenation as an Effective Pathway in Biomass Upgrading. *ACS Catal.* **2016**, *6* (3), 1420−1436.
(17) He, J.; Li, H.; Lu, Y.; Liu, Y.; Wu, Z.; Hu, D.; Yang, S. Cascade catalytic transfer hydrogenation−cyclization of ethyl levulinate to γ -valerolactone with Al−Zr mixed oxides. *Appl. Catal., A* **2016**, *510*, 11−19.
(18) Yang, Z.; Huang, Y.-B.; Guo, Q.-X.; Fu, Y. RANEY® Ni catalyzed transfer hydrogenation of levulinate esters to γ-valerolactone at room temperature. *Chem. Commun.* **2013**, *49* (46), 5328−5330.
(19) Song, J.; Wu, L.; Zhou, B.; Zhou, H.; Fan, H.; Yang, Y.; Meng, Q.; Han, B. A new porous Zr-containing catalyst with a phenate group: an efficient catalyst for the catalytic transfer hydrogenation of ethyl levulinate to γ-valerolactone. *Green Chem.* **2015**, *17* (3), 1626−1632.
(20) Wang, J.; Jaenicke, S.; Chuah, G.-K. Zirconium−Beta zeolite as a robust catalyst for the transformation of levulinic acid to γ-valerolactone via Meerwein−Ponndorf−Verley reduction. *RSC Adv.* **2014**, *4* (26), 13481−13489.
(21) Li, J. R.; Sculley, J.; Zhou, H. C. Metal-organic frameworks for separations. *Chem. Rev.* **2012**, *112* (2), 869−932.
(22) Kreno, L. E.; Leong, K.; Farha, O. K.; Allendorf, M.; Van Duyne, R. P.; Hupp, J. T. Metal−Organic Framework Materials as Chemical Sensors. *Chem. Rev.* **2012**, *112* (2), 1105−1125.
(23) Dhakshinamoorthy, A.; Asiri, A. M.; Garcia, H. Mixed-metal or mixed-linker metal organic frameworks as heterogeneous catalysts. *Catal. Sci. Technol.* **2016**, *6* (14), 5238−5261.
(24) Zhao, M.; Yuan, K.; Wang, Y.; Li, G.; Guo, J.; Gu, L.; Hu, W.; Zhao, H.; Tang, Z. Metal−organic frameworks as selectivity regulators for hydrogenation reactions. *Nature* **2016**, *539* (7627), 76−80.
(25) Zou, L.; Feng, D.; Liu, T.-F.; Chen, Y.-P.; Yuan, S.; Wang, K.; Wang, X.; Fordham, S.; Zhou, H.-C. A versatile synthetic route for the preparation of titanium metal−organic frameworks. *Chem. Sci.* **2016**, *7* (2), 1063−1069.
(26) Furukawa, H.; Cordova, K. E.; O'Keeffe, M.; Yaghi, O. M. The Chemistry and Applications of Metal-Organic Frameworks. *Science (Washington, DC, U. S.)* **2013**, *341* (6149), 1230444−1230444.
(27) Herbst, A.; Janiak, C. MOF catalysts in biomass upgrading towards value-added fine chemicals. *CrystEngComm* **2017**, *19* (29), 4092−4117.
(28) Valekar, A. H.; Cho, K.-H.; Chitale, S. K.; Hong, D.-Y.; Cha, G.-Y.; Lee, U.-H.; Hwang, D. W.; Serre, C.; Chang, J.-S.; Hwang, Y. K. Catalytic transfer hydrogenation of ethyl levulinate to γ-valerolactone over zirconium-based metal−organic frameworks. *Green Chem.* **2016**, *18* (16), 4542−4552.
(29) Kuwahara, Y.; Kango, H.; Yamashita, H. Catalytic Transfer Hydrogenation of Biomass-Derived Levulinic Acid and Its Esters to γ-Valerolactone over Sulfonic Acid-Functionalized UiO-66. *ACS Sustainable Chem. Eng.* **2017**, *5* (1), 1141−1152.
(30) Klet, R. C.; Liu, Y.; Wang, T. C.; Hupp, J. T.; Farha, O. K. Evaluation of Brønsted acidity and proton topology in Zr- and Hf-based metal−organic frameworks using potentiometric acid−base titration. *J. Mater. Chem. A* **2016**, *4* (4), 1479−1485.
(31) Ling, S.; Slater, B. Dynamic acidity in defective UiO-66. *Chem. Sci.* **2016**, *7* (7), 4706−4712.
(32) Cirujano, F. G.; Corma, A.; Llabrés I Xamena, F. X. Zirconium-containing metal organic frameworks as solid acid catalysts for the esterification of free fatty acids: Synthesis of biodiesel and other compounds of interest. *Catal. Today* **2015**, *257*, 213−220.
(33) Trickett, C. A.; Gagnon, K. J.; Lee, S.; Gándara, F.; Bürgi, H. B.; Yaghi, O. M. Definitive Molecular Level Characterization of Defects in UiO-66 Crystals. *Angew. Chem., Int. Ed.* **2015**, *54* (38), 11162−11167.
(34) Wegner, J.; Ceylan, S.; Kirschning, A. Ten key issues in modern flow chemistry. *Chem. Commun.* **2011**, *47* (16), 4583−4592.
(35) Yu, F.; Zhong, R.; Chong, H.; Smet, M.; Dehaen, W.; Sels, B. F. Fast catalytic conversion of recalcitrant cellulose into alkyl levulinates and levulinic acid in the presence of soluble and recoverable sulfonated hyperbranched poly(arylene oxindole)s. *Green Chem.* **2017**, *19* (1), 153−163.
(36) Peng, L.; Lin, L.; Li, H.; Yang, Q. Conversion of carbohydrates biomass into levulinate esters using heterogeneous catalysts. *Appl. Energy* **2011**, *88* (12), 4590−4596.
(37) Cavka, J. H.; Jakobsen, S.; Olsbye, U.; Guillou, N.; Lamberti, C.; Bordiga, S.; Lillerud, K. P. A New Zirconium Inorganic Building Brick Forming Metal Organic Frameworks with Exceptional Stability. *J. Am. Chem. Soc.* **2008**, *130* (42), 13850−13851.
(38) Katz, M. J.; Brown, Z. J.; Colón, Y. J.; Siu, P. W.; Scheidt, K. A.; Snurr, R. Q.; Hupp, J. T.; Farha, O. K. A facile synthesis of UiO-66, UiO-67 and their derivatives. *Chem. Commun.* **2013**, *49* (82), 9449−9451.
(39) Valenzano, L.; Civalleri, B.; Chavan, S.; Bordiga, S.; Nilsen, M. H.; Jakobsen, S.; Lillerud, K. P.; Lamberti, C. Disclosing the complex structure of UiO-66 metal organic framework: A synergic combination of experiment and theory. *Chem. Mater.* **2011**, *23* (7), 1700−1718.
(40) Hernández Enríquez, J. M.; Cortez Lajas, L. A.; García Alamilla, R.; Castillo Mares, A.; Sandoval Robles, G.; García Serrano, L. A. Synthesis and characterization of mesoporous and nano-crystalline phosphate zirconium oxides. *J. Alloys Compd.* **2009**, *483* (1−2), 425−428.

DOI: 10.1021/acssuschemeng.8b00549
ACS Sustainable Chem. Eng. 2018, 6, 6746−6752

8.6. Appendix 6 Mild Ultrasound-Assisted Synthesis of TiO_2 Supported on Magnetic Nanocomposites for Selective Photo-Oxidation of Benzyl Alcohol

Applied Catalysis B: Environmental 183 (2016) 107–112

Contents lists available at ScienceDirect

Applied Catalysis B: Environmental

journal homepage: www.elsevier.com/locate/apcatb

Mild ultrasound-assisted synthesis of TiO_2 supported on magnetic nanocomposites for selective photo-oxidation of benzyl alcohol

Juan C. Colmenares[a,*], Weiyi Ouyang[b], Manuel Ojeda[b], Ewelina Kuna[a], Olga Chernyayeva[a], Dmytro Lisovytskiy[a], Sudipta De[b], Rafael Luque[b], Alina M. Balu[b,**]

[a] Institute of Physical Chemistry PAS, Kasprzaka 44/52, 01-224, Warsaw, Poland
[b] Departamento de Quimica Organica, Universidad de Cordoba, Campus de Rabanales, Edificio Marie Curie, E-14014 Cordoba, Spain

ARTICLE INFO

Article history:
Received 3 September 2015
Received in revised form
29 September 2015
Accepted 14 October 2015
Available online 19 October 2015

Keywords:
Selective photo-oxidation
Ultrasound-assisted impregnation
TiO_2
Aromatic alcohols
Magnetic photocatalysts

ABSTRACT

A simple and effective ultrasound-assisted wet impregnation method was developed for the preparation of magnetically separable TiO_2/maghemite-silica photo-active nanocomposites. The resulting nanomaterials were characterized by several techniques and subsequently tested for their photocatalytic activities in the liquid phase selective oxidation of benzyl alcohol. An unprecedented selectivity in organic media (90% in acetonitrile) towards benzaldehyde was achieved at a benzyl alcohol conversion of ca. 50%, being remarkably superior in terms of activity to any other supported transition metal catalysts reported to date as well as commercial titania Evonik P-25 photocatalyst.

1. Introduction

Photocatalysis is currently considered as one of the most advanced, environment friendly and promising technologies due to excellent merits such as clean, effective, energy-saving, and low cost [1,2]. Photocatalytic oxidation (PCO) could be a promising alternative of aforementioned chemical oxidation technologies for lignin oxidation in terms of selectivity and economic issues. In 1989, Ohnishi et al. studied the performance of different photocatalysts including ZnO, TiO_2, CdS, In_2O_3, WO_3, and Fe_2O_3 on lignin degradation [3]. Doping of noble metals such as Pt, Ag, and Au could further improved the efficiency of the photocatalyst. The next generation photocatalysts will be based on the utilization of a heterojunction between two photoactive materials with different band gap [4].

Among various semiconductor photocatalysts used in the past 3 decades, TiO_2 received most attention due to its biological and chemical inertness, cost effectiveness, and the strong oxidizing power of the photogenerated holes [5,6]. However, one of the major problems of using pure TiO_2 is that only ultraviolet light photons can displace the valence band electrons of TiO_2 due to its high band-gap energy (3.2 eV), making only 5% of the solar radiation utilized. This problem can be solved by doping heteroatoms in the TiO_2 and creating new heterojunctions with TiO_2 materials that improve the photocatalytic properties of TiO_2 by enhancing the light absorption and delaying recombination of photogenerated electron–hole pairs [7].

Selective oxidation of alcohols to their corresponding carbonyl compounds (especially aldehydes) is one of the important organic transformations as carbonyl compounds are widely used in food, beverages, and pharmaceutical industries, and as precursors in chemical industries [8,9]. The conversion of aromatic alcohols to aldehydes is particularly attractive since aromatic alcohols represent themselves as model lignin compounds obtained after the depolymerization of lignin. The main purpose of studying these compounds is that they contain linkages that resemble those found in lignin and thus their reactivity could potentially provide insights into the degradation and reaction of the polymer structure as a whole [10]. Since, benzyl alcohol is a key structural unit of most of lignin model compounds, major focus has been given to its reactivity and transformation strategies. Another advantage relates to the simplicity of benzyl alcohol as aromatic substrate and consequently

* Corresponding author.
** Corresponding author.
E-mail addresses: jcarloscolmenares@ichf.edu.pl (J.C. Colmenares), qo2balua@uco.es (A.M. Balu).

http://dx.doi.org/10.1016/j.apcatb.2015.10.034
0926-3373/

Incorporation of 25 wt% TiO_2 on the surface of MAGSNC was believed to form a close heterojunction of two semiconductors (TiO_2/γ-Fe_2O_3) favoring the electron transfer from γ-Fe_2O_3 (E_g = 1.78 eV) to TiO_2 (photosensitization of titania) and making it more photoselective as compared to TiO_2 P-25 (99% and 32% selectivity towards benzaldehyde, respectively, Table 2) with a good benzyl alcohol conversion (ca. 50%). Additionally, the nanophotocatalyst was proved to be highly stable under the investigated reaction conditions, with no leaching of Fe or Ti after several hours of reaction (undetected by ICP/MS) (Fig. 4).

An increase in the crystallite size of TiO_2 materials produces decreased selectivity in the photo-oxidation process [35]. Highly crystalline materials possess lower surface areas due to which the surface hydroxyl group density decreases and consequently result lower activity. Our photoactive nanocomposite material possessed a high surface area (292 m^2 g^{-1}, Table 1), and its TiO_2 component has very small crystallite size of approx. 4 nm and exclusively composed of anatase phase (Fig. 1). The adsorptive affinity of rutile for organic compounds (e.g. benzyl alcohol) is lower to that of anatase and rutile exhibits higher rates of recombination electron–hole (lower photo-catalytic activity) in comparison to anatase [36].

4. Conclusions

Magnetically separable TiO_2/MAGSNC photocatalysts were synthesized following the improved wet impregnation method assisted by ultrasonic irradiation. The spatially ordered heterojuntion between TiO_2 and γ-Fe_2O_3 and a potential co-catalytic incorporation of Fe^{3+} (from the support MAGSNC) into the titania structure might significantly increase the sensitization and decreased the band gap energy of TiO_2, effectively improving the photocatalytic activity and selectivity of the materials towards selective oxidation of benzyl alcohol to benzaldehyde. Solvents played a significant role in the photo-oxidation process with materials showed very good conversion and selectivity in acetonitrile but not in aqueous conditions. This work provided a simple low-cost preparation of magnetically separable titania supported photocatalysts for the selective oxidation of aromatic alcohols which has a promising potential in future studies towards the photochemical conversion of phenolic-type compounds.

Acknowledgements

Prof. Colmenares would like to thank the Institute of Physical Chemistry of the Polish Academy of Sciences for all support. Rafael Luque gratefully acknowledges Spanish MICINN for financial support via the concession of a RyC contract (ref: RYC-2009-04199) and funding under project CTQ2011-28954-C02-02 (MEC). Consejeria de Ciencia e Innovacion, Junta de Andalucia is also gratefully acknowledged for funding project P10-FQM-6711. JCC, AMB and RL gratefully acknowledge support from COST Action FP1306 for networking and possibilities for meetings and future students exchange.

References

[1] X. Lang, X. Chen, J. Zhao, Chem. Soc. Rev. 43 (2014) 473–486.
[2] J.C. Colmenares, R. Luque, Chem. Soc. Rev. 43 (2014) 765–778.
[3] H. Ohnishi, M. Matsumura, H. Tsubomura, M. Iwasaki, Ind. Eng. Chem. Res. 28 (1989) 719–724.
[4] (a) A.V. Emeline, V.N. Kunznetsov, V.K. Ryabchuk, Environ. Sci. Pollut. Res. Int. 19 (2012) 3666–3675;
(b) A.V. Serpone, J. Phys. Chem. Lett. 3 (2012) 673–677.
[5] J.C. Colmenares, R. Luque, J.M. Campelo, F. Colmenares, Z. Karpiński, A.A. Romero, Materials 2 (2009) 2228–2258.
[6] Q. Xu, Y. Ma, J. Zhang, X.L. Wang, Z.C. Feng, C. Li, J. Catal. 278 (2011) 329–335.
[7] J.T. Chang, Y.F. Lai, J.L. He, Surf. Coating Technol. 200 (2005) 1640–1644.
[8] A. Maldotti, A. Molinari, R. Amadelli, Chem. Rev. 102 (2002) 3811–3836.
[9] X. Lang, W. Ma, C. Chen, H. Ji, J. Zhao, Acc. Chem. Res. 47 (2014) 355–363.
[10] J. Zakzeski, P.C.A. Bruijnincx, A.L. Jongerius, B.M. Weckhuysen, Chem. Rev. 110 (2010) 3552–3599.
[11] S. Yurdakal, G. Palmisano, V. Loddo, V. Augugliaro, L. Palmisano, J. Am. Chem. Soc. 130 (2008) 1568–1569.
[12] S. Yurdakal, G. Palmisano, V. Loddo, O. Alagoz, V. Augugliaro, L. Palmisano, Green Chem. 13 (2009) 510–516.
[13] C.J. Li, G.R. Xu, B.H. Zhang, J.R. Gong, Appl. Catal. B 115 (2012) 201–208.
[14] T. Shishido, T. Miyatake, K. Teramura, Y. Hitomi, H. Yamashita, T. Tanaka, J. Phys. Chem. C 113 (2009) 18713–18718.
[15] S.R. Kadam, V.R. Mate, R.P. Panmand, L.K. Nikam, M.V. Kulkarni, R.S. Sonawane, B.B. Kale, RSC Adv. 4 (2014) 60626–60635.
[16] A. Tanaka, K. Hashimoto, H. Kominami, Chem. Commun. 47 (2011) 10446–10448.
[17] Y. Zhang, N. Zhang, Z.R. Tang, Y.J. Xu, ACS Sustain. Chem. Eng. 1 (2013) 1258–1266.
[18] W. Zhai, S. Xue, A. Zhu, Y. Luo, Y. Tian, ChemCatChem 3 (2011) 127–130.
[19] M. Qamar, R.B. Elsayed, K.R. Alhooshani, M.I. Ahmed, D.W. Bahnemann, ACS Appl. Mater. Interfaces 7 (2015) 1257–1269.
[20] L. Yuan, Q. Yu, Y. Zhang, Y.J. Xu, RSC Adv. 4 (2014) 15264–15270.
[21] X. Dai, M. Xie, S. Meng, X. Fu, S. Chen, Appl. Catal. B 158 (2014) 382–390.
[22] N. Zhang, Y. Zhang, X. Pan, X. Fu, S. Liu, Y.J. Xu, J. Phys. Chem. C 115 (2011) 23501–23511.
[23] J.C. Colmenares, A. Magdziarz, O. Chernyayeva, D. Lisovytskiy, K. Kurzydlowski, J. Grzonka, ChemCatChem 5 (2013) 2270–2277.
[24] J.C. Colmenares, A. Magdziarz, K. Kurzydlowski, J. Grzonka, O. Chernyayeva, D. Lisovytskiy, Appl. Catal. B 134–135 (2013) 136–144.
[25] M. Ojeda, A. Pineda, A.A. Romero, V. Barron, R. Luque, ChemSusChem 7 (2014) 1876–1880.
[26] J.C. Colmenares, P. Lisowski, D. Łomot, RSC Adv. 3 (2013) 20186–20192.
[27] S. Sakthivel, H. Kisch, Angew. Chem. Int. Ed. 42 (2003) 4908–4911.
[28] R. Cornell, U. Schertmann, Iron Oxides in the Laboratory: Preparation and Characterization, VCH, Weinheim, 1991.
[29] W. Choi, A. Termin, M.R. Hoffman, J. Phys. Chem. 98 (1994) 13669–13679.
[30] K.B. Qi, B. Fei, J.H. Xin, Thin Solid Films 519 (2011) 2438–2444.
[31] J.C. Colmenares, ChemSusChem 7 (2014) 1512–1527.
[32] (a) Y. Ma, X.-T. Zhang, Z.-S. Guan, Y.-A. Cao, J.-N. Yao, J. Mater. Res. 16 (2001) 2928–2933;
(b) M. Litter, J.A. Navio, J. Photochem. Photobiol. A 98 (1996) 171–181.
[33] Y. Shiraishi, T. Hirai, J. Photochem. Photobiol. C 9 (2008) 157–170.
[34] A. Maldotti, A. Molinari, Top. Curr. Chem. 303 (2011) 185–216.
[35] C.-J. Li, G.-R. Xu, B. Zhang, J.R. Gong, Appl. Catal. B 115–116 (2012) 201–208.
[36] K.A. Stafford, P.V. Gray, Chem. Phys. Lett. 205 (1993) 55–61.

8.7. Appendix 7 Facile Mechanochemical Modification of g-C_3N_4 for Selective Photo-Oxidation of Benzyl Alcohol

ARTICLE IN PRESS

Chemical Engineering Science xxx (2018) xxx–xxx

Contents lists available at ScienceDirect

Chemical Engineering Science

journal homepage: www.elsevier.com/locate/ces

Facile mechanochemical modification of g-C_3N_4 for selective photo-oxidation of benzyl alcohol

Kenneth Cerdan [a], Weiyi Ouyang [a], Juan C. Colmenares [b], Mario J. Muñoz-Batista [a], Rafael Luque [a,c,*], Alina M. Balu [a,*]

[a] Departamento de Quimica Organica, Universidad de Cordoba, Edificio Marie Curie (C-3), Ctra Nnal IV-A, Km 396, E14014 Cordoba, Spain
[b] Institute of Physical Chemistry, Polish Academy of Sciences, Kasprzaka 44/52, 01-224 Warsaw, Poland
[c] Peoples Friendship University of Russia (RUDN University), 6 Miklukho-Maklaya Str., Moscow 117198, Russia

HIGHLIGHTS

- Facile mechanochemical synthesis of g-C_3N_4-ZnO and -Fe_2O_3 composite photocatalyts.
- Maximum benzaldehyde selectivity (70%) for the g-C_3N_4-Fe_2O_3 composite sample.
- Crystallinity and surface concentration of the oxides control the selectivity of benzyl alcohol oxidation.

GRAPHICAL ABSTRACT

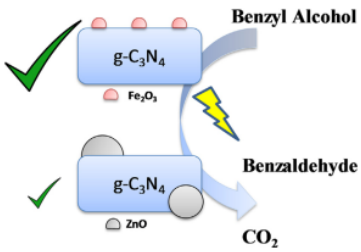

ARTICLE INFO

Article history:
Received 24 January 2018
Received in revised form 23 March 2018
Accepted 1 April 2018
Available online xxxx

Keywords:
Photo-catalysis
Graphitic carbon nitride
Mechanochemical
Benzyl alcohol
ZnO
Fe_2O_3

ABSTRACT

Graphitic carbon nitride (CN) enriched with ZnO or Fe_2O_3 were synthesized using a simple one-pot mechanochemical method. By using this method, composite samples were synthetized without the production of any potentially hazardous waste. Synthesized materials were used as catalysts during selective photo-oxidation of benzyl alcohol. Both composite materials displayed an enhancement of activity and benzaldehyde selectivity with respect to the pure CN. The most active catalyst was Fe_2O_3/g-C_3N_4 (Fe/CN). Conversion and benzaldehyde selectivity of this sample were 20 and 70%, respectively. It showed a considerable increase of benzaldehyde selectivity compared to the pure CN and TiO_2 P25 commercial reference. A complete structural and electronic characterization using Scanning Electron Microscopy-Energy Dispersive (SEM-EDX), BET measurements, X-ray diffraction (XRD), X-ray Photoelectron (XPS), and UV–visible spectroscopies was carried out. The characterization analysis pointed out the leading role of the crystallinity and surface concentration over the activity and benzaldehyde selectivity of the reaction.

1. Introduction

As a fundamental field of science, photochemistry development has been improved significantly during the last decades (Schultz and Yoon, 2011). Advanced oxidation processes and particularly heterogeneous photocatalysis have evolved as powerful technologies to facilitate the control and elimination of pollutants, energy production, as well as selective synthesis of high added value

* Corresponding authors at: Departamento de Quimica Organica, Universidad de Cordoba, Edificio Marie Curie (C-3), Ctra Nnal IV-A, Km 396, E14014 Cordoba, Spain (R. Luque).
E-mail address: rafael.luque@uco.es (R. Luque).

https://doi.org/10.1016/j.ces.2018.04.001
0009-2509/

Yan, S.C., Li, Z.S., Zou, Z.G., 2009. Photodegradation performance of g-C_3N_4 fabricated by directly heating melamine. Langmuir 25, 10397–10401. https://doi.org/10.1021/la900923z.

Yang, M.-Q., Xu, Y.-J., 2013. Selective photoredox using graphene-based composite photocatalysts. Phys. Chem. Chem. Phys. 15, 19102. https://doi.org/10.1039/c3cp53325e.

Zhang, G., Zhang, J., Zhang, M., Wang, X., 2012. Polycondensation of thiourea into carbon nitride semiconductors as visible light photocatalysts. J. Mater. Chem. 22, 8083–8091. https://doi.org/10.1039/c2jm00097k.

Zhang, N., Yang, M.-Q., Liu, S., Sun, Y., Xu, Y.-J., 2015. Waltzing with the versatile platform of graphene to synthesize composite photocatalysts. Chem. Rev. 115, 10307–10377. https://doi.org/10.1021/acs.chemrev.5b00267.

Zhang, N., Yang, M.-Q., Tang, Z.-R., Xu, Y.-J., 2014. Toward Improving the graphene-semiconductor composite photoactivity via the addition of metal ions as generic interfacial mediator. ACS Nano 8, 623–633. https://doi.org/10.1021/nn405242t.

Zhang, Y., Pan, Q., Chai, G., Liang, M., Dong, G., Zhang, Q., Qiu, J., 2013a. Synthesis and luminescence mechanism of multicolor-emitting g-C_3N_4 nanopowders by low temperature thermal condensation of melamine. Sci. Rep. 3, 1943. https://doi.org/10.1038/srep01943.

Zhang, Y., Zhang, N., Tang, Z.-R., Xu, Y.-J., 2013b. A unique silk mat-like structured Pd/CeO_2 as an efficient visible light photocatalyst for green organic transformation in water. ACS Sustain. Chem. Eng. 1, 1258–1266. https://doi.org/10.1021/sc400116k.

Zhao, Z., Sun, Y., Dong, F., 2015. Graphitic carbon nitride based nanocomposites: a review. Nanoscale 7, 15–37. https://doi.org/10.1039/c4nr03008g.

Zhou, J., Zhang, M., Zhu, Y., 2015. Photocatalytic enhancement of hybrid C_3N_4/TiO_2 prepared via ball milling method. Phys. Chem. Chem. Phys. 17, 3647–3652. https://doi.org/10.1039/C4CP05173D.

Please cite this article in press as: Cerdan, K., et al. Facile mechanochemical modification of g-C_3N_4 for selective photo-oxidation of benzyl alcohol. Chem. Eng. Sci. (2018), https://doi.org/10.1016/j.ces.2018.04.001

8.8. Appendix 8 Continuous Flow Alcoholysis of Furfuryl Alcohol to Alkyl Levulinates Using Zeolites

ACS Sustainable Chemistry & Engineering

Research Article

Cite This: ACS Sustainable Chem. Eng. 2018, 6, 6901−6909

pubs.acs.org/journal/ascecg

Continuous Flow Alcoholysis of Furfuryl Alcohol to Alkyl Levulinates Using Zeolites

Deyang Zhao,[†] Pepijn Prinsen,[‡] Yantao Wang,[†] Weiyi Ouyang,[‡] Frederic Delbecq,[§] Christophe Len,[†,∥] and Rafael Luque[*,‡,⊥]

[†]Centre de Recherche Royallieu, Sorbonne Universités, Université de Technologie de Compiègne, CS 60 319, F-60203 Compiègne Cedex, France

[‡]Departamento de Química Orgánica, Universidad D Cordoba, Campus de Rabanales, Edificio Marie Curie, Ctra. Nnal. IV, Km. 396, E-14014, Cordoba, Spain

[§]Ecole Supérieure de Chimie Organique et Minérale (ESCOM), 1 Allée du Réseau Jean Marie Buckmaste, F-60200 Compiègne, France

[∥]PSL Research University, Chimie ParisTech, CNRS, Institut de Recherche de Chimie Paris, 11 rue Pierre et Marie Curie, F-75231 Paris Cedex 05, France

[⊥]Peoples Friendship University of Russia (RUDN University), 6 Miklukho-Maklaya Street, Moscow 117198, Russia

Supporting Information

ABSTRACT: The present work explores the catalytic activity of various zeolites for the production of methyl levulinates from hemicellulose derived furfuryl alcohol and explores the performance of H-ZSM-5-50 zeolite in continuous flow alcoholysis. Methyl levulinate yields up to 80% were achieved at 170 °C (50 bar) using a high load (1.6 M furfuryl alcohol) feed at 0.2 mL min^{-1} flow rate. Angelica lactones were produced in significant amounts as one of the side products, albeit in lower amounts in continuous flow mode. Catalyst deactivation occurred at high furfuryl alcohol load through formation of pore blocking polyfurfuryl alcohols. The zeolites showed good reusability after regeneration at 500 °C. The levulinate yields in ethanol and *n*-propanol were 20% lower.

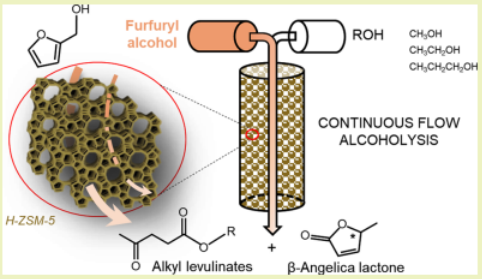

KEYWORDS: *Furfuryl alcohol, Continuous flow alcoholysis, Zeolites, Alkyl levulinates, Angelica lactones*

INTRODUCTION

Recent advances in the field of catalytic valorization of lignocellulose for the production of biofuels and chemicals aim to reach high yields of (1) hexitols through hydrogenation or (2) 5-hydroxymethylfurfural (HMF) through isomerization and dehydration of glucose or oligomers, produced from cellulose hydrolysis.[1,2] Similarly, furfural can be produced from xylose, as the major hydrolysis product from hemicelluloses.[3,4] Levulinic acid, as the 5-HMF hydrolysis product, is among the top target chemicals in lignocellulose biorefinery and it can be converted into various derivatives with several applications, particularly into alkyl levulinates as biofuel additive or precursor.[5] Alkyl levulinates can be obtained via esterification of levulinic acid with various alcohols.[6] Levulinic acid can be produced directly from various biomass sources in acidic aqueous media, but this process deals with the production of waste, a high cost for mineral acid recovery, humin formation, and a rather difficult separation of the highly polar molecule levulinic acid.[7,8] Some promising results were obtained using ionic liquids and with the carbohydrate derived solvent γ-valerolactone and by using solid acid catalysts, as demonstrated recently for H-ZSM-5 in aqueous THF.[9] Alcoholysis is a promising alternative to tackle these problems and opens ways for direct conversion of sugar monomers,[10,11] as demonstrated very recently for methyl levulinate starting from glucose using sulfated zirconia.[12] The alcoholysis processes can also be started from 5-HMF (Scheme 1, pathway displayed in green), without the need for isolation of levulinic acid from aqueous product streams. Likewise, alkyl levulinates can also be produced via selective hydrogenation of furfural to furfuryl alcohol (FA) followed by conversion in various alcohols (ROH), as illustrated in Scheme 1 (pathway displayed in blue). This conversion allows to increase the overall yield of a levulinate production plant from lignocellulose by converting a minor coproduct, furfural or furfuryl alcohol, into its main product.

Various solid acid catalysts have been demonstrated to work well for the conversion of FA to alkyl levulinates, as recently reviewed for ethyl levulinate by Haider and co-workers.[12] The

Received: February 12, 2018
Revised: March 15, 2018
Published: April 2, 2018

DOI: 10.1021/acssuschemeng.8b00726
ACS Sustainable Chem. Eng. 2018, 6, 6901−6909

(25) Ouyang, W.; Yepez, A.; Romero, A. A.; Luque, R. Towards industrial furfural conversion: selectivity and stability of palladium and platinum catalysts under continuous flow regime. *Catal. Today* **2017**, DOI: 10.1016/j.cattod.2017.07.011.
(26) Brasholz, M.; von Känel, K.; Hornung, C. H.; Saubern, S.; Tsanaktsidis, J. Highly efficient dehydration of carbohydrates to 5-(chloromethyl)furfural (CMF), 5-(hydroxymethyl)furfural (HMF) and levulinic acid by biphasic continuous flow processing. *Green Chem.* **2011**, *13*, 1114−1117.
(27) Xing, R.; Qi, W.; Huber, G. W. Production of furfural and carboxylic acids from waste aqueous hemicellulose solutions from the pulp and paper and cellulosic ethanol industries. *Energy Environ. Sci.* **2011**, *4*, 2193−2205.
(28) Serrano-Ruiz, J. C.; Luque, R.; Campelo, J. M.; Romero, A. A. Continuous-flow processes in heterogeneously catalyzed transformations of biomass derivatives into fuels and chemicals. *Challenges* **2012**, *3*, 114−132.
(29) Grob, R. L.; Barry, E. F. *Modern Practice of Gas Chromatography*; John Wiley & Sons, Inc., 2004.
(30) Xin, J.; Zhang, S.; Yan, D.; Ayodele, O.; Lu, X.; Wang, J. Formation of C-C bonds for the bio-alkanes production at mild conditions. *Green Chem.* **2014**, *16*, 3589−3595.
(31) Karwa, S.; Gajiwala, V. M.; Heltzel, J.; Patil, S. K. R.; Lund, C. R. F. Reactivity of levulinic acid during aqueous, acid-catalyzed HMF hydration. *Catal. Today* **2016**, *263*, 16−21.
(32) Lima, C. G. S.; Monteiro, J. L.; Lima, T.; Paixão, M. W.; Corrêa, A. G. Angelica lactones: from biomass-derived platform chemicals to value-added products. *ChemSusChem* **2018**, *11*, 25−47.
(33) Prinsen, P.; Luque, R.; González-Arellano, C. Zeolite catalyzed palmitic acid esterification. *Microporous Mesoporous Mater.* **2018**, *262*, 133−139.
(34) Li, H.; Yang, S.; Riisager, A.; Pandey, A.; Sangwan, R. S.; Saravanamurugan, S.; Luque, R. Zeolite and zeotype-catalysed transformations of biofuranic compounds. *Green Chem.* **2016**, *18*, 5701−5735.

DOI: 10.1021/acssuschemeng.8b00726
ACS Sustainable Chem. Eng. 2018, 6, 6901−6909

8.9. Appendix 9 Designer Hydrogenated Wrinkled Yolk@Shell TiO_2 Architectures towards Advanced Visible Light Photocatalysts for Selective Alcohol Oxidation

Journal of Materials Chemistry A

PAPER

View Article Online
View Journal

Cite this: DOI: 10.1039/c8ta02012d

Designer hydrogenated wrinkled yolk@shell TiO_2 architectures towards advanced visible light photocatalysts for selective alcohol oxidation†

Abolfazl Ziarati, [a] Alireza Badiei, *[a] Rafael Luque *[bc] and Weiyi Ouyang[b]

Received 2nd March 2018
Accepted 14th April 2018

DOI: 10.1039/c8ta02012d

rsc.li/materials-a

Smart architectures of TiO_2 are attracting increasing attention due to their outstanding properties in a broad range of fields. Herein, we report the preparation of an unprecedented yolk/shell wrinkled TiO_2 architecture with excellent photocatalytic activities under visible light irradiation. This method includes solvothermal, partial etching and hydrogen treatment sequential preparation steps. The solvothermal step leads to yolk@shell TiO_2 (Y@S-TiO_2) structures which can generate multiple reflections of incident light so as to promote an efficient light harvesting due to an enhanced surface area and light scattering ability based on the hydrothermal alkaline partial etching. The hydrogen treatment process generated Ti^{3+} species on the surface of TiO_2 which facilitate electron–hole separation, decreasing the band gap of titania to the visible region. The resultant yolk@hydrogenated wrinkled shell TiO_2 architecture exhibited high efficiency in visible light oxidation of alcohols to the corresponding aldehydes (up to 90% in conversion and 97% in selectivity).

Introduction

TiO_2 has received widespread attention as a favourable candidate for use in water splitting, dye-sensitized solar cells and photocatalysis reactions in recent years due to its outstanding chemical and physical properties including photo-corrosion resistance, chemical stability, low toxicity and suitable electronic band structure.[1–4] The ability to adjust nanostructured TiO_2 to diverse polymorphs and morphologies is the key to efficiently design advanced functional materials for the aforementioned applications.[5–7]

Several TiO_2 morphologies have been extensively investigated including nanotubes, nanowires, hollow spheres, and core@shell and yolk@shell architectures.[8–14] Yolk@shell architectures have attracted particular attention and emerged as a modern generation of smart functional structures.[15,16] These structures generally include a functional core and a hollow porous shell. Owing to their unique structural properties including the presence of interstitial hollow spaces, the permeability of shells and the tunable functionalities in both the inner core and outer shell, yolk@shell architectures have been employed in various fields such as biomedicine, sorption, electrochemistry, catalysis and especially in energy conversion.[17–22] For example, Li *et al.* have prepared TiO_2 mesoporous yolk@shell microspheres with a high light scattering ability.[23] Feng *et al.* synthesized Y@S-TiO_2 structures composed of a single anatase TiO_2 phase with high light conversion abilities.[24]

All reported yolk@shell structures displayed an improved light harvesting activity as compared to commercial TiO_2 because of their larger specific surface areas and light-scattering abilities.

A large diversity of living organisms with wrinkled structures can be found in nature. These include plant seeds, pollens and several microorganisms. Wrinkled structures can provide large surface areas which improve surface properties including tracking, adhesiveness and capturing functions. Furthermore, the structural stability and light utilization efficiency have been reported to be improved in wrinkled surfaces.[25] Inspired by such a concept in nature, this contribution was aimed to design artificial wrinkled surfaces based on Y@S-TiO_2 structures as advanced functional photonanocatalysts.

The development of stable and highly active visible light absorption titania photocatalysts still remains a significant challenge since TiO_2 uses are critically hindered by ineffective operation of visible light (43% of the total solar energy) which results from its wide band gap (3.2 eV). The preparation of reduced TiO_2 nanomaterials containing Ti^{3+} species has been considered as a promising environmentally friendly strategy to enhance visible light photoactivity.[26–31] In fact, hydrogenated

[a]School of Chemistry, College of Science, University of Tehran, Tehran, Iran. E-mail: abadiei@khayam.ut.ac.ir; Fax: +98-21-61112614; Tel: +98-21-61112614

[b]Departamento de Quimica Organica, Universidad de Cordoba, Campus de Rabanales, Edificio Marie Curie, E-14014 Cordoba, Spain. E-mail: rafael.luque@uco.es

[c]Peoples Friendship University of Russia (RUDN University), 6 Miklukho-Maklaya str., 117198, Moscow, Russia

† Electronic supplementary information (ESI) available: Details of the materials and apparatus used, formation process of the Y@S-TiO_2 microspheres, UV-Vis spectra and nitrogen adsorption–desorption isotherms of some of the structures, and the reusability study of the Y@HWS-TiO_2 architecture. See DOI: 10.1039/c8ta02012d

31 Q. Zhu, Y. Peng, L. Lin, C.-M. Fan, G.-Q. Gao, R.-X. Wang and A.-W. Xu, *J. Mater. Chem. A*, 2014, **2**, 4429–4437.
32 X. Chen, L. Liu and F. Huang, *Chem. Soc. Rev.*, 2015, **44**, 1861–1885.
33 Y. Yan, M. Han, A. Konkin, T. Koppe, D. Wang, T. Andreu, G. Chen, U. Vetter, J. R. Morante and P. Schaaf, *J. Mater. Chem. A*, 2014, **2**, 12708–12716.
34 Z. Wang, C. Yang, T. Lin, H. Yin, P. Chen, D. Wan, F. Xu, F. Huang, J. Lin and X. Xie, *Adv. Funct. Mater.*, 2013, **23**, 5444–5450.
35 X. Yu, B. Kim and Y. K. Kim, *ACS Catal.*, 2013, **3**, 2479–2486.
36 A. Sinhamahapatra, J.-P. Jeon and J.-S. Yu, *Energy Environ. Sci.*, 2015, **8**, 3539–3544.
37 H. Eskandarloo, M. Hashempour, A. Vicenzo, S. Franz, A. Badiei, M. A. Behnajady and M. Bestetti, *Appl. Catal., B*, 2016, **185**, 119–132.
38 J. Poostforooshan, A. Badiei, M. Kolahdouz and A. P. Weber, *ACS Appl. Mater. Interfaces*, 2016, **8**, 21731–21741.
39 J. Lai, S. Li, F. Wu, M. Saqib, R. Luque and G. Xu, *Energy Environ. Sci.*, 2016, **9**, 1210–1214.
40 S. De, J. Zhang, R. Luque and N. Yan, *Energy Environ. Sci.*, 2016, **9**, 3314–3347.
41 J. C. Colmenares, W. Ouyang, M. Ojeda, E. Kuna, O. Chernyayeva, D. Lisovytskiy, S. De, R. Luque and A. M. Balu, *Appl. Catal., B*, 2016, **183**, 107–112.
42 A. Ziarati, A. Badiei, G. M. Ziarani and H. Eskandarloo, *Catal. Commun.*, 2017, **95**, 77–82.
43 J. Huo, Y. Hu, H. Jiang and C. Li, *Nanoscale*, 2014, **6**, 9078–9084.
44 X. Chen, L. Liu, Y. Y. Peter and S. S. Mao, *Science*, 2011, **331**, 746–750.
45 J. Su, X.-X. Zou, Y.-C. Zou, G.-D. Li, P.-P. Wang and J.-S. Chen, *Inorg. Chem.*, 2013, **52**, 5924–5930.
46 X. Jiang, Y. Zhang, J. Jiang, Y. Rong, Y. Wang, Y. Wu and C. Pan, *J. Phys. Chem. C*, 2012, **116**, 22619–22624.
47 J. Chen, Z. Ding, C. Wang, H. Hou, Y. Zhang, C. Wang, G. Zou and X. Ji, *ACS Appl. Mater. Interfaces*, 2016, **8**, 9142–9151.
48 T. Xia and X. Chen, *J. Mater. Chem. A*, 2013, **1**, 2983–2989.
49 W. Wei, N. Yaru, L. Chunhua and X. Zhongzi, *RSC Adv.*, 2012, **2**, 8286–8288.
50 M. Sugawara, *Phys. Rev. B: Condens. Matter Mater. Phys.*, 1995, **51**, 10743.
51 M. Xing, W. Fang, M. Nasir, Y. Ma, J. Zhang and M. Anpo, *J. Catal.*, 2013, **297**, 236–243.

A work paving the way
for
the development of environmentally sound solutions
towards
a more sustainable future